

HARMONIC REPRESENTATION APPLIED  
TO ATMOSPHERIC DYNAMICS

[HARMONIC REPRESENTATION APPLIED TO  
LARGE SCALE ATMOSPHERIC DYNAMICS]

by

Philip E. Merilees

A thesis submitted to the Faculty of Graduate Studies  
and Research in partial fulfillment of the requirements  
for the degree of Doctor of Philosophy.

Department of Meteorology

McGill University

Montreal

April, 1966

To my wife, Micheline

## TABLE OF CONTENTS

	Page
Acknowledgements	i
List of Tables	ii
List of Figures	iv
List of Appendices	vii
Abstract	viii
1. Introduction	1
2. The Dynamical Equations in Spectral Form	8
The Spectral Transformation	8
The Energy Equations	27
3. Three-Component Barotropic Systems	38
Model 1 - Motion on the "f-plane"	38
Model 2 - Motion on the " $\beta$ -plane"	45
Model 3 - Motion on a Spherical Surface	62
4. Data Analysis in Terms of Spherical Harmonics	78
The Analysis of the Geopotential Height Field	79
Properties of Numerical Quadrature	80
The Linear Balance Equation	93
Hemispheric Analysis	99
The Details of the Method Used	99
The Random Error Noise Level	103

	Page
The Statistics of the Flow at 500 mb for September 1957	109
The Geopotential Height Field	109
Noise level in the Height Field Analysis	112
The Stream Function	117
Representation of the Mean Zonal Flow	123
Fluctuations of the Large Scale Components	128
Zonal	128
Non-zonal	130
5. Summary and Conclusions	155
Bibliography	158
Appendix A	162
Appendix B	164

## ACKNOWLEDGEMENTS

The organization of a global field of data for 500 mb by Professor B. W. Boville made a large part of this study possible. The author wishes to express his gratitude to his research supervisor, Professor Boville, and to his many other colleagues in the Arctic Meteorology Research Group for their stimulating discussions and helpful suggestions. Thanks are also due to Miss Susan Hoblyn, who prepared the typescript, and Mrs. H. B. Kruczkowska and Miss N. Walters, who prepared the diagrams.

## LIST OF TABLES

Table		Page
2.1	The spectral form of the vorticity equation	24
2.2	The spectral form of the divergence equation	25
2.3	The spectral forms of the thermodynamic, continuity and hydrostatic equations	26
3.1	Possible unstable combinations of (s, k) in Model 3.	67
4.1a	Quadrature matrix - trapezoidal rule for m=0	83
4.1b	Quadrature matrix - trapezoidal rule for m=4	84
4.2a	Quadrature matrix - Simpson's rule for m=0	85
4.2b	Quadrature matrix - Simpson's rule for m=4	86
4.3a	Quadrature matrix - Gaussian plus interpolation for m=0	87
4.3b	Quadrature matrix - Gaussian plus interpolation for m=4	88
4.4a	Quadrature matrix - over Gaussian latitudes for m=0	90
4.4b	Quadrature matrix - over Gaussian latitudes for m=4	91
4.5	Solution of linear balance equation in spectral domain	95
4.6	Distribution of variance of the mean of randomly generated height fields	101
4.7	Distribution of mean variance of the randomly generated height fields	102
4.8	Distribution of variance of the mean of stream fields obtained from randomly generated height fields	104

Table		Page
4.9	Distribution of mean variance of the stream fields obtained from randomly generated height fields	105
4.10	Distribution of variance of mean 500 mb height field for September 1957	107
4.11	Distribution of mean variance of the 500 mb height field for September 1957	108
4.12	Distribution of kinetic energy of the 500 mb mean flow, September 1957	114
4.13	Distribution of mean kinetic energy of the 500 mb flow, September 1957	115
4.14	Accumulated mean zonal wind profiles	121
4.15	Character of the fluctuations of spherical harmonic waves	149

## LIST OF FIGURES

Figure		Page
3.1a	Fluctuations of components of Model 1 - stable case	41
3.1b	Fluctuations of components of Model 1 - unstable case	41
3.2a	Fluctuations of components of Model 1 - stable case - subcritical	43
3.2b	Fluctuations of components of Model 1 - stable case - supercritical	43
3.3	Zonal flow profile for Model 2	51
3.4	Linear phase speeds for Model 2	49
3.5	Linear growth rates for Model 2	50
3.6	Fluctuation of components of Model 2 - stable, short wave case	52
3.7	Fluctuation of components of Model 2 - unstable case	54
3.8	Fluctuation of components of Model 2 - stable, long wave case	55
3.9	Fluctuation of components of Model 2 - stable, long wave case with large initial perturbation.	57
3.10	Fluctuation of components of Model 2 - stable, short wave case with large initial perturbation.	58
3.11	Amplitude of fluctuation of zonal component as a function of $\alpha$	61

Figure		Page
3.12 to 3.15	Linear phase speeds and growth rates for Model 3	70-73
3.16	Fluctuations of Model 3 - unstable case	75
3.17	Fluctuations of Model 3 - stable case	76
4.1	Distribution of variance of 500 mb height field over the three wave numbers for September 1957	110
4.2	Distribution of mean kinetic energy at 500 mb over the three wave numbers for September 1957	116
4.3	Distribution of mean kinetic energy at 500 mb in the northern hemisphere for January 1957 (from Eliassen and Machenhauer (1965) )	118
4.4	Corrected distribution of mean kinetic energy at 500 mb over the three wave numbers for September 1957	120
4.5	Comparison of accumulated mean zonal wind profiles	122
4.6	Comparison of mean zonal stream winds with geostrophically computed winds	124
4.7	Daily values of zonal stream function components (n = 1-5)	126
4.8	Daily values of zonal stream function components (n = 6-9)	127
4.9	Daily values of zonal stream function components (n = 10, 11)	129
4.10 to 4.15	Phase diagrams for global stream components	131-136
4.16 to 4.19	Phase diagrams for northern and southern hemispheric height components	138-141

Figure		Page
4. 20 to	Phase diagrams for northern and southern	
4. 23	hemispheric height components	143-146
4. 24 to	Phase diagrams for northern and southern	
4. 25	hemispheric height components	151-152

## LIST OF APPENDICES

Appendix		Page
A	Properties of Legendre functions	162
B	Evaluation of interaction matrices	164

Abstract

Spectral analysis (primarily in terms of spherical harmonics) is applied to the atmospheric dynamical equations in general, to truncated barotropic systems in particular and, in addition, to the global geopotential height field of the 500 mb surface for September 1957.

The complete set of equations governing adiabatic frictionless flow transform into the spectral domain, and are energetically consistent under practically any truncation procedure. Analysis of truncated barotropic systems leads to a reinterpretation of barotropic instability in terms of the frequency of momentum transport.

There is no evidence that the fluctuations of spherical harmonic waves at 500 mb are global in character, but the lack of data in the southern hemisphere limits the validity of this conclusion. Hemispheric analysis of the geopotential height field at 500 mb for the northern hemisphere indicates that the planetary waves are composed of a quasi-stationary component and a rapidly retrogressive component whose phase speeds are a large fraction of the theoretical Rossby-Haurwitz phase speeds.

## 1. INTRODUCTION

The systematic investigation of the properties of the meteorologically significant wave motions in the atmosphere has proceeded apace since the pioneer work of Rossby, Haurwitz and Bilinova in the late 1930's and early 1940's. By introducing the "beta plane" approximation, Rossby (1939) formulated the vorticity principle which governs the motion of long waves in a barotropic atmosphere. Haurwitz (1940) and Bilinova (1943) extended this work without the "beta plane" approximation, using spherical harmonics, and obtained the corresponding phase speed formula for barotropic waves on a spherical earth. Craig (1945) and Neamtan (1946) found a particular solution of the non-linear vorticity equation in terms of spherical harmonics. Kuo (1949) considered the barotropic problem more realistically by permitting variations of zonal wind with latitude, which introduced the possibility of developing unstable waves in this current. Extensions of the physical model from one which conserved absolute vorticity to one which conserved potential vorticity led to the classic studies of the baroclinic problem by Charney (1947), Eady (1949) and Fjortoft (1950). In these studies the essential physical relationships between energy conversion from potential to kinetic, and the corresponding motions necessary to achieve the conversion, were demonstrated. As well, the vertical wind shear was shown to be the predominant parameter for the stability of such motions.

A major limitation of these studies was the mathematical

necessity of linearizing the equations of motion. This process consists of choosing a dynamic and thermodynamic state which is a solution of the equations; then considering small deviations from this state, determining whether these deviations tend to grow, decay, or remain the same. In principle one is interested in the deviations and their behaviour, since they constitute the greater part of the day-to-day variability of the atmosphere. In fact, however, linearization shifts the emphasis of the study to the basic state, and as soon as the deviations from the state become large (e. g., for an unstable basic state) the linearized equations break down. Also, there appear to be many physical systems which are stable to small perturbations, but unstable for large perturbations, and hence beyond the scope of linearized equations.

One solution to this difficulty is to abandon the analytical study of the equations of motion and to integrate them by numerical grid-point techniques. The fact that the equations are non-linear does not present any fundamental difficulty. This approach was initiated by Charney and collaborators in the late 1940's, in order to do actual forecasting of upper level wind patterns. Since then, the technique of numerical integration has been applied to many physical models of the atmosphere, both from a forecasting and a general circulation point of view. These models have done remarkably well in reproducing the atmosphere's complex motions, at least in a statistical sense. However, most of the models simulate the atmosphere in having very many degrees of freedom, so that the physical processes represented

by the non-linear terms in the equations are not subject to much more particular scrutiny than if one looked at actual atmospheric data.

There is another approach to the problem. In 1954, Silberman presented a method by which the advection term (a non-linear term) in the barotropic vorticity equation may be evaluated in the form of a Fourier transform. In his method, the fields of dynamic variables, rather than being represented by a finite number of grid points, are represented by the amplitudes of a finite number of functions; in his case spherical harmonics. The most obvious advantage of this method is the explicit continuity in space of the dynamic fields. The disadvantages lie in the necessity of computing the initial amplitudes from the original grid of data and the computation of the so-called "interaction matrices" which represent the non-linear advection term.

Lorenz (1960a) used Silberman's idea to study barotropic motion on a flat earth. He discovered the remarkable property that, if one transformed the equations into a spectral form (i. e., to a set of equations describing the variations of the amplitudes of specified spatial functions), then not only were the conservation theorems (i. e., conservation of kinetic energy and mean square vorticity) valid for an infinite set of amplitudes, but also for a highly truncated set of amplitudes. Further, by considering only the very minimum number of degrees of freedom necessary to represent a physical process, one

could integrate the non-linear equations of motion analytically. Platzman (1960, 1962) applied spherical harmonics to the barotropic vorticity equation in the manner of Silberman and proved that the conservation theorems for truncated systems hold in this function domain as well. He also did a systematic delineation of those truncated systems (applied to the barotropic vorticity equation) which could be integrated analytically. By applying the spectral method to a system of equations governing the rotating dish-pan experiments Lorenz (1962) was able to reproduce the curve of transition from a Hadley to a Rossby regime obtained experimentally by Fultz (1959), and also explain to some extent the hysteresis effect of the transition by a non-linear process.

The method of spectral representation of the equations of motion, because of its conservation properties, was recognized as being very useful in the field of numerical weather prediction. Baer (1964) integrated a spectral barotropic model from generated initial conditions and demonstrated the feasibility of this process. Recently Ellsaesser (1965) has integrated a spectral barotropic model from actual initial conditions with good results.

The spectral method has also found its way into general circulation experiments. Bryan (1959) considered a highly truncated spectral version (13 degrees of freedom) of a two-level baroclinic model with heating and friction, but found that the number of degrees of freedom was not sufficient to produce a definite life cycle in the

disturbances. However, his analysis of the horizontal momentum transport in the model pointed out the importance of the "differential  $\beta$ -effect" in determining the direction of momentum transport (see chapter 3). Robert (1965) applied the technique to a primitive equation model, to demonstrate its feasibility for this type of equation, and Peng (1965) was able to provide a reasonable explanation for the up-gradient heat transport in the lower stratosphere by consideration of a truncated spectral form of the equations of motion.

There are two major applications of the spectral method. One may take advantage of its conservation properties and apply it with high resolution to produce better prediction or general circulation models. More importantly, one may also apply this method with very low resolution to specific physical models to gain insight into the non-linear processes inherent in the equations.

The application of spectral representation to observational studies of the atmosphere has proceeded at a much slower pace than the theoretical studies because of the lack of adequate data coverage. One-dimensional Fourier analysis at latitude circles has been used by many authors, Boville (1961), Eliassen (1958), etc., to determine the distribution of horizontal kinetic energy as a function of wavelength as well as to measure the contribution of various scales to the maintenance of the atmosphere's budgets (e. g., heat, momentum). Whether this approach can adequately define the dominant scales of motion is questionable, because it lacks the determination of a wave-

length in the north-south direction. In fact, in most studies the large variation of the phase angle of a given wave with latitude indicates that the dominant scales of motion are considerably smaller than those which would be determined by counting the number of waves around a latitude circle (Phillips, 1963, pp. 161-162).

One of the first attempts at representing atmospheric fields by two-dimensional waves was made by Haurwitz and Craig (1952). Lacking data even for a single hemisphere they resorted to a statistical best fit method of analysis in terms of spherical harmonics. The results were disappointing in the sense that no simple model could account for the behaviour of the waves. However, they did show how remarkably few waves were necessary to represent the large scale features. Apart from isolated attempts at using Chebyshev polynomials for the representation in the north-south direction, spherical harmonics have been used to analyze data fields into two dimensional waves. Most recent observational studies (Eliassen and Machenhauer (1965), Deland (1965) ) have used data from the Northern Hemisphere and assumed either symmetry or antisymmetry for the missing Southern Hemisphere data. One attempt has been made at a global analysis of the 500 mb height field, using the data obtained during the IGY (Steinberg, 1965). (A detailed comparison of the last three studies referred to will be made in a subsequent chapter; suffice here to say that a reasonable picture of the behaviour of spherical harmonic waves is emerging.)

The present study is divided into four sections:

1. The transformation of the general dynamical equations into spectral form, and a study of the truncation properties of the energy equations.
2. A detailed study of highly truncated systems representing barotropic motion with a view to providing some insight into barotropic instability.
3. A study of spherical harmonic analysis techniques and their application to global, as well as hemispheric, analysis.
4. An attempt to apply the concepts formulated in (2) concerning the non-linear behaviour of waves to the observed behaviour of these waves.

## 2. THE DYNAMICAL EQUATIONS IN SPECTRAL FORM

In this chapter the dynamical equations of atmospheric flow will be transformed into their spectral form using spherical harmonics. The corresponding energy equations in spectral form will be studied to determine the conditions imposed on a truncated system in order that energy (potential plus kinetic) be conserved.

### The Spectral Transformations

By Helmholtz' theorem any horizontal wind field may be represented as the sum of an irrotational field and a non-divergent field, i. e.

$$\mathbf{V} = \mathbf{V}_\psi + \mathbf{V}_\chi \quad 2.1$$

$$\text{where } \mathbf{V}_\psi = \mathbf{k} \times \nabla \psi \quad \mathbf{V}_\chi = \nabla \chi \quad 2.2$$

Here  $\psi$  is a stream function,  $\chi$  is a velocity potential and  $\mathbf{k}$  is the unit vertical vector. From these definitions it follows that the vertical component of relative vorticity (hereafter referred to simply as vorticity) and the horizontal divergence are given by

$$\begin{aligned} \zeta &\equiv \mathbf{k} \cdot \nabla \times \mathbf{V} = \nabla^2 \psi \\ D &\equiv \nabla \cdot \mathbf{V} = \nabla^2 \chi \end{aligned} \quad 2.3$$

The components of the horizontal wind field are then

$$u_x = \frac{1}{a \sin \theta} \frac{\partial \chi}{\partial \lambda}$$

$$u_\psi = \frac{1}{a} \frac{\partial \psi}{\partial \theta}$$

2.4

$$v_x = -\frac{1}{a} \frac{\partial \chi}{\partial \theta}$$

$$v_\psi = \frac{1}{a \sin \theta} \frac{\partial \psi}{\partial \lambda}$$

where  $\theta$  is colatitude,  $\lambda$  is longitude and  $a$  is the radius of the earth.

Using this wind representation, the horizontal equations of motions in a relative coordinate system  $(\lambda, \theta, \rho, t)$  may be transformed into the vorticity equation and the divergence equation,

$$\frac{\partial \zeta}{\partial t} = -k \times \nabla \psi \cdot \nabla \zeta - \nabla \chi \cdot \nabla \zeta - \omega \frac{\partial \zeta}{\partial \rho} - k \times \nabla \psi \cdot \nabla f$$

2.5

$$- \nabla \chi \cdot \nabla f - \zeta D - f D - k \cdot \nabla \omega \times \nabla \frac{\partial \chi}{\partial \rho} - \nabla \omega \cdot \nabla \frac{\partial \psi}{\partial \rho}$$

$$\frac{\partial D}{\partial t} = -\nabla^2 \left( \frac{V_\psi \cdot V_\psi}{2} \right) - \nabla^2 \left( \frac{V_x \cdot V_x}{2} \right) - \nabla^2 (V_\psi \cdot V_x) + \nabla \psi \cdot \nabla \zeta$$

$$- \omega \frac{\partial D}{\partial \rho} - k \times \nabla \chi \cdot \nabla f + \nabla \psi \cdot \nabla f + \zeta^2 + f \zeta$$

2.6

$$+ k \cdot \nabla \omega \times \nabla \frac{\partial \psi}{\partial \rho} - \nabla \omega \cdot \nabla \frac{\partial \chi}{\partial \rho} - \nabla^2 \Phi$$

where  $f$  is the Coriolis parameter ( $2\Omega \cos \theta$ ),  $\omega$  is the vertical motion in pressure coordinates ( $\omega = \frac{\delta p}{\delta t}$ )\*, and  $\Phi$  is the geopotential of a constant pressure surface. These two equations coupled with the continuity equation,

$$\nabla^2 \chi + \frac{\partial \omega}{\partial p} = 0 \quad 2.7$$

the adiabatic thermodynamic equation ( $\Theta$  is potential temperature);

$$\frac{\partial \Theta}{\partial t} = -k \times \nabla \psi \cdot \nabla \Theta - \nabla \chi \cdot \nabla \Theta - \omega \frac{\partial \Theta}{\partial p} \quad 2.8$$

and the hydrostatic equation ( $\kappa = R/c_p$ )

$$\frac{\partial \Phi}{\partial p} + \frac{R p^{\kappa-1}}{p_0^\kappa} \Theta = 0 \quad 2.9$$

form a complete set of equations governing adiabatic, frictionless flow.

These equations will now be transformed term by term into the spectral domain in terms of spherical harmonics. It will become apparent that the expressions obtained in this process depend entirely on the geometric configuration of the individual terms. So that, having worked through each term in the vorticity equation, most of the terms in the other equations can be transformed by inspection.

As a first step, some elementary properties of the

---

\*  $\frac{\delta}{\delta t}$  is the total derivative; while  $\frac{d}{dt}$  is used to denote the horizontal derivative, i. e. at constant pressure.

spectral functions will be considered. Let  $Y_n^m = P_n^m e^{im\lambda}$  denote a spherical harmonic of degree  $n$  and rank  $m$ . Then, if  $\lambda$  and  $\theta$  denote longitude and colatitude respectively, and  $a$  is the radius of the earth;

$$\nabla^2 Y_n^m = -\frac{n(n+1)}{a^2} Y_n^m \quad 2.10$$

where  $\nabla^2 \equiv \frac{1}{a^2 \sin \theta} \left( \frac{\partial}{\partial \theta} \left( \sin \theta \frac{\partial}{\partial \theta} \right) + \frac{1}{\sin \theta} \frac{\partial^2}{\partial \lambda^2} \right)$

and  $P_n^m$  is a normalized associated Legendre function;

$$P_n^m \equiv \frac{1}{2^n n!} \left( \frac{2n+1}{2} \frac{(n-m)!}{(n+m)!} \right)^{\frac{1}{2}} (1-\mu^2)^{\frac{m}{2}} \frac{d^{n+m}}{d\mu^{n+m}} (\mu^2-1)^n; \mu = \cos \theta$$

$$P_n^{-m} = (-1)^m P_n^m$$

The  $P_n^m$  are orthonormal in  $\theta$ ;

$$\int_0^\pi P_n^m P_k^m \sin \theta d\theta = \begin{cases} 1 & \text{if } n=k \\ 0 & \text{if } n \neq k \end{cases} = \delta_{nk}^n \quad 2.11$$

so that the corresponding spherical harmonics are orthogonal over the surface of a sphere;

$$\frac{1}{2\pi} \int_0^{2\pi} \int_0^\pi Y_n^{*m} Y_k^j \sin \theta d\theta d\lambda = \delta_j^m \delta_k^n \quad 2.12$$

where the asterisk denotes the complex conjugate. The index  $n$  may be any positive integer or zero;  $m$  may be any integer.

However, as can be seen from the definition of the  $P_n^m$ , if  $m > n$   $P_n^m \equiv 0$ . So that  $m$  is usually restricted to range from  $-n$  to  $+n$ .

The notation may be simplified by following Platzman (1962) in defining a complex wave vector  $\gamma = n_\gamma + i m_\gamma$ . In this notation equation 2.10 and 2.12 become

$$\nabla^2 Y_\gamma = -\frac{n_\gamma(n_\gamma+1)}{a^2} Y_\gamma$$

2.13

$$\frac{1}{2\pi} \int_0^{2\pi} \int_0^\pi Y_\alpha^* Y_\beta \sin\theta d\theta d\lambda = \delta_{\alpha\beta}$$

Further properties of these functions are given in Appendix A.

The expansion of the stream function and the potential function in terms of spherical harmonics gives

$$\psi = a^2 \sum_\gamma \psi_\gamma Y_\gamma$$

2.14

$$\chi = a^2 \sum_\gamma \chi_\gamma Y_\gamma$$

where the spectral amplitudes are defined as,

$$\psi_{\gamma} = \frac{1}{2\pi a^2} \int_0^{2\pi} \int_0^{\pi} \Psi Y_{\gamma}^* \sin \theta d\theta d\lambda$$

2.15

$$\chi_{\gamma} = \frac{1}{2\pi a^2} \int_0^{2\pi} \int_0^{\pi} \chi Y_{\gamma}^* \sin \theta d\theta d\lambda$$

Because of equations (2.3) the vorticity and divergence are simply related to these amplitudes.

$$\zeta = - \sum_{\gamma} c_{\gamma} \psi_{\gamma} Y_{\gamma}$$

2.16

$$D = - \sum_{\gamma} c_{\gamma} \chi_{\gamma} Y_{\gamma}$$

where  $c_{\gamma} = n_{\gamma}(n_{\gamma} + 1)$

The spectral amplitudes are in general complex. In order that the representation be real the amplitudes must satisfy,

$$\psi_{\gamma}^* = (-1)^{m_{\gamma}} \psi_{\gamma^*}$$

2.17

$$\chi_{\gamma}^* = (-1)^{m_{\gamma}} \chi_{\gamma^*}$$

where  $\gamma^* = n_{\gamma} - i m_{\gamma}$ . This result is obtained by taking the complex conjugate of equations (2.14).

Other derived parameters of the flow can be represented simply in terms of the spectral amplitudes.

The mean zonal angular momentum  $\overline{M}$  ;

$$\overline{M} \equiv \frac{1}{4\pi} \int_0^{2\pi} \int_0^{\pi} (a u \sin \theta) \sin \theta d\theta d\lambda = -a^2 \left(\frac{2}{3}\right)^{\frac{1}{2}} \psi_1^0 \quad 2.18$$

the mean horizontal kinetic energy  $\overline{E}$  ;

$$\overline{E} \equiv \frac{1}{4\pi} \int_0^{2\pi} \int_0^{\pi} \frac{1}{2} (\mathbf{V} \cdot \mathbf{V}) \sin \theta d\theta d\lambda = \frac{a^2}{4} \sum_{\gamma} c_{\gamma} (\psi_{\gamma} \psi_{\gamma}^* + \chi_{\gamma} \chi_{\gamma}^*) \quad 2.19$$

the mean square vorticity  $\overline{\zeta^2}$  ;

$$\overline{\zeta^2} \equiv \frac{1}{4\pi} \int_0^{2\pi} \int_0^{\pi} \zeta^2 \sin \theta d\theta d\lambda = \frac{1}{2} \sum_{\gamma} c_{\gamma}^2 \psi_{\gamma} \psi_{\gamma}^* \quad 2.20$$

In non-divergent barotropic flow all of these quantities are conserved (Platzman 1960).

Integration of equation (2.7) with respect to pressure from  $p = 0$  to  $p$  with the boundary condition that  $\omega = 0$  at  $p = 0$  results in,

$$\omega = - \int_0^p \nabla^2 \chi dp \quad 2.21$$

so that substituting  $\nabla^2 \chi$  from 2.16, 2.21 becomes,

$$\omega = \sum_{\gamma} c_{\gamma} \overline{\chi}_{\gamma} Y_{\gamma} \quad 2.22$$

where the bar denotes integration from  $\rho=0$  to  $\rho$ .

The process of transformation consists of expressing the quantity in terms of its spectral amplitudes; multiplying by  $(2\pi)^{-1} Y_\gamma^* \sin\theta d\theta d\lambda$  and integrating over a sphere.

Hence,

$$A \equiv \frac{\partial}{\partial t} (\nabla^2 \psi) = - \sum_{\alpha} C_{\alpha} \frac{d\psi_{\alpha}}{dt} Y_{\alpha}$$

Transforming, we obtain

$$A_{\gamma} = \frac{1}{2\pi} \int_0^{2\pi} \int_0^{\pi} A Y_{\gamma}^* \sin\theta d\theta d\lambda = -\frac{1}{2\pi} \sum_{\alpha} C_{\alpha} \frac{d\psi_{\alpha}}{dt} \int_0^{2\pi} \int_0^{\pi} Y_{\alpha} Y_{\gamma}^* \sin\theta d\theta d\lambda$$

which, in view of the orthogonal relations 2.12, becomes

$$A_{\gamma} = -C_{\gamma} \frac{d\psi_{\gamma}}{dt} \quad 2.23^*$$

$$E \equiv -kx \nabla \psi \cdot \nabla f = \left( -\frac{1}{a \sin\theta} \frac{\partial \psi}{\partial \lambda} \right) \left( -\frac{1}{a} \frac{\partial f}{\partial \theta} \right) = -\frac{1}{a^2} 2\Omega \frac{\partial \psi}{\partial \lambda}$$

Substituting for  $\psi$  in the above expression, we obtain

$$E = -2\Omega \frac{\partial}{\partial \lambda} \sum_{\alpha} \psi_{\alpha} P_{\alpha} e^{im_{\alpha}\lambda} = -i2\Omega \sum_{\alpha} m_{\alpha} \psi_{\alpha} Y_{\alpha}$$

Transforming as before, we have

---

\* See footnote p. 10

$$E_Y = -i 2 \Omega m_Y \Psi_Y$$

2. 24

$$F \equiv -\nabla \chi \cdot \nabla f = -\left(-\frac{1}{a} \frac{\partial \chi}{\partial \theta}\right) \left(-\frac{1}{a} \frac{\partial f}{\partial \theta}\right) = \frac{2\Omega}{a^2} \sin \theta \frac{\partial \chi}{\partial \theta}$$

Substitution for  $\chi$  yields

$$F = 2\Omega \sin \theta \frac{\partial}{\partial \theta} \sum_{\alpha} \chi_{\alpha} Y_{\alpha} = 2\Omega \sum_{\alpha} \chi_{\alpha} \sin \theta \frac{dP_{\alpha}^{m_Y}}{d\theta} e^{i m_Y \lambda}$$

which, under transformation, becomes

$$F_Y = 2\Omega \sum_{n_{\alpha}} \chi_{n_{\alpha}}^{m_Y} \left[ \int_0^{\pi} P_{n_Y}^{m_Y} \sin \theta \frac{dP_{n_{\alpha}}^{m_Y}}{d\theta} \sin \theta d\theta \right]$$

As shown in Appendix B, the integral in the square brackets is non-zero only when  $n_{\alpha} = n_Y \pm 1$ .

Thus,

$$F_Y = 2\Omega \left( (n_Y - 1) \epsilon_Y \chi_{Y-1} - (n_Y + 2) \epsilon_{Y+1} \chi_{Y+1} \right)$$

2. 25

where  $\epsilon_Y = \left[ \frac{n_Y^2 - m_Y^2}{4n_Y^2 - 1} \right]^{\frac{1}{2}}$

$$\begin{aligned}
 N &\equiv -f \nabla^2 \chi = (-2\Omega \cos \theta) \left( -\sum_{\alpha} C_{\alpha} \chi_{\alpha} Y_{\alpha} \right) \\
 &= 2\Omega \sum_{\alpha} C_{\alpha} \chi_{\alpha} \cos \theta P_{\alpha} e^{i m_{\alpha} \lambda}
 \end{aligned}$$

Transforming, we have

$$N_{\gamma} = 2\Omega \sum_{n_{\alpha}} C_{\alpha} \chi_{n_{\alpha}}^{m_{\gamma}} \left[ \int_0^{\pi} P_{n_{\gamma}}^{m_{\gamma}} \cos \theta P_{n_{\alpha}}^{m_{\gamma}} \sin \theta d\theta \right]$$

As in the previous term the integral in the square brackets reduces to two terms (see Appendix B),

$$N_{\gamma} = 2\Omega \left( n_{\gamma} (n_{\gamma} - 1) \epsilon_{\gamma} \chi_{\gamma-1} + (n_{\gamma} + 1) (n_{\gamma} + 2) \epsilon_{\gamma+1} \chi_{\gamma+1} \right) \quad 2.26$$

The above components constitute what may be considered as linear terms, in the sense that no products of amplitudes are involved.

$$B \equiv -k \times \nabla \psi \cdot \nabla \zeta = -\frac{1}{a^2 \sin \theta} \left( \frac{\partial \psi}{\partial \theta} \frac{\partial}{\partial \lambda} - \frac{\partial \psi}{\partial \lambda} \frac{\partial}{\partial \theta} \right) \zeta$$

Substituting the expansions for  $\psi$  and  $\zeta$  we have

$$B = -\frac{i}{\sin \theta} \sum_{\alpha} \sum_{\beta} C_{\beta} \psi_{\alpha} \psi_{\beta} \left( m_{\alpha} P_{\alpha} \frac{dP_{\beta}}{d\theta} - m_{\beta} P_{\beta} \frac{dP_{\alpha}}{d\theta} \right) e^{i(m_{\alpha} + m_{\beta})\lambda}$$

By renaming dummies  $\alpha$ ,  $\beta$ ; adding and dividing by two, the following symmetric form is obtained;

$$B = \frac{-i}{2\sin\theta} \sum_{\alpha} \sum_{\beta} \psi_{\alpha} \psi_{\beta} (c_{\beta} - c_{\alpha}) \left[ m_{\alpha} P_{\alpha} \frac{dP_{\beta}}{d\theta} - m_{\beta} P_{\beta} \frac{dP_{\alpha}}{d\theta} \right] e^{i(m_{\alpha} + m_{\beta})\lambda}$$

Transformation of the above expression leads to

$$B_{\gamma} = i \sum_{\alpha} \sum_{\beta} \psi_{\alpha} \psi_{\beta} H_{\alpha\gamma\beta} \quad 2.27$$

where  $H_{\alpha\gamma\beta} = \frac{c_{\alpha} - c_{\beta}}{2} \int_0^{\pi} P_{\gamma} \left( m_{\alpha} P_{\alpha} \frac{dP_{\beta}}{d\theta} - m_{\beta} P_{\beta} \frac{dP_{\alpha}}{d\theta} \right) d\theta$ ;  $m_{\alpha} + m_{\beta} = m_{\gamma}$

$$H_{\alpha\gamma\beta} = 0 \quad \text{otherwise.}$$

In 2.27 the summation takes place over all possible values of  $\alpha$ ,  $\beta$ . The  $H_{\alpha\gamma\beta}$  for any particular component measures the "effectiveness" of an interaction of components  $\psi_{\alpha}$ ,  $\psi_{\beta}$  in producing a change in a third component  $\psi_{\gamma}$ , through non-divergent advection of vorticity. This transformation was first performed by Silberman (1954) and later extended by Platzman (1960). Silberman has presented analytic formulae for the evaluation of  $H_{\alpha\gamma\beta}$  (see Appendix B).

Application of the same technique as above results in

$$C_{\gamma} \equiv [-\nabla \chi \cdot \nabla \mathcal{S}]_{\gamma} = - \sum_{\alpha} \sum_{\beta} \chi_{\alpha} \psi_{\beta} I_{\alpha\gamma\beta} \quad 2.28$$

where 
$$I_{\alpha\gamma\beta} = c_\beta \int_0^\pi P_\gamma \left( \frac{m_\alpha m_\beta P_\alpha P_\beta}{\sin^2 \theta} - \frac{dP_\alpha}{d\theta} \frac{dP_\beta}{d\theta} \right) \sin \theta d\theta; m_\alpha + m_\beta = m_\gamma$$

$$I_{\alpha\gamma\beta} = 0 \text{ otherwise}$$

and,

$$D_\gamma \equiv \left[ -\omega \frac{\partial \zeta}{\partial \rho} \right]_\gamma = \sum_\alpha \sum_\beta \bar{\chi}_\alpha \frac{\partial \psi_\beta}{\partial \rho} J_{\alpha\gamma\beta} \quad 2.29$$

where 
$$J_{\alpha\gamma\beta} = c_\alpha c_\beta \int_0^\pi P_\alpha P_\gamma P_\beta \sin \theta d\theta; m_\alpha + m_\beta = m_\gamma$$

$$J_{\alpha\gamma\beta} = 0 \text{ otherwise;}$$

and as before, the bar denotes integration from  $\rho = 0$  to  $\rho$ .

Both  $I_{\alpha\gamma\beta}$  and  $J_{\alpha\gamma\beta}$  are subject to calculation using analytic formulae and their evaluation is presented in Appendix B.

Kubota (1960) first considered these transformations. His evaluation of  $I_{\alpha\gamma\beta}$  is somewhat different however.

Thus far, three different forms of interaction matrices have appeared, i. e.  $H_{\alpha\gamma\beta}$ ,  $I_{\alpha\gamma\beta}$ ,  $J_{\alpha\gamma\beta}$ . These three, it will be seen, are sufficient to describe all of the terms in the dynamic equations. These three interaction matrices, in fact, represent the geometrical configuration of the three types of products in the equations, i. e. the scalar triple product, the scalar product, and the ordinary product. So that it is evident that  $G \equiv -(\nabla^2 \psi)(\nabla^2 \chi)$

transforms into

$$G_Y = - \sum_{\alpha} \sum_{\beta} \chi_{\alpha} \psi_{\beta} J_{\alpha\gamma\beta} \quad 2.30$$

$$R = -k \cdot \nabla \omega \times \nabla \frac{\partial \chi}{\partial \rho} = \frac{1}{a^2 \sin \theta} \left( \frac{\partial \omega}{\partial \lambda} \frac{\partial}{\partial \theta} - \frac{\partial \omega}{\partial \theta} \frac{\partial}{\partial \lambda} \right) \frac{\partial \chi}{\partial \rho}$$

Substituting for  $\omega, \chi$  we obtain

$$R = \frac{i}{\sin \theta} \sum_{\alpha} \sum_{\beta} c_{\alpha} \bar{\chi}_{\alpha} \frac{\partial \chi_{\beta}}{\partial \rho} \left( m_{\alpha} P_{\alpha} \frac{dP_{\beta}}{d\theta} - m_{\beta} P_{\beta} \frac{dP_{\alpha}}{d\theta} \right) e^{i(m_{\alpha} + m_{\beta})\lambda}$$

which through transformation becomes,

$$R_Y = i \sum_{\alpha} \sum_{\beta} c_{\alpha} \bar{\chi}_{\alpha} \frac{\partial \chi_{\beta}}{\partial \rho} L_{\alpha\gamma\beta} \quad 2.31$$

where  $L_{\alpha\gamma\beta} = \int_0^{\pi} P_{\gamma} \left( m_{\alpha} P_{\alpha} \frac{dP_{\beta}}{d\theta} - m_{\beta} P_{\beta} \frac{dP_{\alpha}}{d\theta} \right) d\theta$  ;  $m_{\alpha} + m_{\beta} = m_{\gamma}$

$$L_{\alpha\gamma\beta} = 0 \quad \text{otherwise}$$

This is not a new interaction matrix because in fact

$$H_{\alpha\gamma\beta} = \frac{c_{\alpha} - c_{\beta}}{2} L_{\alpha\gamma\beta}$$

$$Q = -\nabla\omega \cdot \nabla \frac{\partial\psi}{\partial p} = -\frac{1}{a^2} \left( \frac{1}{\sin^2\theta} \frac{\partial\omega}{\partial\lambda} \frac{\partial}{\partial\lambda} + \frac{\partial\omega}{\partial\theta} \frac{\partial}{\partial\theta} \right) \frac{\partial\psi}{\partial p}$$

substituting and transforming, we obtain

$$Q_\gamma = \sum_\alpha \sum_\beta \bar{\chi}_\alpha \frac{\partial\psi_\beta}{\partial p} I_{\beta\gamma\alpha} \quad 2.32$$

It has now been shown how each of the terms in the vorticity equation can be transformed into the spectral domain. The non-linear terms are represented as infinite sums of selected spectral amplitudes multiplied by an element of an interaction matrix. All of these interaction matrices are subject to calculation using analytical formulae. The remainder of the dynamic equations may be transformed into the spectral domain using the same techniques as above with the following expansions for the geopotential and potential temperature,

$$\Phi = a^2 \sum_\gamma \bar{\Phi}_\gamma \Upsilon_\gamma$$

2.33

$$\Theta = \sum_\gamma \bar{\Theta}_\gamma \Upsilon_\gamma$$

The only term in these transformations that requires further analysis is the Laplacian of kinetic energy. In equation 2.6  $\nabla^2 \left( \frac{1}{2} \mathbf{V} \cdot \mathbf{V} \right)$  has been split into three parts which will be considered separately.

$$\frac{1}{2} \nabla \cdot \nabla = \frac{1}{2} (u_\psi^2 + v_\psi^2) + \frac{1}{2} (u_x^2 + v_x^2) + u_\psi u_x + v_\psi v_x$$

or written in terms of  $\psi, \chi$  using 2.4,

$$\frac{1}{2} \nabla \cdot \nabla = \frac{1}{2} \{ \psi \} + \frac{1}{2} \{ \chi \} + \frac{1}{a^2 \sin \theta} \left[ \frac{\partial \chi}{\partial \lambda} \frac{\partial \psi}{\partial \theta} - \frac{\partial \chi}{\partial \theta} \frac{\partial \psi}{\partial \lambda} \right]$$

$$\text{where } \{ \} = \frac{1}{a^2} \left[ \frac{1}{\sin^2 \theta} \left( \frac{\partial}{\partial \lambda} \right)^2 + \left( \frac{\partial}{\partial \theta} \right)^2 \right]$$

Now suppose  $\{ \chi \} = \sum_Y \{ \chi \}_Y Y_Y$  ; then it follows that

$$\nabla^2 \{ \chi \} = - \sum_Y \frac{C_Y}{a^2} \{ \chi \}_Y Y_Y \quad 2.34$$

now, substitution for  $\chi$  from 2.14 gives

$$\{ \chi \} = -a^2 \sum_{\alpha} \sum_{\beta} \chi_{\alpha} \chi_{\beta} \left( \frac{m_{\alpha} m_{\beta} P_{\alpha} P_{\beta}}{\sin^2 \theta} - \frac{dP_{\alpha}}{d\theta} \frac{dP_{\beta}}{d\theta} \right) e^{i(m_{\alpha} + m_{\beta})\lambda}$$

Transforming, we obtain

$$\{ \chi \}_Y = -a^2 \sum_{\alpha} \sum_{\beta} \chi_{\alpha} \chi_{\beta} \frac{I_{\alpha \gamma \beta}}{C_{\beta}}$$

Substitution of the above expression into 2.34 leads to

$$\left[ \nabla^2 \{ \chi \} \right]_{\gamma} = \sum_{\alpha} \sum_{\beta} \frac{c_{\gamma}}{c_{\beta}} \chi_{\alpha} \chi_{\beta} I_{\alpha \gamma \beta} \quad 2.35$$

Similarly, we obtain

$$\left[ \nabla^2 \{ \psi \} \right]_{\gamma} = \sum_{\alpha} \sum_{\beta} \frac{c_{\gamma}}{c_{\beta}} \psi_{\alpha} \psi_{\beta} I_{\alpha \gamma \beta} \quad 2.36$$

Using similar arguments as above, the cross terms

$$\eta = \frac{1}{a^2 \sin \theta} \left[ \frac{\partial \chi}{\partial \lambda} \frac{\partial \psi}{\partial \theta} - \frac{\partial \chi}{\partial \theta} \frac{\partial \psi}{\partial \lambda} \right]$$

may be expressed as

$$\left[ \nabla^2 \eta \right]_{\gamma} = i \sum_{\alpha} \sum_{\beta} c_{\gamma} \chi_{\alpha} \psi_{\beta} L_{\alpha \gamma \beta} \quad 2.37$$

or finally, we have

$$\left[ -\nabla^2 \left( \frac{1}{2} (u_{\psi}^2 + v_{\psi}^2) \right) \right]_{\gamma} = \frac{1}{2} c_{\gamma} \sum_{\alpha} \sum_{\beta} \psi_{\alpha} \psi_{\beta} \frac{I_{\alpha \gamma \beta}}{c_{\beta}} \quad 2.38$$

$$\left[ -\nabla^2 \left( \frac{1}{2} (u_{\chi}^2 + v_{\chi}^2) \right) \right]_{\gamma} = \frac{1}{2} c_{\gamma} \sum_{\alpha} \sum_{\beta} \chi_{\alpha} \chi_{\beta} \frac{I_{\alpha \gamma \beta}}{c_{\beta}} \quad 2.39$$

$$\left[ -\nabla^2 (u_{\psi} u_{\chi} + v_{\psi} v_{\chi}) \right]_{\gamma} = -i c_{\gamma} \sum_{\alpha} \sum_{\beta} \chi_{\alpha} \psi_{\beta} L_{\alpha \gamma \beta} \quad 2.40$$

TABLE 2.1

SPECTRAL FORM OF THE VORTICITY EQUATION		
TERM	SPECTRAL REPRESENTATION	CLASS
$\frac{\partial \zeta}{\partial t}$	$-c_{\gamma} \frac{d\psi_{\gamma}}{dt}$	-
$-k \times \nabla \psi \cdot \nabla \zeta$	$i \sum_{\alpha} \sum_{\beta} \psi_{\alpha} \psi_{\beta} H_{\alpha \gamma \beta}$	2, 2, 2
$-\nabla \chi \cdot \nabla \zeta$	$-\sum_{\alpha} \sum_{\beta} \chi_{\alpha} \psi_{\beta} I_{\alpha \gamma \beta}$	2, 2, 3
$-\omega \frac{\partial \zeta}{\partial p}$	$\sum_{\alpha} \sum_{\beta} \bar{\chi}_{\alpha} \frac{\partial \psi_{\beta}}{\partial p} J_{\alpha \gamma \beta}$	2, 2, 3
$-k \times \nabla \psi \cdot \nabla f$	$-i 2 \Omega m_{\gamma} \psi_{\gamma}$	2, 2
$-\nabla \chi \cdot \nabla f$	$2 \Omega \left[ (n_{\gamma}-1) \epsilon_{\gamma} \chi_{\gamma-1} - (n_{\gamma}+2) \epsilon_{\gamma+1} \chi_{\gamma+1} \right]$	2, 3
$-\zeta D$	$-\sum_{\alpha} \sum_{\beta} \chi_{\alpha} \psi_{\beta} J_{\alpha \gamma \beta}$	2, 2, 3
$-f D$	$2 \Omega \left[ n_{\gamma} (n_{\gamma}-1) \epsilon_{\gamma} \chi_{\gamma-1} + (n_{\gamma}+1) (n_{\gamma}+2) \epsilon_{\gamma+1} \chi_{\gamma+1} \right]$	2, 3
$-k \cdot \nabla \omega \times \nabla \frac{\partial \chi}{\partial p}$	$i \sum_{\alpha} \sum_{\beta} c_{\alpha} \bar{\chi}_{\alpha} \frac{\partial \chi_{\beta}}{\partial p} L_{\alpha \gamma \beta}$	2, 3, 3
$-\nabla \omega \cdot \nabla \frac{\partial \psi}{\partial p}$	$\sum_{\alpha} \sum_{\beta} \bar{\chi}_{\alpha} \frac{\partial \psi_{\beta}}{\partial p} I_{\beta \gamma \alpha}$	2, 2, 3

TABLE 2.2

SPECTRAL FORM OF THE DIVERGENCE EQUATION		
TERM	SPECTRAL REPRESENTATION	CLASS
$\frac{\partial D}{\partial t}$	$-c_\gamma \frac{dX_\gamma}{dt}$	-
$-\nabla^2 \left( \frac{V_\psi \cdot V_\psi}{2} \right)$	$\frac{1}{2} c_\gamma \sum_\alpha \sum_\beta \psi_\alpha \psi_\beta \frac{I_{\alpha\gamma\beta}}{c_\beta}$	2, 2, 3
$-\nabla^2 \left( \frac{V_x \cdot V_x}{2} \right)$	$\frac{1}{2} c_\gamma \sum_\alpha \sum_\beta \chi_\alpha \chi_\beta \frac{I_{\alpha\gamma\beta}}{c_\beta}$	3, 3, 3
$-\nabla^2 (V_\psi \cdot V_x)$	$-i c_\gamma \sum_\alpha \sum_\beta \chi_\alpha \psi_\beta L_{\alpha\gamma\beta}$	2, 3, 3
$\nabla \psi \cdot \nabla \zeta$	$\sum_\alpha \sum_\beta \psi_\alpha \psi_\beta I_{\alpha\gamma\beta}$	2, 2, 3
$-\omega \frac{\partial D}{\partial p}$	$\sum_\alpha \sum_\beta \bar{\chi}_\alpha \frac{\partial \chi_\beta}{\partial p} J_{\alpha\gamma\beta}$	3, 3, 3
$-kx \nabla x \cdot \nabla f$	$-i 2\Omega m_\gamma \chi_\gamma$	3, 3
$\nabla \psi \cdot \nabla f$	$-2\Omega \left[ (n_\gamma - 1) \epsilon_\gamma \psi_{\gamma-1} - (n_\gamma + 2) \epsilon_{\gamma+1} \psi_{\gamma+1} \right]$	2, 3
$\zeta^2$	$\sum_\alpha \sum_\beta \psi_\alpha \psi_\beta J_{\alpha\gamma\beta}$	2, 2, 3
$f\zeta$	$-2\Omega \left[ n_\gamma (n_\gamma - 1) \epsilon_\gamma \psi_{\gamma-1} + (n_\gamma + 1)(n_\gamma + 2) \epsilon_{\gamma+1} \psi_{\gamma+1} \right]$	2, 3
$k \cdot \nabla \omega \times \nabla \frac{\partial \psi}{\partial p}$	$-i \sum_\alpha \sum_\beta c_\alpha \bar{\chi}_\alpha \frac{\partial \psi_\beta}{\partial p} L_{\alpha\gamma\beta}$	2, 3, 3
$-\nabla \omega \cdot \nabla \frac{\partial x}{\partial p}$	$\sum_\alpha \sum_\beta \bar{\chi}_\alpha \frac{\partial \chi_\beta}{\partial p} I_{\beta\gamma\alpha}$	3, 3, 3
$-\nabla^2 \Phi$	$c_\gamma \Phi_\gamma$	1, 3

TABLE 2.3

SPECTRAL FORM OF THE THERMODYNAMIC EQUATION		
TERM	SPECTRAL REPRESENTATION	CLASS
$\frac{\partial \theta}{\partial t}$	$\frac{d\theta_\gamma}{dt}$	-
$-k \chi \nabla \psi \cdot \nabla \theta$	$i \sum_{\alpha} \sum_{\beta} \psi_{\alpha} \theta_{\beta} L_{\alpha\gamma\beta}$	2,3
$-\nabla \chi \cdot \nabla \theta$	$\sum_{\alpha} \sum_{\beta} \chi_{\alpha} \theta_{\beta} \frac{I_{\alpha\gamma\beta}}{c_{\beta}}$	1,3
$-\omega \frac{\partial \theta}{\partial p}$	$-\sum_{\alpha} \sum_{\beta} \bar{\chi}_{\alpha} \frac{\partial \theta_{\beta}}{\partial p} \frac{J_{\alpha\gamma\beta}}{c_{\beta}}$	1,3

SPECTRAL FORM OF THE CONTINUITY EQUATION		
TERM	SPECTRAL REPRESENTATION	CLASS
$D$	$-c_{\gamma} \chi_{\gamma}$	-
$-\frac{\partial \omega}{\partial p}$	$-\frac{\partial \omega_{\gamma}}{\partial p}$	-

SPECTRAL FORM OF THE HYDROSTATIC EQUATION		
TERM	SPECTRAL REPRESENTATION	CLASS
$\frac{\partial \Phi}{\partial p}$	$a^2 \frac{\partial \Phi_{\gamma}}{\partial p}$	-
$-\frac{R p^{k-1}}{\rho_0^k} \theta$	$-\frac{R p^{k-1}}{\rho_0^k} \theta_{\gamma}$	-

In Tables 2.1, 2.2, 2.3 the transformations of the complete set of dynamical equation as well as the class of each term according to Lorenz (1960b) are presented.

The tables are to be read as follows: the indicated equation is formed by equating the first line of the table to the sum of the remaining lines. Neither friction nor heating have been considered, but these may be added to the right hand sides of the equations in their spectral forms.

#### The Energy Equations

In this section the energy equations in spectral form are studied with the view of determining under what truncation conditions the energy conservation theorem holds. Following Lorenz (1960b) total potential energy  $P + I$  is defined as

$$P + I = c_p p_0^{-k} \int p^k \Theta dM \quad 2.41$$

where  $dM$  indicates the integration performed over the entire mass of the atmosphere. Separation of the integration over mass into an integration over the surface of a sphere plus an integration with respect to pressure, and substitution for  $\Theta$  in terms of its spectral amplitudes gives

$$\begin{aligned}
 P+I &= \frac{c_p}{g} p_0^{-k} \int_0^{\infty} \int_0^{2\pi} \int_0^{\pi} p^k (\sum_{\gamma} \Theta_{\gamma} \Upsilon_{\gamma}) a^2 \sin \theta d\theta d\lambda dp \\
 &= \frac{c_p}{g} p_0^{-k} \frac{\sigma}{\sqrt{2}} \int_p^{\infty} p^k \Theta_0^{\circ} dp
 \end{aligned} \tag{2.42}$$

where  $\sigma = 4\pi a^2$

Then the time rate of change of  $P+I$  is given as

$$\begin{aligned}
 \frac{\partial}{\partial t} (P+I) &= \frac{c_p}{g} p_0^{-k} \frac{\sigma}{\sqrt{2}} \int_p^{\infty} p^k \frac{d\Theta_0^{\circ}}{dt} dp \\
 &= \frac{c_p}{g} p_0^{-k} \frac{\sigma}{\sqrt{2}} \int_p^{\infty} p^k \left[ i \sum_{\alpha} \sum_{\beta} \Psi_{\alpha} \Theta_{\beta} L_{\alpha 0 \beta}^{\circ} + \sum_{\alpha} \sum_{\beta} \chi_{\alpha} \Theta_{\beta} \frac{I_{\alpha 0 \beta}^{\circ}}{c_{\beta}} \right. \\
 &\quad \left. - \sum_{\alpha} \sum_{\beta} \bar{\chi}_{\alpha} \frac{\partial \Theta_{\beta}}{\partial p} \frac{J_{\alpha 0 \beta}^{\circ}}{c_{\beta}} \right] dp
 \end{aligned} \tag{2.43}$$

using the spectral form of the thermodynamic equation. Now, as can be determined from their definitions,

$$L_{\alpha 0 \beta}^{\circ} \equiv 0 \quad ; \quad \frac{I_{\alpha 0 \beta}^{\circ}}{c_{\beta}} = -\frac{c_{\alpha}}{\sqrt{2}} (-1)^{m_{\alpha}} \delta_{\beta}^{\alpha*} = \frac{J_{\alpha 0 \beta}^{\circ}}{c_{\beta}}$$

Thus it follows that 2.43 becomes

$$\frac{\partial}{\partial t} (P+I) = \frac{c_p}{2g} p_0^{-k} \sigma \int_p^{\infty} p^k \left[ -\sum_{\alpha} c_{\alpha} (-1)^{m_{\alpha}} (\chi_{\alpha} \Theta_{\alpha*} + \bar{\chi}_{\alpha} \frac{\partial \Theta_{\alpha*}}{\partial p}) \right] dp$$

Application of the condition of reality of the representation results in

$$\frac{\partial}{\partial t} (P+I) = -\frac{c_p}{2g} p_0^{-\kappa} \sigma \int_p^p \sum_{\alpha} c_{\alpha} \left( \chi_{\alpha} \Theta_{\alpha}^* + \bar{\chi}_{\alpha} \frac{\partial \Theta_{\alpha}^*}{\partial p} \right) dp \quad 2.44$$

Now  $\bar{\chi}_{\alpha} = \int_0^p \chi_{\alpha} dp$ , therefore it follows that

$$\frac{\partial}{\partial p} (\bar{\chi}_{\alpha} \Theta_{\alpha}^*) = \chi_{\alpha} \Theta_{\alpha}^* + \bar{\chi}_{\alpha} \frac{\partial \Theta_{\alpha}^*}{\partial p}$$

Substitution of this expression and integration by parts results in

$$\frac{\partial}{\partial t} (P+I) = \frac{R}{2g} p_0^{-\kappa} \sigma \int_p^p \sum_{\gamma} c_{\gamma} \bar{\chi}_{\gamma} \Theta_{\gamma}^* dp \quad 2.45$$

where  $\alpha$  has been replaced by  $\gamma$  as the dummy index.

The integrated horizontal kinetic energy,

$$K = \int \frac{1}{2} (\mathbf{V} \cdot \mathbf{V}) dM \quad 2.46$$

may be expressed as an integral over pressure of equation 2.19

$$K = \frac{\sigma a^2}{4g} \int_p^p \sum_{\gamma} c_{\gamma} (\psi_{\gamma} \psi_{\gamma}^* + \chi_{\gamma} \chi_{\gamma}^*) dp \quad 2.47$$

The problem now is the determination of  $\frac{\partial K}{\partial t}$ . As Lorenz (1960b) shows, the logical independence of the thermodynamic variables (class 1), non-divergent wind (class 2) and the divergent wind (class 3) requires that terms classified in this manner (see Tables 2.1, 2.2, 2.3) must cancel each other identically in a closed system. One can therefore consider each class separately and determine the conditions imposed on the truncation of the representation in order to achieve this result. Differentiating 2.47 with respect to time, we have

$$\frac{\partial K}{\partial t} = -\frac{\sigma a^2}{4g} \int_p^{\infty} \frac{\partial \bar{K}}{\partial t} dp \quad 2.48$$

$$\text{where } \frac{\partial \bar{K}}{\partial t} = \sum_{\gamma} \left[ \psi_{\gamma} (-c_{\gamma} \frac{d\psi_{\gamma}^*}{dt}) + \psi_{\gamma}^* (-c_{\gamma} \frac{d\psi_{\gamma}}{dt}) + \chi_{\gamma} (-c_{\gamma} \frac{d\chi_{\gamma}^*}{dt}) + \chi_{\gamma}^* (-c_{\gamma} \frac{d\chi_{\gamma}}{dt}) \right]$$

The contribution made by each class to  $\frac{\partial \bar{K}}{\partial t}$ , (which will be denoted as  $\frac{\partial \bar{K}}{\partial t} (2,2)$ ,  $\frac{\partial \bar{K}}{\partial t} (3,3)$  etc.) will now be considered.

Firstly,

$$\frac{\partial \bar{K}}{\partial t} (2,2) = \sum_{\gamma} -i2\Omega m_{\gamma} \psi_{\gamma} \psi_{\gamma}^* + i2\Omega m_{\gamma} \psi_{\gamma}^* \psi_{\gamma} = 0 \quad 2.49$$

$$\frac{\partial \bar{K}}{\partial t} (3,3) = \sum_{\gamma} -i2\Omega m_{\gamma} \chi_{\gamma} \chi_{\gamma}^* + i2\Omega m_{\gamma} \chi_{\gamma}^* \chi_{\gamma} = 0 \quad 2.50$$

The vanishing of these terms simply requires that any wave present in the truncation must be free to propagate (Platzman 1960). In the remaining discussion this condition will be implicitly assumed. Now consider class (2, 2, 2).

$$\begin{aligned} \frac{\partial \bar{K}}{\partial t}(2,2,2) &= \sum_{\gamma} \left( i \sum_{\alpha} \sum_{\beta} \psi_{\alpha} \psi_{\beta} \psi_{\gamma}^* H_{\alpha\gamma\beta} - i \sum_{\alpha} \sum_{\beta} \psi_{\alpha}^* \psi_{\beta}^* \psi_{\gamma} H_{\alpha\gamma\beta} \right) \\ &= \frac{i}{2} \sum_{\gamma} \sum_{\alpha} \sum_{\beta} \left[ (c_{\alpha} - c_{\beta}) (\psi_{\alpha} \psi_{\beta} \psi_{\gamma}^* - \psi_{\alpha}^* \psi_{\beta}^* \psi_{\gamma}) L_{\alpha\gamma\beta} \right] \end{aligned}$$

By renaming dummy indices twice, adding and dividing by three we have,

$$\begin{aligned} \frac{\partial \bar{K}}{\partial t}(2,2,2) &= \frac{i}{6} \sum_{\alpha} \sum_{\beta} \sum_{\gamma} \left[ (c_{\alpha} - c_{\beta}) (\psi_{\alpha} \psi_{\beta} \psi_{\gamma}^* - \psi_{\alpha}^* \psi_{\beta}^* \psi_{\gamma}) L_{\alpha\gamma\beta} \right. \\ &\quad \left. + (c_{\beta} - c_{\gamma}) (\psi_{\beta} \psi_{\gamma} \psi_{\alpha}^* - \psi_{\beta}^* \psi_{\gamma}^* \psi_{\alpha}) L_{\beta\alpha\gamma} + (c_{\gamma} - c_{\alpha}) (\psi_{\gamma} \psi_{\alpha} \psi_{\beta}^* - \psi_{\gamma}^* \psi_{\alpha}^* \psi_{\beta}) L_{\gamma\beta\alpha} \right] \end{aligned}$$

Since the waves have been assumed to be free to propagate, for each  $\alpha, \beta, \gamma$  in the summation there is a corresponding  $\alpha^*, \beta^*, \gamma^*$ . So that we may at any time change an index to its conjugate without affecting the summation. This process will be referred to as conjugation.

Conjugating  $\beta$  and  $\alpha$  respectively in the last two

terms of the above expression, we obtain

$$\begin{aligned} \frac{\partial \bar{K}}{\partial t}(2,2,2) = & \frac{i}{6} \sum_{\alpha} \sum_{\beta} \sum_{\gamma} \left[ (c_{\alpha} - c_{\beta})(\psi_{\alpha} \psi_{\beta} \psi_{\gamma}^* - \psi_{\alpha}^* \psi_{\beta}^* \psi_{\gamma}) L_{\alpha\gamma\beta} \right. \\ & + (c_{\beta} - c_{\gamma})(\psi_{\beta}^* \psi_{\gamma} \psi_{\alpha}^* - \psi_{\beta} \psi_{\gamma}^* \psi_{\alpha}) L_{\beta^* \alpha \gamma} (-1)^{m_{\beta}} \\ & \left. + (c_{\gamma} - c_{\alpha})(\psi_{\gamma} \psi_{\alpha}^* \psi_{\beta}^* - \psi_{\gamma}^* \psi_{\alpha} \psi_{\beta}) L_{\gamma\beta\alpha^*} (-1)^{m_{\alpha}} \right] \end{aligned}$$

Now (see Appendix B)  $L_{\beta^* \alpha \gamma} = (-1)^{m_{\beta}} L_{\beta\gamma\alpha} = (-1)^{m_{\beta}+1} L_{\alpha\gamma\beta}$

and  $L_{\gamma\beta\alpha^*} = (-1)^{m_{\alpha}} L_{\beta\gamma\alpha} = (-1)^{m_{\alpha}+1} L_{\alpha\gamma\beta}$

so that

$$\frac{\partial \bar{K}}{\partial t}(2,2,2) = \frac{i}{6} \sum_{\alpha} \sum_{\beta} \sum_{\gamma} (c_{\alpha} - c_{\beta}) Q + (c_{\beta} - c_{\gamma}) Q + (c_{\gamma} - c_{\alpha}) Q = 0 \quad 2.51$$

where  $Q = (\psi_{\alpha} \psi_{\beta} \psi_{\gamma}^* - \psi_{\alpha}^* \psi_{\beta}^* \psi_{\gamma}) L_{\alpha\gamma\beta}$

This form of energy term illustrates the Fjortoft blocking theorem (Fjortoft 1953). This equation also shows that if any three components can exchange energy, i. e.  $L_{\alpha\gamma\beta} \neq 0$ , then they do so in the manner of the Fjortoft theorem.

The contribution from class (2, 3) is

$$\begin{aligned} \frac{\partial \bar{K}}{\partial t}(2,3) = 2\Omega \sum_{\gamma} & \left[ (\eta_{\gamma-1}) \epsilon_{\gamma} (\chi_{\gamma-1} \psi_{\gamma}^* + \chi_{\gamma-1}^* \psi_{\gamma}) - (\eta_{\gamma+2}) \epsilon_{\gamma+1} (\chi_{\gamma+1} \psi_{\gamma}^* \right. \\ & + \chi_{\gamma+1}^* \psi_{\gamma}) + \eta_{\gamma} (\eta_{\gamma}-1) \epsilon_{\gamma} (\chi_{\gamma-1} \psi_{\gamma}^* + \chi_{\gamma-1}^* \psi_{\gamma}) + (\eta_{\gamma}+1)(\eta_{\gamma}+2) \epsilon_{\gamma+1} (\chi_{\gamma+1} \psi_{\gamma}^* \\ & + \chi_{\gamma+1}^* \psi_{\gamma}) - (\eta_{\gamma}-1) \epsilon_{\gamma} (\psi_{\gamma-1} \chi_{\gamma}^* + \psi_{\gamma-1}^* \chi_{\gamma}) + (\eta_{\gamma}+2) \epsilon_{\gamma+1} (\psi_{\gamma+1} \chi_{\gamma}^* + \psi_{\gamma+1}^* \chi_{\gamma}) \\ & \left. - \eta_{\gamma} (\eta_{\gamma}-1) \epsilon_{\gamma} (\psi_{\gamma-1} \chi_{\gamma}^* + \psi_{\gamma-1}^* \chi_{\gamma}) - (\eta_{\gamma}+1)(\eta_{\gamma}+2) \epsilon_{\gamma+1} (\psi_{\gamma+1} \chi_{\gamma}^* + \psi_{\gamma+1}^* \chi_{\gamma}) \right] \end{aligned}$$

if we let  $\bar{F}_{1,\gamma} = \eta_{\gamma} (\eta_{\gamma}+2) \epsilon_{\gamma+1} [\chi_{\gamma+1}^* \psi_{\gamma} + \chi_{\gamma+1} \psi_{\gamma}^*]$

$\bar{F}_{2,\gamma} = \eta_{\gamma} (\eta_{\gamma}+2) \epsilon_{\gamma+1} [\psi_{\gamma+1}^* \chi_{\gamma} + \psi_{\gamma+1} \chi_{\gamma}^*]$

and since  $\eta_{\gamma-1} = \eta_{\gamma} - 1$  we have

$$\frac{\partial \bar{K}}{\partial t}(2,3) = 2\Omega \sum_{\gamma} \left[ (\bar{F}_{1,\gamma} - \bar{F}_{1,\gamma-1}) - (\bar{F}_{2,\gamma} - \bar{F}_{2,\gamma-1}) \right]$$

For a summation to infinity, all terms except the first cancel in pairs so that since  $\eta_0 = 0$

$$\frac{\partial \bar{K}}{\partial t}(2,3) = 2\Omega (\bar{F}_{2,0} - \bar{F}_{1,0}) = 0$$

2.52

For a truncated system, say truncated at  $\gamma = \gamma_0$ , we have

$$\frac{\partial \bar{K}}{\partial t}(2,3) = 2\Omega \left( \bar{F}_{2,0} - \bar{F}_{1,0} + \bar{F}_{1,\gamma_0} - \bar{F}_{2,\gamma_0} \right) \quad 2.53$$

Now  $\bar{F}_{1,\gamma_0}$  and  $\bar{F}_{2,\gamma_0}$  involve components  $\psi_{\gamma_0+1}$  and  $\chi_{\gamma_0+1}$ ; so to preserve the property  $\frac{\partial \bar{K}}{\partial t}(2,3) = 0$  one concludes that any components outside the truncation must be considered to be identically zero. This implies that although the spectral form of the terms of class (2,3) may indicate a non-zero time derivative for a component outside the truncation, it must be ignored in order to preserve energy.

By similar techniques to above, the expressions for the contributions of the remaining classes of terms may be obtained.

Thus one finds that

$$\frac{\partial \bar{K}}{\partial t}(3,3,3) = \frac{1}{4} \sum_{\alpha} \sum_{\beta} \sum_{\gamma} \frac{\partial}{\partial p} \left[ \chi_{\alpha} \chi_{\beta} \bar{\chi}_{\gamma}^* + \chi_{\alpha}^* \chi_{\beta}^* \bar{\chi}_{\gamma} \right] c_{\gamma} [c_{\alpha} + c_{\beta} - c_{\gamma}] M_{\alpha\gamma\beta} \quad 2.54$$

$$\frac{\partial \bar{K}}{\partial t}(2,3,3) = i \sum_{\alpha} \sum_{\beta} \sum_{\gamma} \frac{\partial}{\partial p} \left[ \chi_{\alpha}^* \bar{\chi}_{\gamma}^* \psi_{\beta} - \chi_{\alpha} \bar{\chi}_{\gamma} \psi_{\beta}^* \right] c_{\gamma} L_{\alpha\gamma\beta} \quad 2.55$$

$$\frac{\partial \bar{K}}{\partial t}(2,2,3) = \frac{1}{4} \sum_{\alpha} \sum_{\beta} \sum_{\gamma} \frac{\partial}{\partial p} \left[ \bar{\chi}_{\gamma}^* \psi_{\alpha} \psi_{\beta} + \bar{\chi}_{\gamma} \psi_{\alpha}^* \psi_{\beta}^* \right] c_{\gamma} [c_{\alpha} + c_{\beta} - c_{\gamma}] M_{\alpha\gamma\beta} \quad 2.56$$

where  $M_{\alpha\gamma\beta} = \int_0^\pi p_\alpha p_\gamma p_\beta \sin\theta d\theta$  ;  $m_\alpha + m_\beta = m_\gamma$

Remembering equation (2.22), i.e.  $\omega_\gamma = c_\gamma \bar{\chi}_\gamma$  , it is evident that 2.54 and 2.56 represent the divergence of the vertical flux of divergent kinetic energy and non-divergent kinetic energy respectively. In a closed system, therefore, their contributions would be zero. Otherwise they represent a boundary flux of kinetic energy. Equation 2.55 also represents a vertical flux of kinetic energy and arises because the vertical motion may be correlated with the term  $\nabla_\psi \cdot \nabla_\chi$  in the expression for the kinetic energy, although  $\nabla_\psi \cdot \nabla_\chi$  does not enter the expression for the horizontal mean of kinetic energy.

The final class considered is (1,3),

$$\frac{\partial \bar{K}}{\partial t} (1,3) = \sum_\gamma c_\gamma (\bar{\Phi}_\gamma \chi_\gamma^* + \bar{\Phi}_\gamma^* \chi_\gamma) \quad 2.57$$

From the hydrostatic equation we have

$$a^2 \frac{\partial \bar{\Phi}_\gamma}{\partial p} = - \frac{R p^{\kappa-1}}{\rho_0^\kappa} \Theta_\gamma$$

so that we may derive

$$a^2 \chi_\gamma^* \bar{\Phi}_\gamma = a^2 \frac{\partial}{\partial p} (\bar{\chi}_\gamma^* \bar{\Phi}_\gamma) + \bar{\chi}_\gamma^* \frac{R p^{\kappa-1}}{\rho_0^\kappa} \Theta_\gamma$$

Hence,

$$\begin{aligned} \frac{\partial \bar{K}}{\partial t} (1,3) = & \sum_{\gamma} c_{\gamma} \left[ \frac{\partial}{\partial p} (\bar{\chi}_{\gamma} \Phi_{\gamma}^* + \bar{\chi}_{\gamma}^* \Phi_{\gamma}) \right. \\ & \left. + \frac{R p^{k-1}}{p_0^k a^2} (\bar{\chi}_{\gamma} \Theta_{\gamma}^* + \bar{\chi}_{\gamma}^* \Theta_{\gamma}) \right] \end{aligned} \quad 2.58$$

The first term represents the divergence of the vertical flux of geopotential, and the second the  $\omega, \Theta$  covariance. For a closed system integration of equation 2.58 with respect to pressure leads to

$$\int \frac{\partial \bar{K}}{\partial t} (1,3) dp = \frac{R}{p_0^k a^2} \int \sum_{\gamma} c_{\gamma} (\bar{\chi}_{\gamma} \Theta_{\gamma}^* + \bar{\chi}_{\gamma}^* \Theta_{\gamma}) p^{k-1} dp \quad 2.59$$

Substituting this expression into 2.48 we find

$$\frac{\partial K}{\partial t} = -\frac{\sigma R}{4g p_0^k} \int \sum_{\gamma} c_{\gamma} (\bar{\chi}_{\gamma} \Theta_{\gamma}^* + \bar{\chi}_{\gamma}^* \Theta_{\gamma}) p^{k-1} dp \quad 2.60$$

By conjugating  $\gamma$  in 2.60 we may obtain

$$\frac{\partial K}{\partial t} = -\frac{R}{2g} p_0^{-k} \sigma \int p^{k-1} \left( \sum_{\gamma} c_{\gamma} \bar{\chi}_{\gamma} \Theta_{\gamma}^* \right) dp \quad 2.61$$

Comparing 2.61 with 2.45 it is found that

$$\frac{\partial}{\partial t} (P + I + K) = 0 \quad 2.62$$

To summarize, if the set of equations used is an energetically consistent one (deletions of terms are made class by class), then a truncated spectral version of the equations will be energetically consistent as long as i) the waves are free to propagate and ii) any wave outside the truncation is considered to be identically zero. Continuity in pressure has been assumed, so that any division into pressure levels must modify those terms whose vanishing depends on an integration over pressure (Lorenz 1960b).

### 3. THREE-COMPONENT BAROTROPIC SYSTEMS

One of the most important properties of spectral forms of the dynamic equation is that very highly truncated versions of the equations satisfy the same conservation theorems as the full set of equations. Further, these truncated forms have the ability of representing in a very simple manner the non-linear effects inherent in the full dynamical equations. In this section we will study three truncated systems representing barotropic flow. The first model was presented by Lorenz (1960a) and considers barotropic motion on a flat earth where the Coriolis parameter is constant (the "f-plane"); the second is the extension of Lorenz's model to the " $\beta$ -plane"; the third is an equivalent three component system in spherical harmonics which accounts for the sphericity of the earth. Because of the geometry of the first two models the relevant functions to be used in the spectral representation of the dynamic equations are trigonometric functions of  $x, y$ . Where  $x$  is distance measured in an east-west direction,  $y$  is distance measured in a north-south direction.

Model 1 - Motion on the "f-plane"

The equation governing the first model is

$$\frac{\partial}{\partial t} (\nabla^2 \psi) + \mathbf{k} \times \nabla \psi \cdot \nabla (\nabla^2 \psi) = 0$$

3.1

where  $\psi$  is a stream function and  $\mathbf{k}$  is the unit vertical vector. Lorenz shows that by considering flows which are doubly-periodic in  $x$  and  $y$  equation 3.1 may be transformed into spectral form in terms of trigonometric functions of the form  $e^{i(mkx + nly)}$  where  $m, n$  are integers; and  $L_x = \frac{2\pi}{k}$ ,  $L_y = \frac{2\pi}{l}$  define the fundamental region. Further, by truncating the representation he shows that the minimum system capable of reproducing the non-linear effect of the advection term in 3.1 is given by the following equations

$$\nabla^2 \psi = A \cos ly + F \cos kx + 2G \sin ly \sin kx$$

3.2

$$\psi = \frac{-A}{l^2} \cos ly - \frac{F}{k^2} \cos kx - \frac{2G}{k^2 + l^2} \sin ly \sin kx$$

Then the harmonic tendencies equation obtained by substituting in 3.1 are

$$\frac{dA}{dt} = -\frac{1}{\alpha(\alpha^2 + 1)} FG$$

3.3

$$\frac{dF}{dt} = \frac{\alpha^4}{\alpha(\alpha^2 + 1)} AG$$

$$\frac{dG}{dt} = -\frac{\alpha^4 - 1}{2\alpha(\alpha^2 + 1)} AF$$

where  $\alpha = k/l$

The expression for the horizontally averaged kinetic

energy and square vorticity are given by

$$\bar{E} = \frac{1}{4} \left( \frac{A^2}{l^2} + \frac{F^2}{k^2} + \frac{2G^2}{k^2+l^2} \right) ; \quad \bar{V}^2 = \frac{1}{2} (A^2 + F^2 + 2G^2) \quad 3.4$$

and they are both conserved under this truncation, as may be verified by using 3.3.

The three differential equations 3.3 can be solved analytically and the solution can be expressed in terms of elliptic functions. They may also be solved by numerical integration, and it is perhaps somewhat easier to do so, especially if we wish to change parameters and initial conditions to obtain a variety of solutions.

The  $A$  in the equations 3.2, 3.3 represents a zonal flow with a sinusoidal profile,  $F$  and  $G$  being waves superimposed on the zonal flow. Let us then consider a basic zonal flow  $A = \bar{A}$  and perturbations  $F = F'$ ,  $G = G'$ . Then, linearizing equations 3.3, i. e. neglecting products of perturbation quantities, we have

$$\frac{d\bar{A}}{dt} = 0$$

$$\frac{d^2 F'}{dt^2} = - \frac{\alpha^2(\alpha^2 - 1)}{2(\alpha^2 + 1)} \bar{A}^2 F'$$

3.5

with a similar expression for  $G'$ . The above equation is of the form  $\frac{d^2 X}{dt^2} = cX$ ; and solutions to this equation are exponential

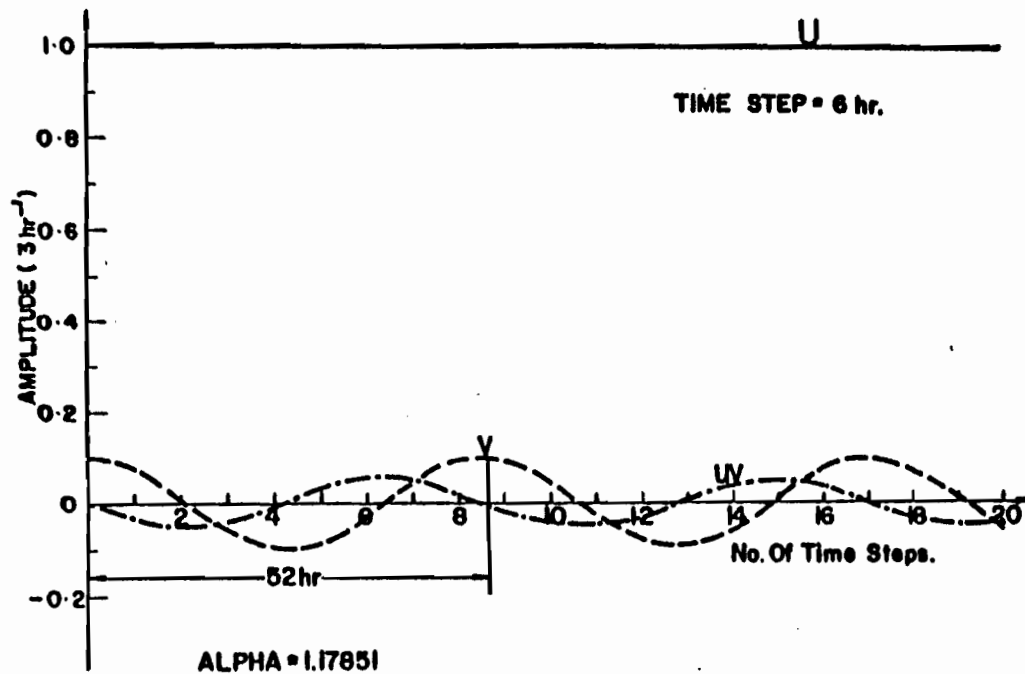


Figure 3.1a: Fluctuations of components of Model 1 for a linearly stable case.

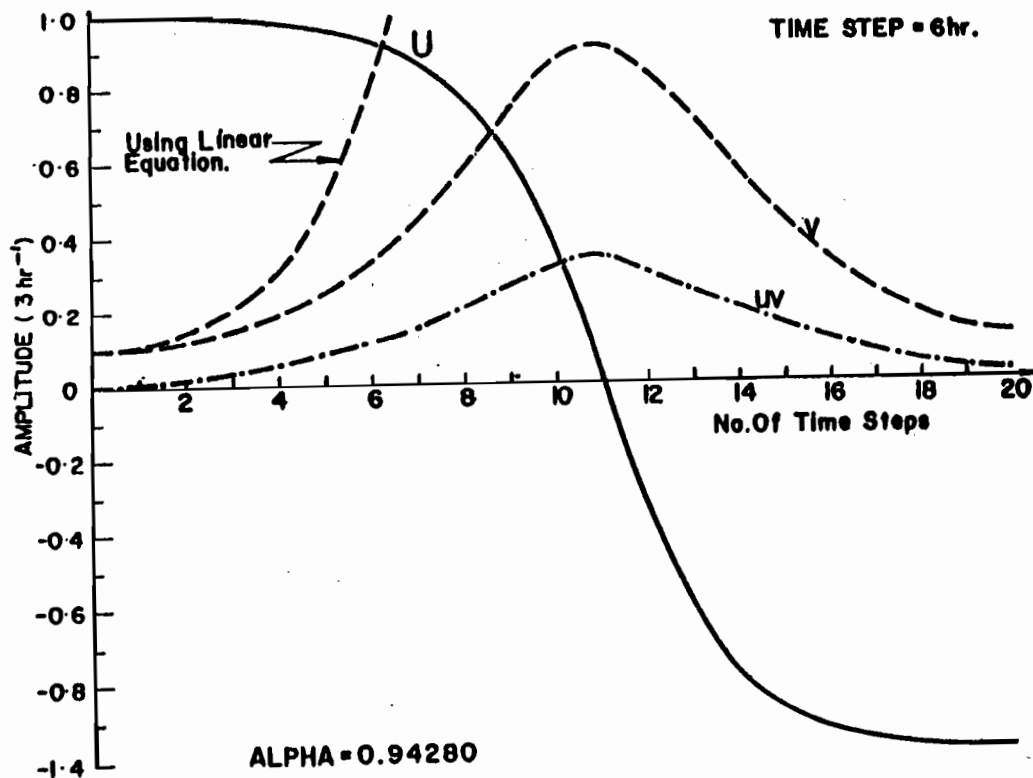


Figure 3.1b: Fluctuations of components of Model 1 for a linearly unstable case.

if  $\mathcal{L} > 0$  and sinusoidal if  $\mathcal{L} < 0$ . Thus for stable oscillations  $\alpha^2 - 1 > 0$  or since  $\alpha \geq 0$ ,  $\alpha > 1$ ; for unstable oscillations  $\alpha^2 - 1 < 0$  or  $\alpha < 1$ . At this point most analyses of the dynamic equations stop. In this system one is not so limited. One may in fact study the non-linear behaviour of the system in conjunction with at worst a simple numerical integration with respect to time.

In figures 3.1a and 3.1b we present the results of two numerical integrations of equations 3.3. Time is measured in units of 3 hours, so that if  $A = 1$ , the vorticity of the zonal flow is of the order of  $f$  in middle latitudes. The time step used was 2 units or 6 hours. The initial conditions were chosen to be perturbation conditions, that is, so that the linearized equations would be valid initially. The curves are labelled  $U$ ,  $v$ ,  $uv$  according to the wind components they imply, i. e.  $U = A$ ,  $v = F$ ,  $uv = G$ .

#### Instability of small perturbations

##### a) Stable case, $\alpha > 1$ Figure 3.1a

The perturbations ( $v$ ,  $uv$ ) initially tend to die out, feeding kinetic energy into the zonal flow. The perturbations then take back their kinetic energy, the net result being that the perturbations move with some fraction of the maximum wind.

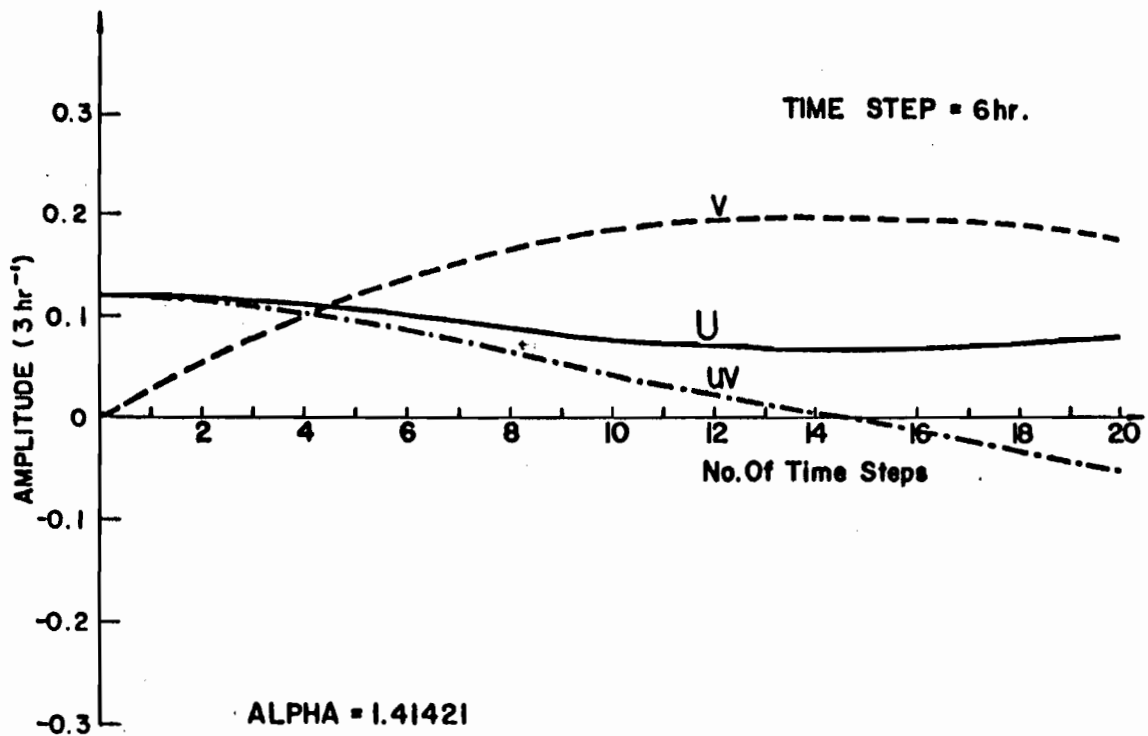


Figure 3. 2a: Fluctuations of component of Model 1 for a linearly stable case with subcritical initial perturbations.

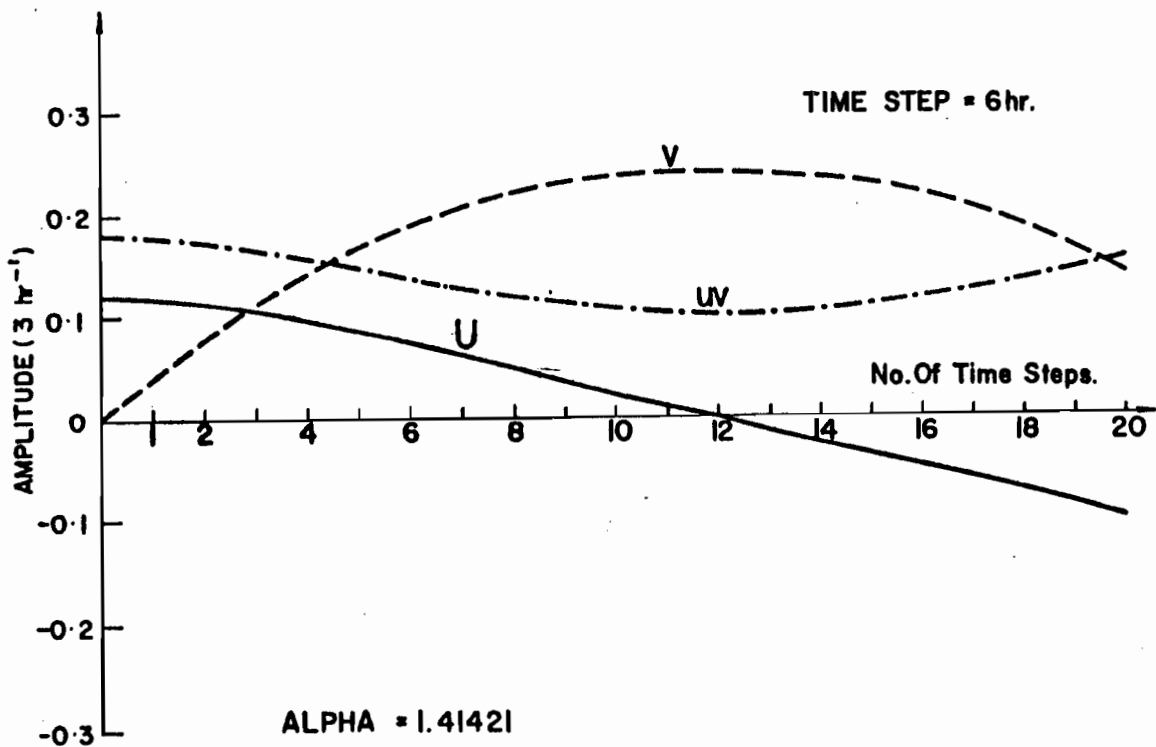


Figure 3. 2b: Fluctuations of components of Model 1 for a linearly stable case with supercritical initial perturbations.

b) Unstable case,  $\alpha < 1$  Figure 3.1b

The perturbations grow right from the start, initially growing exponentially, taking energy from the zonal current. The growth does not proceed without limit but is slowed down as the zonal flow becomes weaker, finally ceasing altogether when the zonal flow becomes zero. The perturbations then decay and feed energy back into the zonal flow which now changes sign. The process of growth and decay then repeats itself.

Another type of instability

In the linearly stable case  $A$  remained practically constant. This is because the perturbations  $F$  and  $G$  were small initially and always remained small. If, however, one starts an integration where  $F$  and  $G$  are no longer small relative to  $A$ , we have the possibility of causing large fluctuations in  $A$ . Figures 3.2a, 3.2b present the results of numerical integration of equations 3.3 for a stable case where perturbation conditions no longer apply.

In figure 3.2a the initial perturbation is not strong enough to take all the energy from the zonal flow, but does cause a large fluctuation. In figure 3.2b the initial perturbation has been increased slightly, and the zonal flow is completely depleted and then reversed in a similar manner to the linearly unstable case.

The above constitutes a minimum system of equations, as devised by Lorenz (1960a), capable of representing non-linear barotropic motion. Stability and instability here appear to involve the same process, and the particular motion and development of a perturbation, stable or unstable in a linear sense, is governed by its non-linear interaction with the basic flow. The only difference between stability and instability is in the amplitude of the fluctuations of the various modes of motion. That this amplitude of fluctuation depends on the relative magnitudes of the perturbations and zonal flow illustrates what may be called instability depending on the size of the perturbation.

#### Model 2 - Motion on the " $\beta$ -plane"

The extension of the Lorenz model to the " $\beta$ -plane" is quite straightforward. The governing equation for this system is

$$\frac{\partial}{\partial t} (\nabla^2 \psi) + \mathbf{k} \times \nabla \psi \cdot \nabla (\nabla^2 \psi) - \beta_0 \frac{\partial \psi}{\partial x} = 0 \quad 3.6$$

and the simplest possible truncation of the system is

$$\nabla^2 \psi = A \cos ly + F_1 \cos kx + F_2 \sin kx + G_1 \sin ly \cos kx + G_2 \sin ly \sin kx$$

$$\psi = -\frac{A}{l^2} \cos ly - \frac{F_1}{k^2} \cos kx - \frac{F_2}{k^2} \sin kx - \frac{G_1}{k^2 + l^2} \sin ly \cos kx - \frac{G_2}{k^2 + l^2} \sin ly \sin kx \quad 3.7$$

where  $k$ ,  $l$  have the same meaning as in the previous model.

Because of the free phase propagation generated by the Rossby term

(  $\beta_0 \frac{\partial \psi}{\partial x}$  ) both the amplitude and phase of each wave must be included.

The harmonic tendency equations resulting from the substitution of the representation 3.7 into 3.6 have the following form,

$$\frac{dA}{dt} = \frac{1}{2\alpha(1+\alpha^2)} (F_2 G_1 - F_1 G_2)$$

$$\frac{dF_1}{dt} = \frac{\alpha^3}{2(1+\alpha^2)} A G_2 + \frac{\beta_0}{k} F_2 \quad ; \quad \frac{dF_2}{dt} = -\frac{\alpha^3}{2(1+\alpha^2)} A G_1 - \frac{\beta_0}{k} F_1 \quad 3.8$$

$$\frac{dG_1}{dt} = -\frac{(1-\alpha^2)}{\alpha} A F_2 + \frac{\beta_0 \alpha^2}{k(1+\alpha^2)} G_2 \quad ; \quad \frac{dG_2}{dt} = \frac{(1-\alpha^2)}{\alpha} A F_1 - \frac{\beta_0 \alpha^2}{k(1+\alpha^2)} G_1$$

where  $\alpha = k/l$

For reference,  $A$  can be identified with the previous  $A$ ,  $F_1$  with  $F$ ,  $G_2$  with  $2G$ . If  $\beta_0 = 0$  then  $F_2$  and  $G_1$  being zero initially, would always remain so. Again,  $A$  may be identified with a zonal flow and  $F_1$ ,  $F_2$ ,  $G_1$ ,  $G_2$  with perturbations on this basic current.

The first step in the discussion of this system will be a linear analysis of the equations 3.8. As before  $A = \bar{A}$ , which is large compared to the perturbations  $F_1'$ ,  $F_2'$ ,  $G_1'$ ,  $G_2'$ .

Neglecting products of perturbations equations 3.8 become

$$\frac{d\bar{A}}{dt} = 0$$

$$\frac{dF_1'}{dt} = \frac{\alpha^3}{2(1+\alpha^2)} \bar{A} G_2' + \frac{\beta_0}{k} F_2' ; \quad \frac{dF_2'}{dt} = -\frac{\alpha^3}{2(1+\alpha^2)} \bar{A} G_1' - \frac{\beta_0}{k} F_1' \quad 3.9$$

$$\frac{dG_1'}{dt} = -\frac{(1-\alpha^2)}{\alpha} \bar{A} F_2' + \frac{\beta_0 \alpha^2}{k(1+\alpha^2)} G_2' ; \quad \frac{dG_2'}{dt} = \frac{(1-\alpha^2)}{\alpha} \bar{A} F_1' - \frac{\beta_0 \alpha^2}{k(1+\alpha^2)} G_1'$$

This set of linear equations can be solved by setting each of the unknowns equal to an amplitude multiplied by  $e^{\omega t}$ , and solving the resulting set of linear equations for the frequencies consistent with a non-trivial solution. This process gives the following frequency equation;

$$\omega^4 + B\omega^2 + C^2 = 0$$

$$B = \frac{\beta_0^2}{k^2} \left( 1 + \left( \frac{\alpha^2}{1+\alpha^2} \right)^2 \right) - \frac{\alpha^2(1-\alpha^2)}{1+\alpha^2} \bar{A}^2 \quad 3.10$$

$$C = \frac{\beta_0^2 \alpha^2}{k^2(1+\alpha^2)} + \frac{\alpha^2(1-\alpha^2)}{2(1+\alpha^2)} \bar{A}^2$$

In this analysis instability corresponds to real positive roots or complex roots with positive real parts.

The solution of the above equation can be expressed in the form

$$\omega^2 = \frac{1}{2} \left( -B \pm \sqrt{B^2 - 4C^2} \right) \quad 3.11$$

CASE I  $B > 0$   $B^2 - 4C^2 > 0$  ; roots are purely imaginary, so that the system is stable

CASE II  $B > 0$   $B^2 - 4C^2 < 0$  ; roots are complex and the system is unstable

CASE III  $B < 0$   $B^2 - 4C^2 > 0$  ; roots are purely real; this case is impossible

CASE IV  $B < 0$   $B^2 - 4C^2 < 0$  ; roots are complex and the system is unstable.

Thus the necessary and sufficient condition for stability is  $B^2 - 4C^2 \geq 0$ .

This is equivalent to  $\bar{A}^2 \leq \frac{(\beta_0/l)^2}{2\alpha^4(1-\alpha^4)}$  ;  $\alpha < 1$

if  $\alpha > 1$  then  $B^2 - 4C^2 \geq 0$  no matter what the value of  $\bar{A}$ .

The stability criterion is quadratic in  $\alpha^4$  so that for given values of the zonal flow  $\bar{A}$ , there will be upper and lower wavelength bounds on the unstable modes.

The roots of the frequency equation were found using the McGill 7044 computer and a standard library routine for the following model of the zonal current, where the amplitude remains variable.

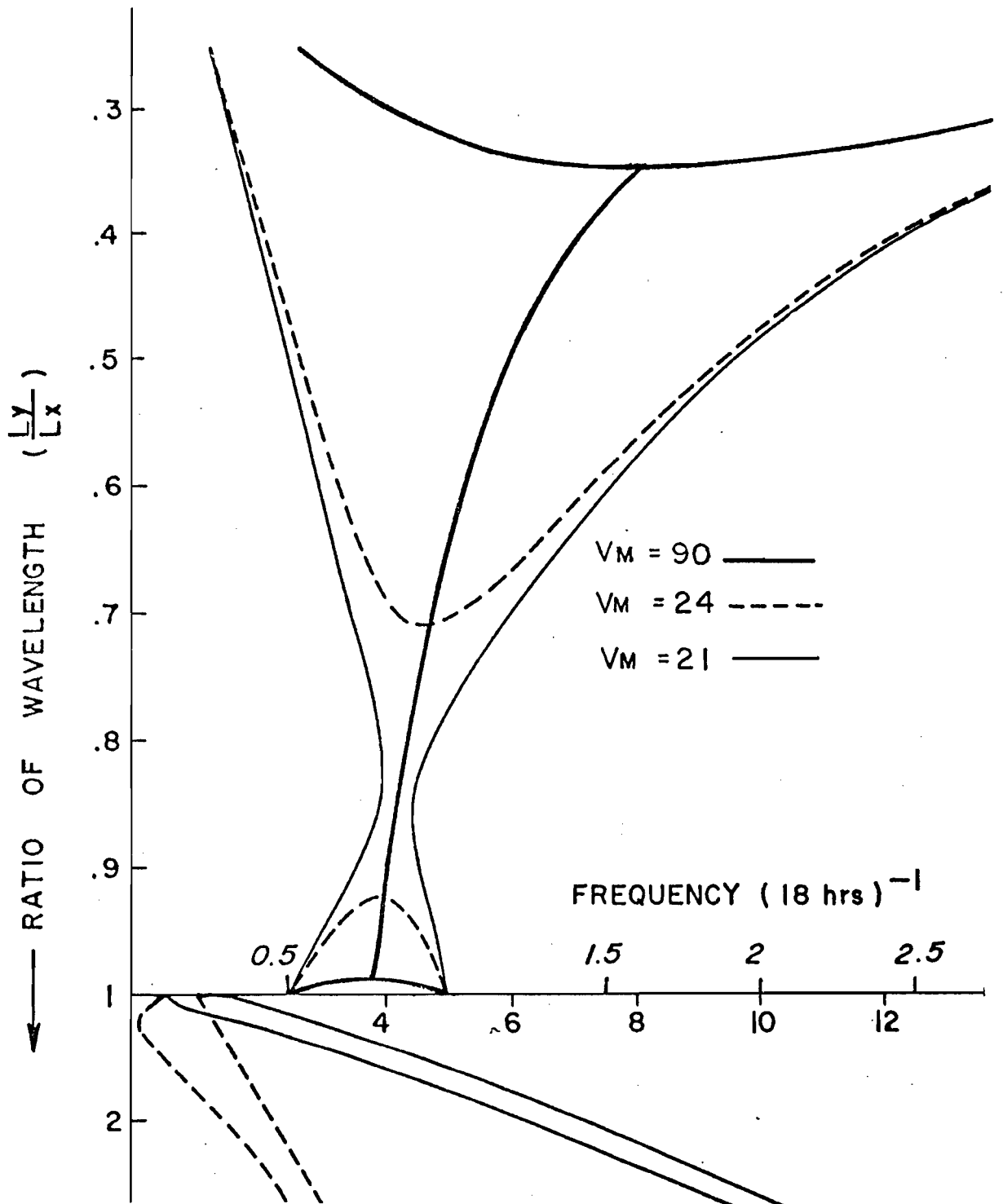


Figure 3.4: The linear phase speeds of the components of Model 2. Curves are labelled with different maximum zonal winds of 90, 24, 21 metres/sec.

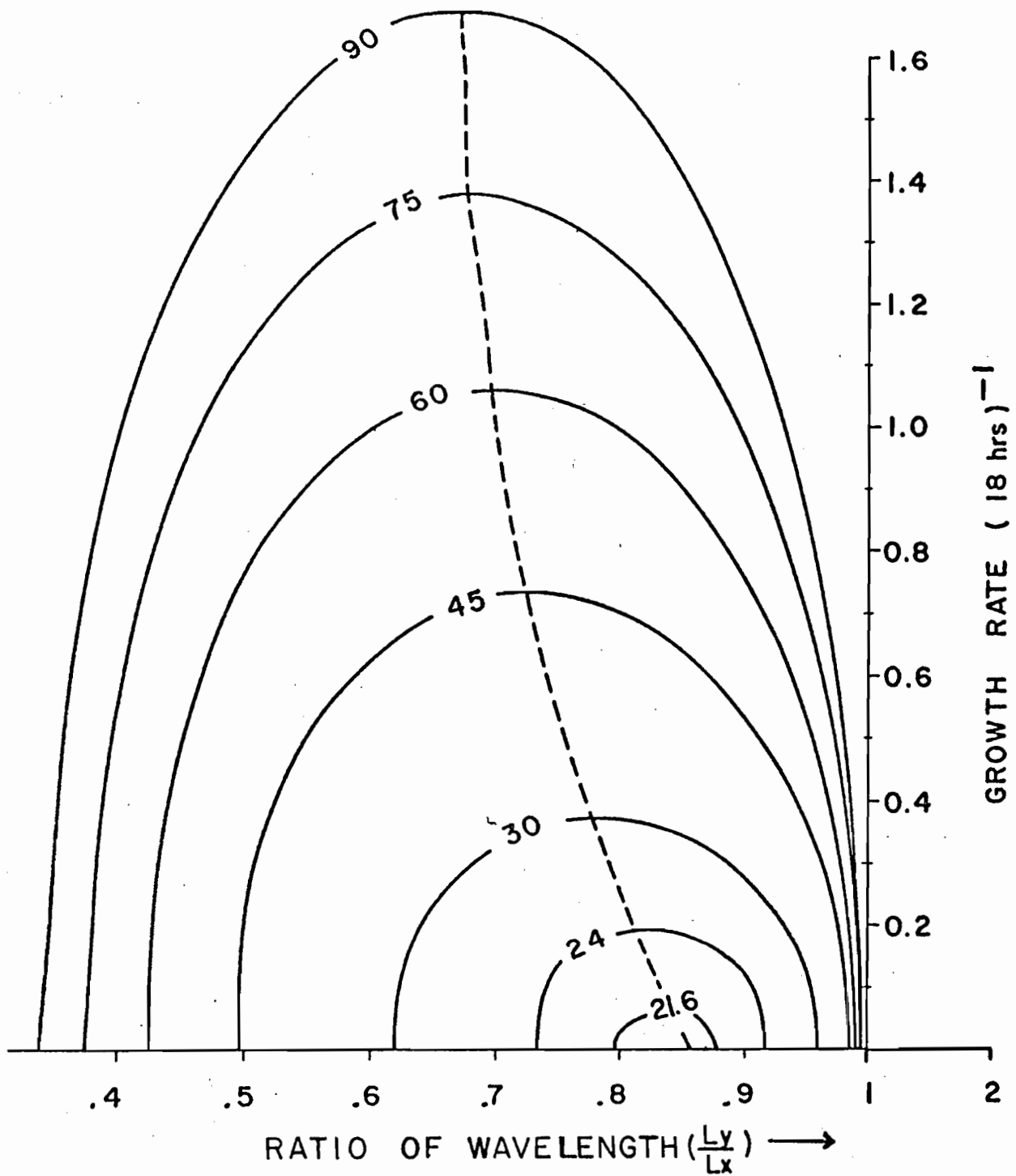
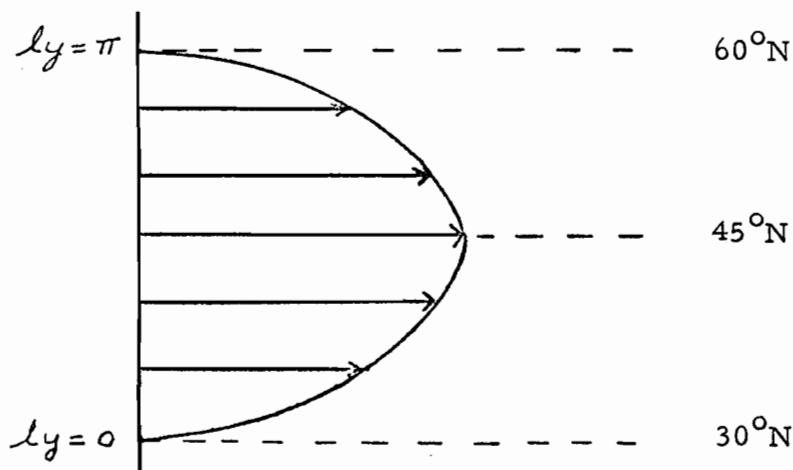


Figure 3.5: Linear growth rates for wave components of Model 2 for various maximum zonal wind values in metres/sec.

Figure 3.3



$$L_y = \frac{a\pi}{3} ; \quad l = \frac{2\pi}{L_y} = \frac{6}{a} ; \quad a = \text{radius of the earth.}$$

Time is measured in units of approximately 18 hours such that

$$f = 6 \text{ and } \beta_0 = \frac{f}{a} = \frac{6}{a} . \quad \text{Thus it follows that } \beta_0/l = 1 .$$

These parameters were also used in the numerical integrations to be described later.

The roots obtained are of the following forms

a) stable regime  $\pm i\omega_1, \pm i\omega_2$ , b) unstable regime  $\pm \omega_1, \pm i\omega_2$  .

Figure 3.4 shows the phase speeds (i. e. imaginary parts) as a function of  $\alpha$  for various maximum zonal winds, while Figure

3.5 shows the growth rates for waves in the unstable regime.

In both of these diagrams only the magnitudes of the roots are

shown. The linear analysis of this system as presented in

Figures 3.4 and 3.5 indicates the following general features.

a) Very long waves ( $\alpha = \frac{L_y}{L_x} \ll 1$ ) are stabilized by the inclusion of the Rossby term. The two phase speeds are very widely different, being determined primarily by the  $\beta_0$  effect.

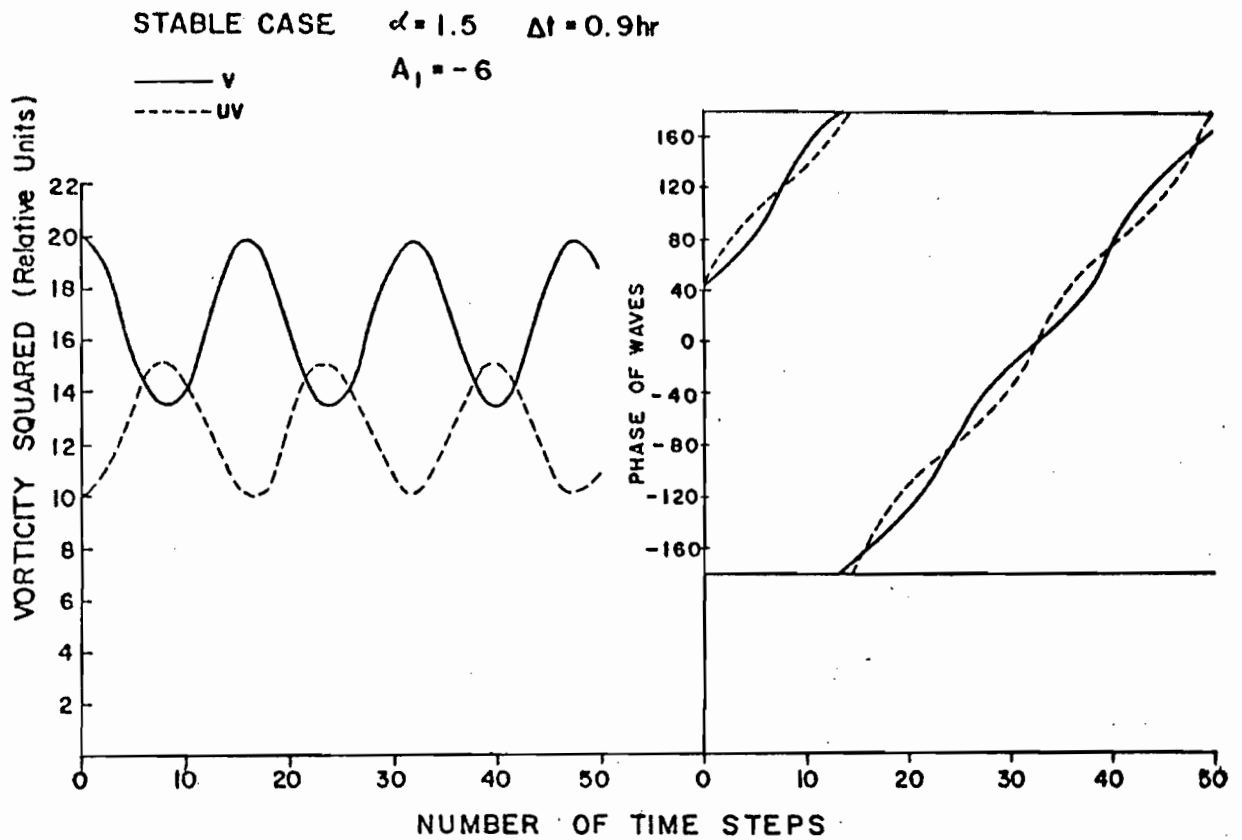


Figure 3.6: The fluctuations of vorticity squared and variation in phase angle in degrees of the components of Model 2 for a stable short-wave configuration.

- b) Short waves ( $\alpha = \frac{L_y}{L_x} > 1$ ) are stable as before, and their phase speeds are determined primarily by the zonal current.
- c) Intermediate wavelengths may be unstable if the zonal current is strong enough.

This picture is consistent with the barotropic analysis of Kuo (1949), although instability is more difficult to achieve in the sense that greater zonal wind shear is required.

The system of equations may be shown to have solutions which are elliptic functions of time (Platzman, 1962), but again by simple numerical integration we may study the non-linear properties of the model.

In the following three cases the initial conditions are the same and correspond to perturbation conditions, i. e.  $A = -6$  ;  
 $F_1 = F_2 = G_1 = G_2 = 0.1$  at  $t = 0$  . The mean square vorticity of each component (which in this system is proportional to the kinetic energy) and the phase angle of the two waves are plotted as functions of time. Here again,  $A$  is referred to as  $\mathcal{U}$  ;  
 $F_1, F_2$  as the "  $v$  " wave, and  $G_1, G_2$  as the "  $uv$  " wave.

CASE I  $\alpha = 1.5$  LINEARLY STABLE (Figure 3.6)

The two waves interchange energy and the zonal current undergoes only very slight changes ( $< .001\%$  and thus is not plotted). The average angular phase speeds of the waves correspond very

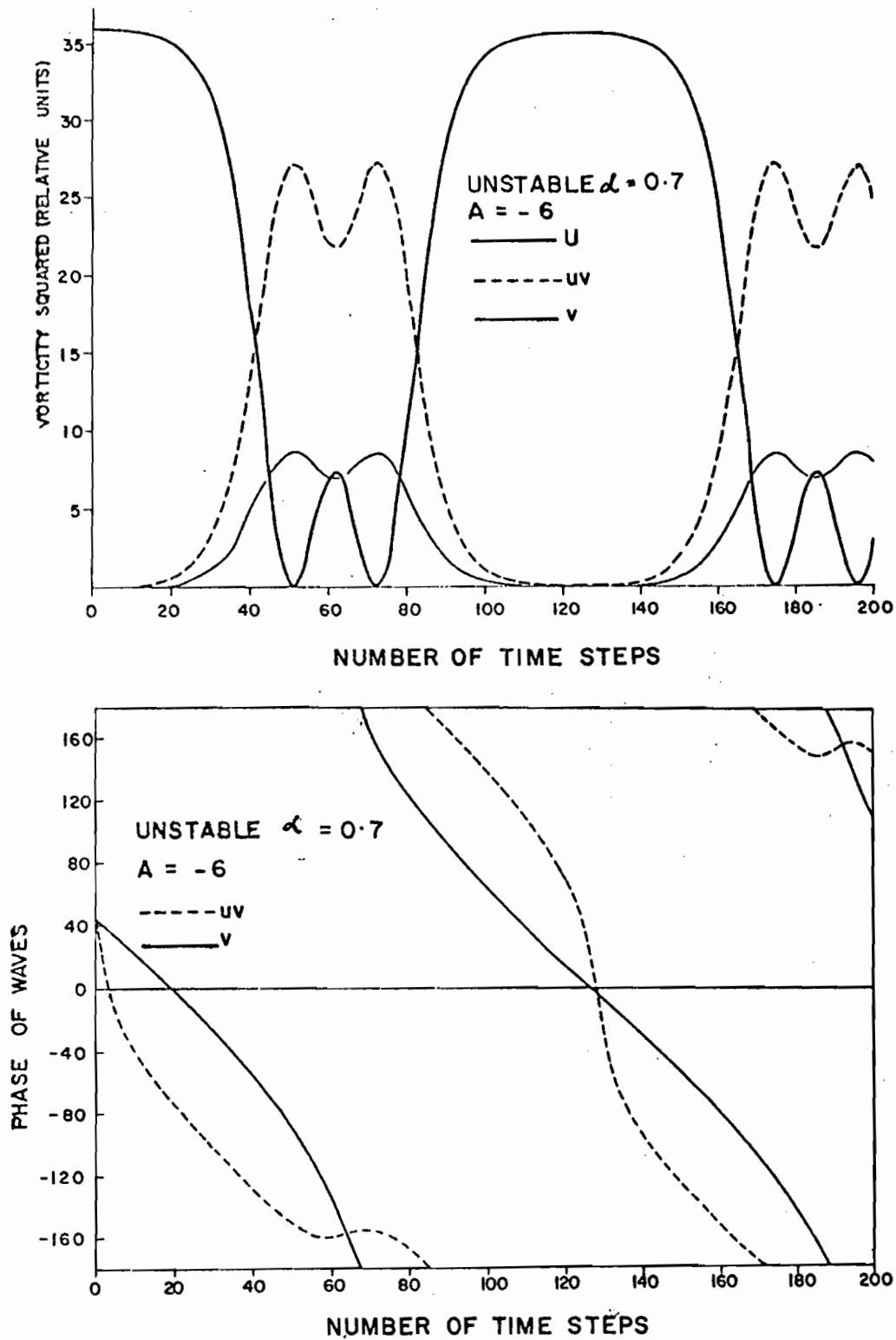


Figure 3.7: The fluctuations of vorticity squared (upper) and variation in phase angle in degrees (lower) of the components of Model 2 for an unstable configuration. Time step = 0.9 hours.

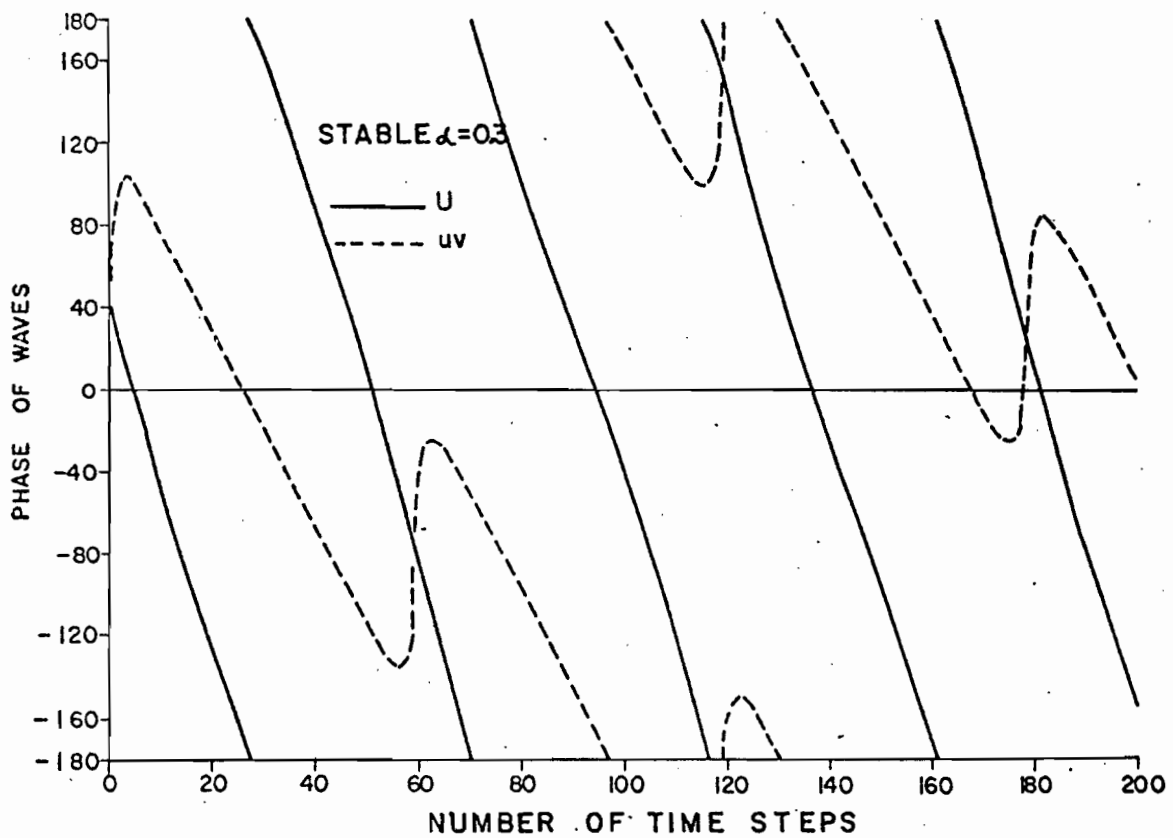
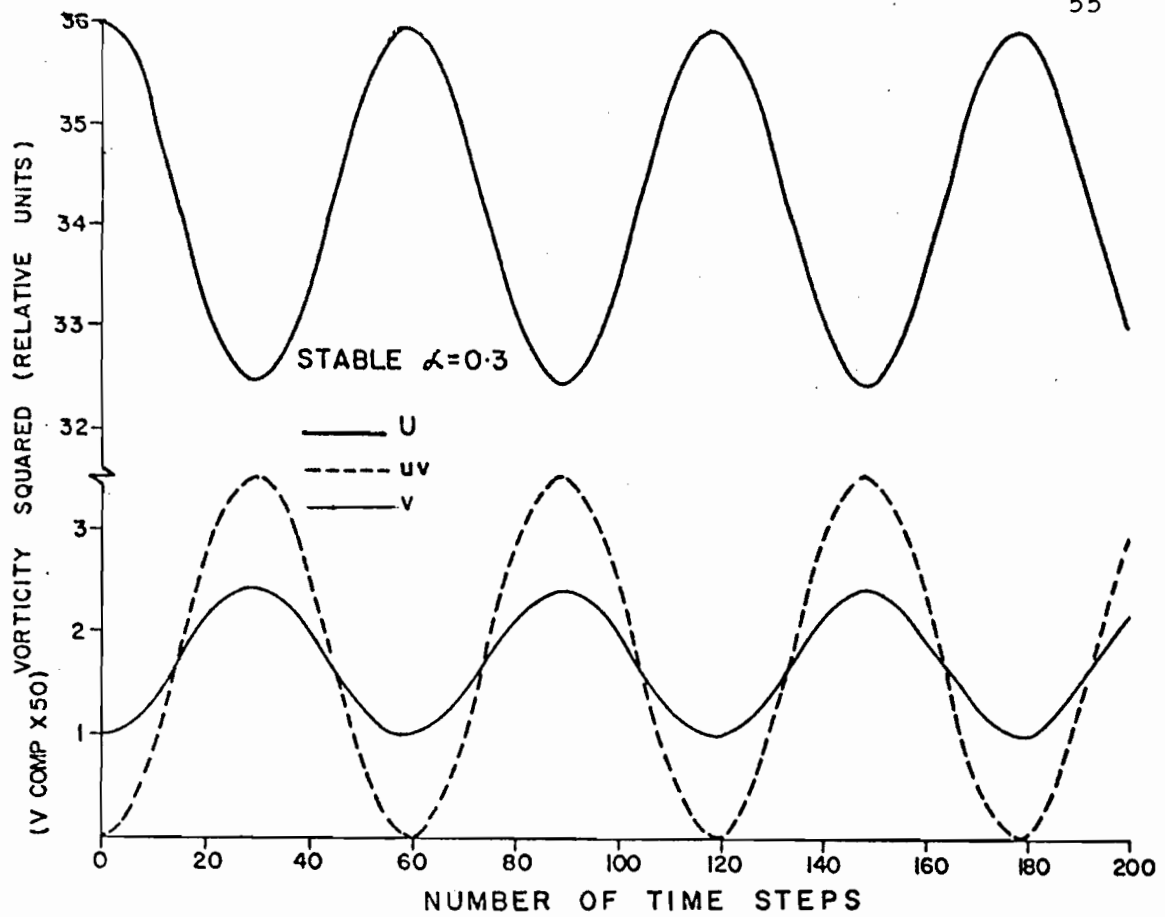


Figure 3.8: The fluctuation of vorticity squared (upper) and variation in phase angle in degrees (lower) of the components of Model 2 for a stable long-wave configuration. Time step = 0.9 hours.

closely to the results of the linear analysis. The two waves do vary their relative positions periodically, but with small amplitude.

CASE II  $\alpha = 0.7$  LINEARLY UNSTABLE (Figure 3.7)

In this case the waves are linearly unstable and start to grow at once, extracting energy from the zonal current. Soon all of the energy is removed from the zonal current which changes sign for a short period, and the perturbations have reached their maximum intensity. The perturbations then decay, feeding their energy back to the zonal current which climbs back to its original value. The " $u$ " wave lags the " $v$ " wave when the zonal current is decreasing westerly and shifts to be leading when the zonal current is increasing westerly.

CASE III  $\alpha = 0.3$  LINEARLY STABLE (Figure 3.8)

The zonal current undergoes a weak sinusoidal fluctuation of about 10% of its amplitude. The perturbations oscillate sinusoidally as well, both being out of phase with the zonal current. The phase progression of the waves is quite different from CASE I. Here the waves are retrogressing and have phase variations which are similar to CASE II. However, because the average phase speeds of the two waves are widely different, the amount of time spent in one phase configuration is small.

As in Model 1 discussed previously, we can cause large

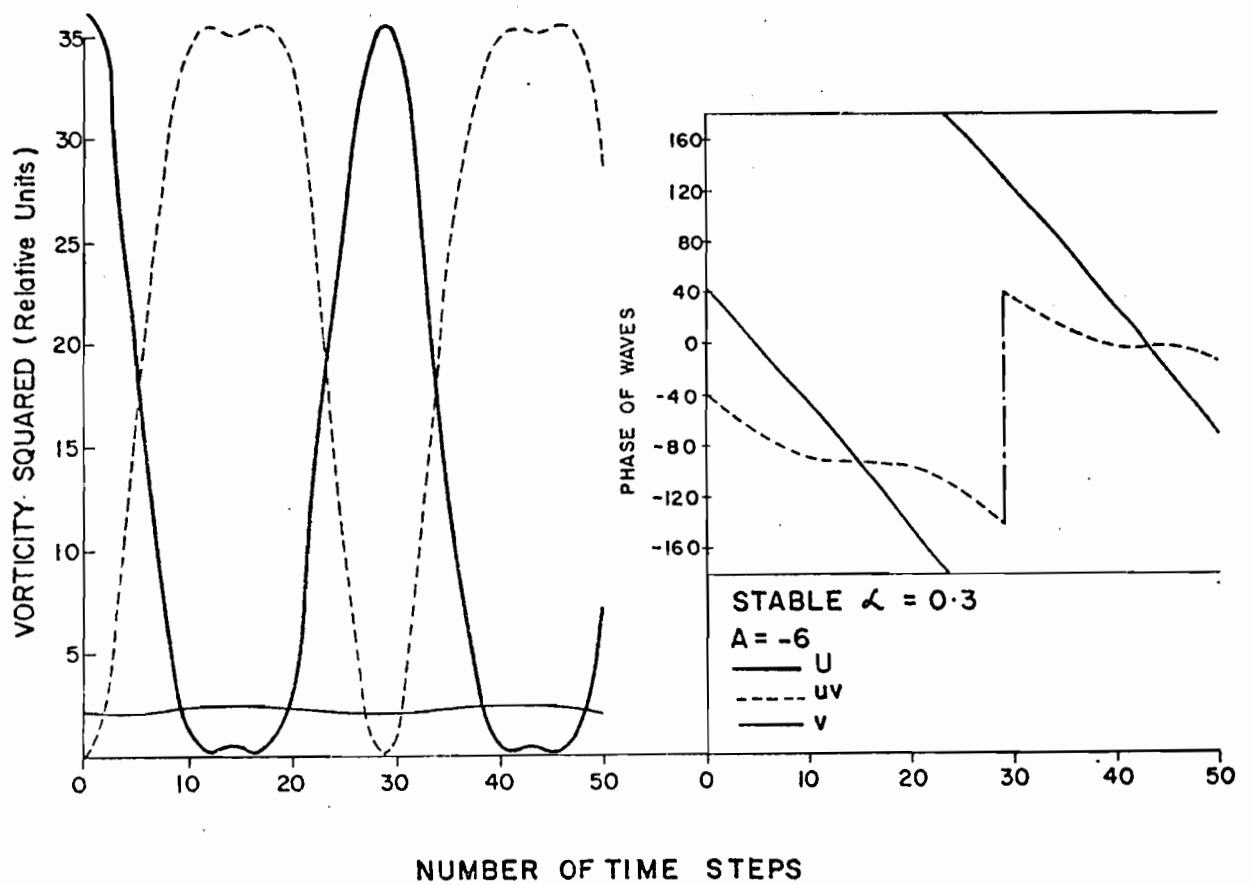


Figure 3.9: The fluctuation of vorticity squared and variation of phase angle in degrees of the components of Model 2 for a long wave non-linear configuration. Time step = 0.9 hours.

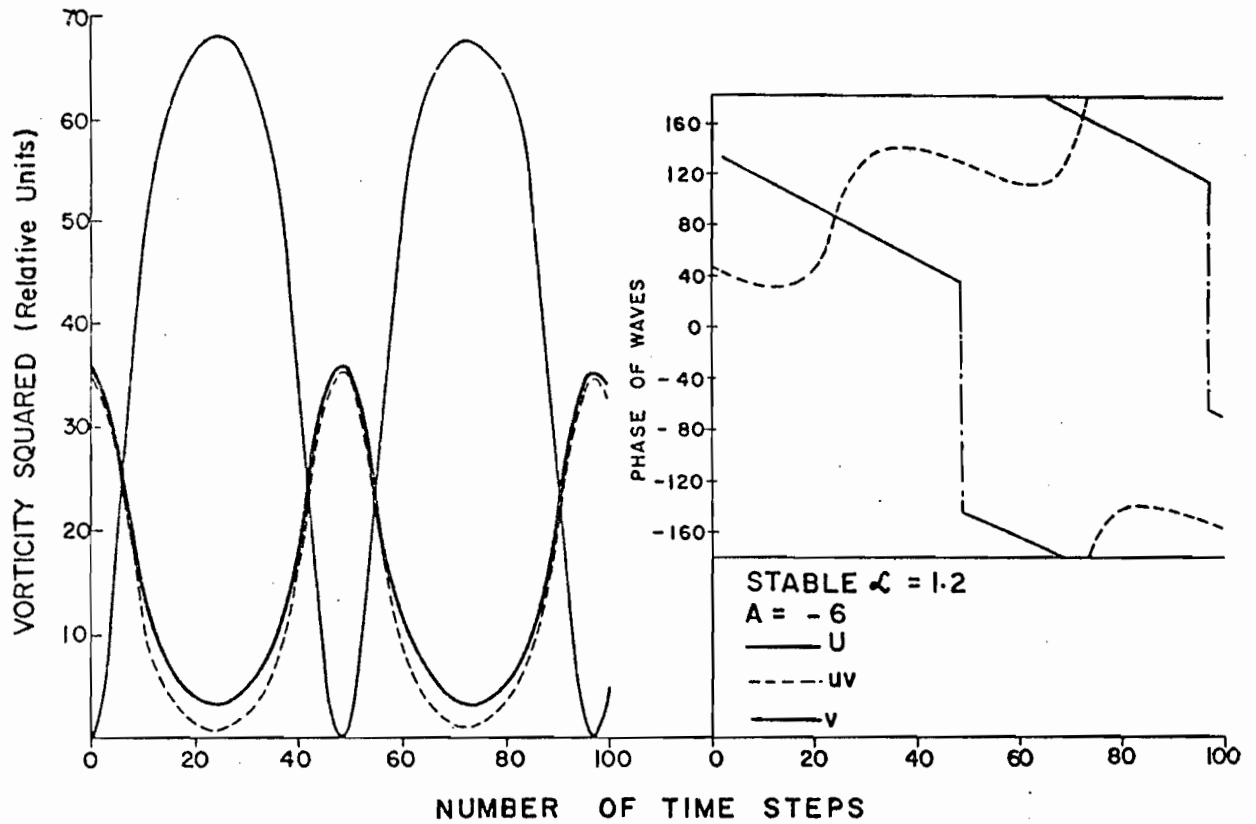


Figure 3.10: The fluctuation of vorticity squared and variation in phase angle in degrees of the components of Model 2 for a short wave non-linear configuration. Time step = 0.9 hours.

fluctuations in a stable zonal current merely by having large enough perturbations initially. Figures 3.9, 3.10 illustrate this for both long wave and short wave cases.

The question now is what physical significance or conclusions can be drawn from this simple non-linear system? Firstly, the non-linear process in operation here is horizontal momentum transport and convergence. The covariance of the convergence of momentum transport and the zonal wind is, of course, the measure of the energy conversion from eddy kinetic energy to zonal kinetic energy. The horizontal momentum transport in this system is given by

$$M_T = \frac{1}{L_x} \int_0^{L_x} (u v) dx = -\frac{1}{2\alpha(1+\alpha^2)} \frac{1}{l^2} (F_2 G_1 - F_1 G_2) \cos ly \quad 3.12$$

The connection with the rate of change of zonal kinetic energy is apparent because

$$\frac{dA}{dt} = \frac{1}{2\alpha(1+\alpha^2)} (F_2 G_1 - F_1 G_2)$$

Now, if we let

$$F_v = (F_1^2 + F_2^2)^{\frac{1}{2}} \quad \text{and} \quad \phi_v = \arctan \frac{F_2}{F_1} \quad 3.13$$

$$G_{uv} = (G_1^2 + G_2^2)^{\frac{1}{2}} \quad \text{and} \quad \phi_{uv} = \arctan \frac{G_2}{G_1} \quad 3.14$$

then 3.12 becomes

$$\begin{aligned}
 M_T &= -\frac{1}{2\alpha(1+\alpha^2)} \frac{1}{L^2} F_V G_{uv} (\sin \phi_V \cos \phi_{uv} - \cos \phi_V \sin \phi_{uv}) \cos ly \\
 &= -\frac{1}{2\alpha(1+\alpha^2)} \frac{1}{L^2} F_V G_{uv} \sin(\phi_V - \phi_{uv}) \cos ly
 \end{aligned}
 \tag{3.15}$$

thus south of the wind maximum we have southward transport of westerly momentum if  $\phi_V > \phi_{uv}$ . Because of the simplicity of the system the momentum convergence has the same profile as the zonal current so that no splitting or north-south motion of the wind maximum can be produced. The important thing to note is that the momentum transport depends on the difference in phase of the "v" and "uv" waves. From this consideration the following physical picture presents itself. The two waves ("v", "uv") are moving in an east-west direction. Even if they are in phase at one particular time, because of their different scales (resulting in different Rossby phase speeds), they become out of phase at a later time; and transport and converge momentum changing the zonal current. This change in the zonal current produces a change in the phase speeds of the two waves and an oscillation has been started. The details of the motion then depend on how much of an effect the perturbations have on the zonal current. If they have little effect then the oscillation is weak and we may consider the system as stable, and if they have a large effect we may consider the system as unstable. The effect must be on the zonal current, and it is not sufficient just to have large

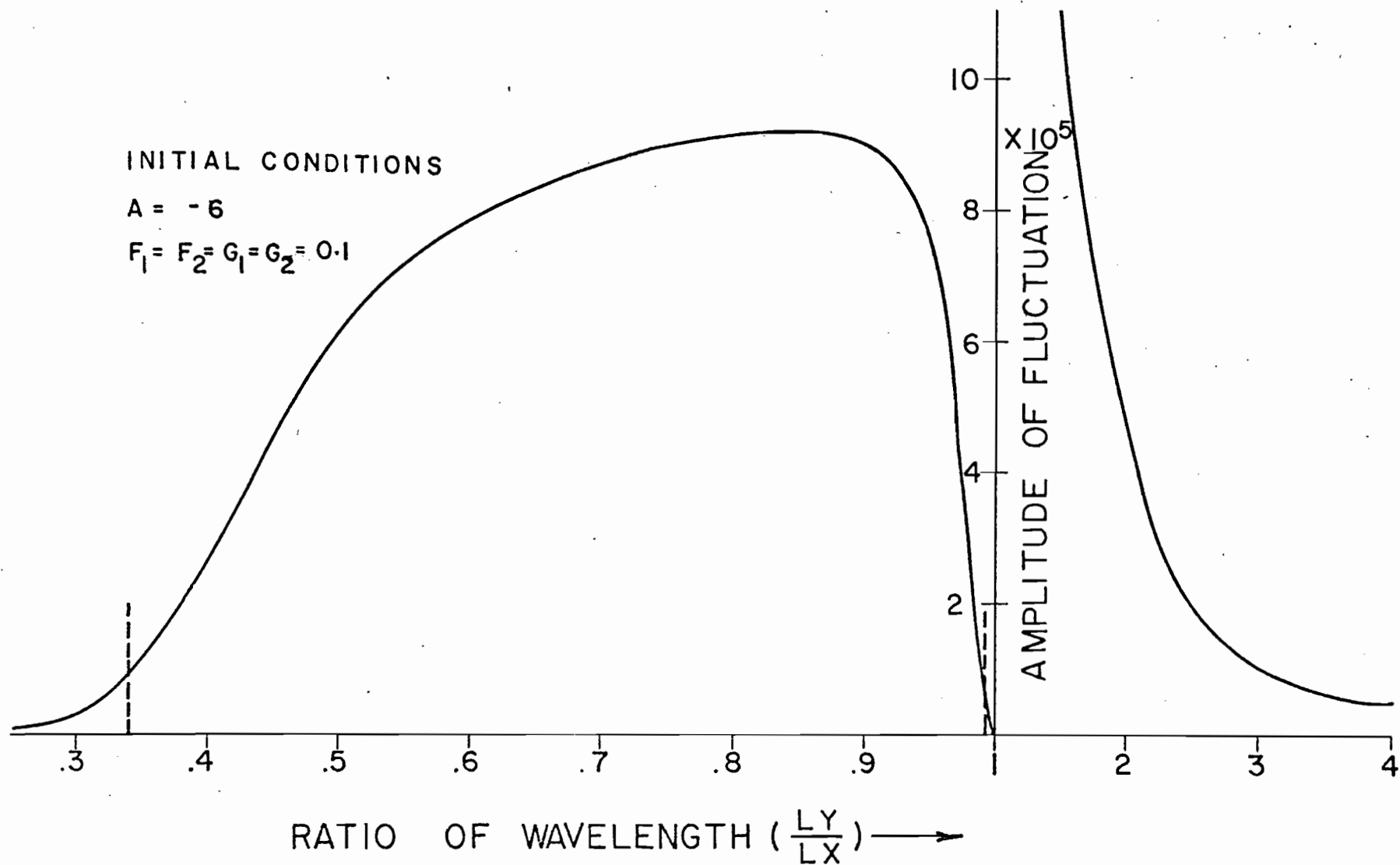


Figure 3.11: Maximum amplitude of fluctuation of the zonal component A subjected to small perturbations. Units are relative to A. Dotted vertical lines mark the limits of linear instability.

momentum transports. In fact, this is the reason why the inclusion of the Rossby term stabilizes the long waves. Because of the large difference in Rossby phase speeds of the " $\psi$ " and " $\mu\psi$ " waves, and although for this scale of motion the momentum transport is large, no significant energy conversion takes place because there is not enough time. In other words, although the amplitude of the momentum transport is large, its time frequency is also large; so that it changes direction before it performs a significant energy conversion.

In the non-linear system the division between stability and instability is not as sharp as in the linearized system. As a measure of instability in this non-linear system one may use the amplitude of fluctuation of the zonal component for given initial values of the perturbations. Figure 3.11 shows the results of the determination of the amplitude of fluctuation as a function of  $\alpha$ . As the initial values of the perturbations are decreased, one may expect that the curve may more closely resemble Figure 3.5.

### Model 3 - Motion on a Spherical Surface

The starting point for this model is the same as for Model 2, i. e. the barotropic vorticity equation, but without the " $\beta$ -plane" approximation. This model does have an added complexity, since for particular components representing the zonal wind it is possible to have a zonal wind which is non-zero when averaged in a north-south direction.

From Table 2.1, the spectral equation describing barotropic flow is

$$-c_Y \frac{d\psi_Y}{dt} = i \sum_{\alpha} \sum_{\beta} \psi_{\alpha} \psi_{\beta} H_{\alpha\gamma\beta} - i2\Omega m_Y \psi_Y \quad 3.16$$

where  $\psi = a^2 \sum_{\gamma} \psi_{\gamma} Y_{\gamma}$

The simplest truncation which produces non-linear exchange is a three-component one. Thus, one component represents the zonal flow  $\psi_n^0$ , and the other two represent perturbations of longitudinal wave number  $m$ ;  $\psi_s^m$  and  $\psi_k^m$  where  $s \neq k$ . This corresponds to Platzman's class L3 (Platzman, 1962). In accordance with the truncation procedure outlined in the previous chapter the components  $\psi_s^{-m}$  and  $\psi_k^{-m}$  must also be included. So that in  $\gamma, \alpha, \beta$  can take on the set of values  $(0, n); (\pm m, k); (\pm m, s)$ .

Performing the indicated summation in 3.16 the following equations are obtained

$$\begin{aligned} -c_n \frac{d\psi_n^0}{dt} &= i \psi_k^m \psi_s^{-m} H_{kn}^{m0-m} + i \psi_s^m \psi_k^{-m} H_{sn}^{m0-m} \\ &\quad + i \psi_k^{-m} \psi_s^m H_{kn}^{-m0m} + i \psi_s^{-m} \psi_k^m H_{sn}^{-m0m} \end{aligned}$$

$$\begin{aligned} -c_s \frac{d\psi_s^m}{dt} &= i \psi_n^0 \psi_k^m H_{ns}^{0mm} + i \psi_k^m \psi_n^0 H_{ks}^{m m 0} \\ &\quad + i \psi_n^0 \psi_s^m H_{ns}^{0mm} + i \psi_n^0 \psi_s^m H_{ss}^{m m 0} - i2\Omega m \psi_s^m \end{aligned}$$

$$\begin{aligned}
-c_k \frac{d\psi_k^m}{dt} &= i\psi_n^0 \psi_s^m H_{nks}^{omm} + i\psi_s^m \psi_n^0 H_{skn}^{mmo} \\
&+ i\psi_n^0 \psi_k^m H_{nkk}^{omm} + i\psi_k^m \psi_n^0 H_{kkn}^{mmo} - i2\Omega m \psi_k^m
\end{aligned}$$

The equations for  $\psi_k^{-m}$ ,  $\psi_s^{-m}$  may be obtained by taking the complex conjugate of the last two equations, and so will be carried implicitly.

Using the symmetry and redundancy properties of the  $H$ 's (Appendix B) the equations may be simplified to

$$\begin{aligned}
-c_n \frac{d\psi_n^0}{dt} &= i(\psi_k^m \psi_s^{*m} - \psi_s^m \psi_k^{*m}) m (c_k - c_s) \xi^0 \\
-c_s \frac{d\psi_s^m}{dt} &= im\psi_n^0 (\psi_k^m (c_n - c_k) \xi^0 - \psi_s^m (c_n - c_s) \alpha_s) - i2\Omega m \psi_s^m \\
-c_k \frac{d\psi_k^m}{dt} &= im\psi_n^0 (\psi_s^m (c_n - c_s) \xi^0 - \psi_k^m (c_n - c_k) \alpha_k) - i2\Omega m \psi_k^m
\end{aligned} \tag{3.17}$$

where

$$\begin{aligned}
\xi^0 &= - \int_0^\pi P_k^m P_s^m \frac{dP_n^0}{d\theta} d\theta \\
\alpha_s &= \int_0^\pi P_s^{m^2} \frac{dP_n^0}{d\theta} d\theta \\
\alpha_k &= \int_0^\pi P_k^{m^2} \frac{dP_n^0}{d\theta} d\theta
\end{aligned}$$

The horizontal mean of kinetic energy in this system is

$$\begin{aligned}\bar{E} &= \frac{a^2}{4} (c_n \psi_n^{\circ 2} + 2c_k \psi_k^m \psi_k^{*m} + 2c_s \psi_s^m \psi_s^{*m}) \\ &= \frac{a^2}{4} (E_n^{\circ} + E_k^m + E_s^m)\end{aligned}\quad 3.18$$

while the mean square vorticity is given by

$$\begin{aligned}\bar{\zeta}^2 &= \frac{1}{2} (c_n^2 \psi_n^{\circ 2} + 2c_k^2 \psi_k^m \psi_k^{*m} + 2c_s^2 \psi_s^m \psi_s^{*m}) \\ &= \frac{1}{2} (\bar{\zeta}_n^{\circ 2} + \bar{\zeta}_k^{2m} + \bar{\zeta}_s^{2m})\end{aligned}\quad 3.19$$

Using the tendency equations 3.17 the energy exchange in this system is described by

$$\begin{aligned}\frac{dE_n^{\circ}}{dt} &= (c_s - c_k)Q & \frac{d\bar{\zeta}_n^{\circ 2}}{dt} &= c_n(c_s - c_k)Q \\ \frac{dE_k^m}{dt} &= (c_n - c_s)Q & \frac{d\bar{\zeta}_k^{2m}}{dt} &= c_k(c_n - c_s)Q \\ \frac{dE_s^m}{dt} &= (c_k - c_n)Q & \frac{d\bar{\zeta}_s^{2m}}{dt} &= c_s(c_k - c_n)Q\end{aligned}$$

where  $Q = 2i \psi_n^{\circ} (\psi_k^m \psi_s^{*m} - \psi_k^{*m} \psi_s^m) m \bar{\zeta}$

This is again the Fjortoft blocking theorem; and it can be seen that  $\frac{d\bar{E}}{dt} = \frac{d\bar{\zeta}^2}{dt} = 0$ .

Linearizing the equations and considering time variations of the form  $e^{im\sigma t}$  the following frequency equation is obtained

$$\sigma^2 - \sigma(\gamma_s + \gamma_k) + \gamma_s \gamma_k - \delta_s \delta_k = 0 \quad 3.20$$

where  $\gamma_s = \frac{2\Omega + \psi_n^0 \alpha_s (c_n - c_s)}{c_s}$  ,  $\delta_s = \frac{\psi_n^0 (c_n - c_s) \xi}{c_s}$

$$\gamma_k = \frac{2\Omega + \psi_n^0 \alpha_k (c_n - c_k)}{c_k} , \quad \delta_k = \frac{\psi_n^0 (c_n - c_k) \xi}{c_k}$$

Thus the necessary and sufficient condition for stability is that

$$\delta_s \delta_k \geq -\frac{1}{4} (\gamma_s - \gamma_k)^2 \quad 3.21$$

and the phase speeds are given by

$$\sigma = \frac{\gamma_s + \gamma_k}{2} \pm \frac{1}{2} \sqrt{(\gamma_s - \gamma_k)^2 + 4 \delta_s \delta_k} \quad 3.22$$

The physical meaning of the parameters are the following:

$\gamma_s, \gamma_k$  are the Rossby phase speeds (or convective phase speeds)

$\delta_s, \delta_k$  are non-linear phase speeds (depending on momentum transport).

Now, if  $\delta_s \delta_k \geq 0$  then waves are stable. From their definitions given

Table 3.1

## POSSIBLE UNSTABLE MODES FOR A GIVEN ZONAL COMPONENT

n	1	2	3	4	5	6
S, K	NONE	NONE	2, 4	2, 5	2, 6	2, 7
V				3, 6	3, 7	3, 8
A					4, 6	4, 7
L					4, 8	4, 7
U						5, 8
E						5, 10
S						

after 3.20 we have

$$\delta_s \delta_k = \frac{\psi_n^{02} \xi^2}{c_s c_k} (c_n - c_s)(c_n - c_k)$$

thus, it follows that unless the zonal wave scale is intermediate to the other two, and  $\xi \neq 0$ , the waves are stable. Since the equations are symmetric in  $s, k$  let  $s > k$ . Then waves are stable unless

$$k < n < s \quad \text{and} \quad \xi \neq 0$$

Now,  $\xi = -\frac{1}{m} L_{s k n}^{m m 0} \neq 0$  if  $s+k+n = \text{odd}$   
and  $|s-n| < k < s+n$

thus the number of possible unstable modes is quite restricted.

The combinations of  $(s, k)$  which can be unstable for a given zonal component are given in Table 3.1.

As indicated previously, this model has the added feature that a purely convective phase speed (one that does not require energy exchange) involving the zonal component is possible. This is measured by the parameters  $\alpha_s$  and  $\alpha_k$ . It is instructive therefore to compare the case where  $\alpha_s = \alpha_k = 0$  with the stability criterion of Model 2. Since

$$\alpha_s = \int_0^\pi P_s^{m^2} \frac{dP_n^0}{d\theta} d\theta$$

it follows that  $P_n^0$  must be even, i.e.  $n = \text{even}$ ; which corresponds to an odd zonal wind field. Assuming that  $k < n < s$  and

$\xi \neq 0$  the condition for instability is

$$\psi_n^{0^2} \geq \frac{(\gamma_s - \gamma_k)^2 c_s c_k}{4 \xi^2 (c_n - c_s)(c_s - c_n)} \quad 3.33$$

where  $\gamma_s = \frac{2\Omega}{c_s}$  ;  $\gamma_k = \frac{2\Omega}{c_k}$  i.e. the Rossby phase speeds for a zero zonal wind. Now, the wavelengths of the components are defined as  $L_n^2 = a^2/c_n$  etc. where  $a$  is the radius of the earth so that 3.33 becomes

$$\psi_n^{0^2} \leq \frac{(\gamma_s - \gamma_k)^2}{4 \xi^2 \left( \left( \frac{L_k}{L_n} \right)^2 - 1 \right) \left( 1 - \left( \frac{L_s}{L_n} \right)^2 \right)}$$

It may be shown that the stability criterion in Model 2 can be written as

$$\left( \frac{A}{\ell^2} \right)^2 \leq \frac{(\gamma_v - \gamma_{uv})^2}{2 \left( \left( \frac{L_v}{L_v} \right)^2 - 1 \right) \left( 1 - \left( \frac{L_{uv}}{L_v} \right)^2 \right)}$$

where  $\gamma_v$ ,  $\gamma_{uv}$  are the Rossby speeds, and  $L_v$ ,  $L_{uv}$  are the wavelengths of the components. Thus Model 2 and this case of Model 3 are physically equivalent. Model 2 could be made completely physically equivalent to Model 3 if a constant zonal wind was

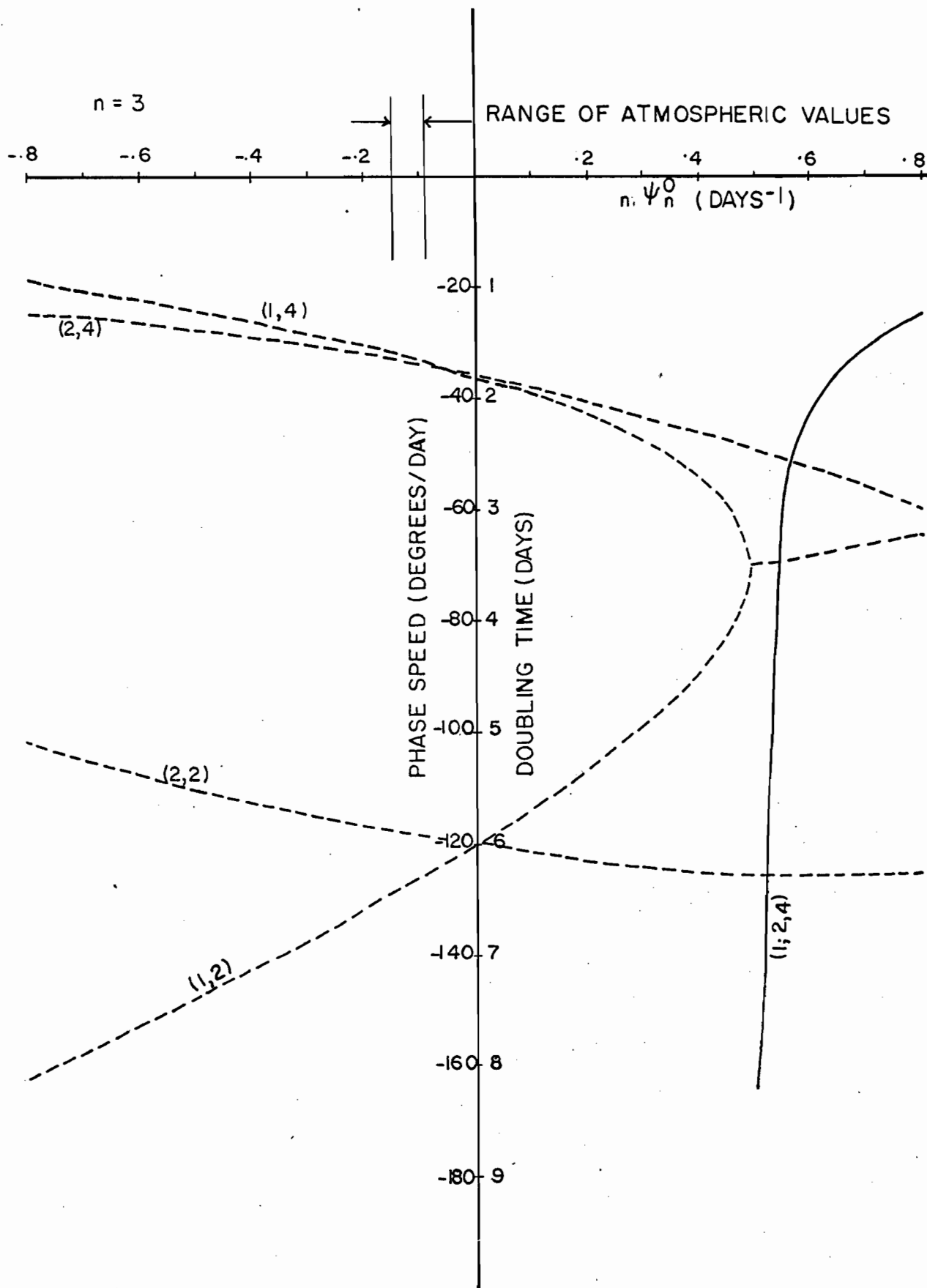


Figure 3.12: Linear phase speeds and growth rates of waves in Model 3. Abscissa is  $n$  times the amplitude of the zonal current. The curves are labelled such that the first index is the east-west wave number, the second is the total wave number.

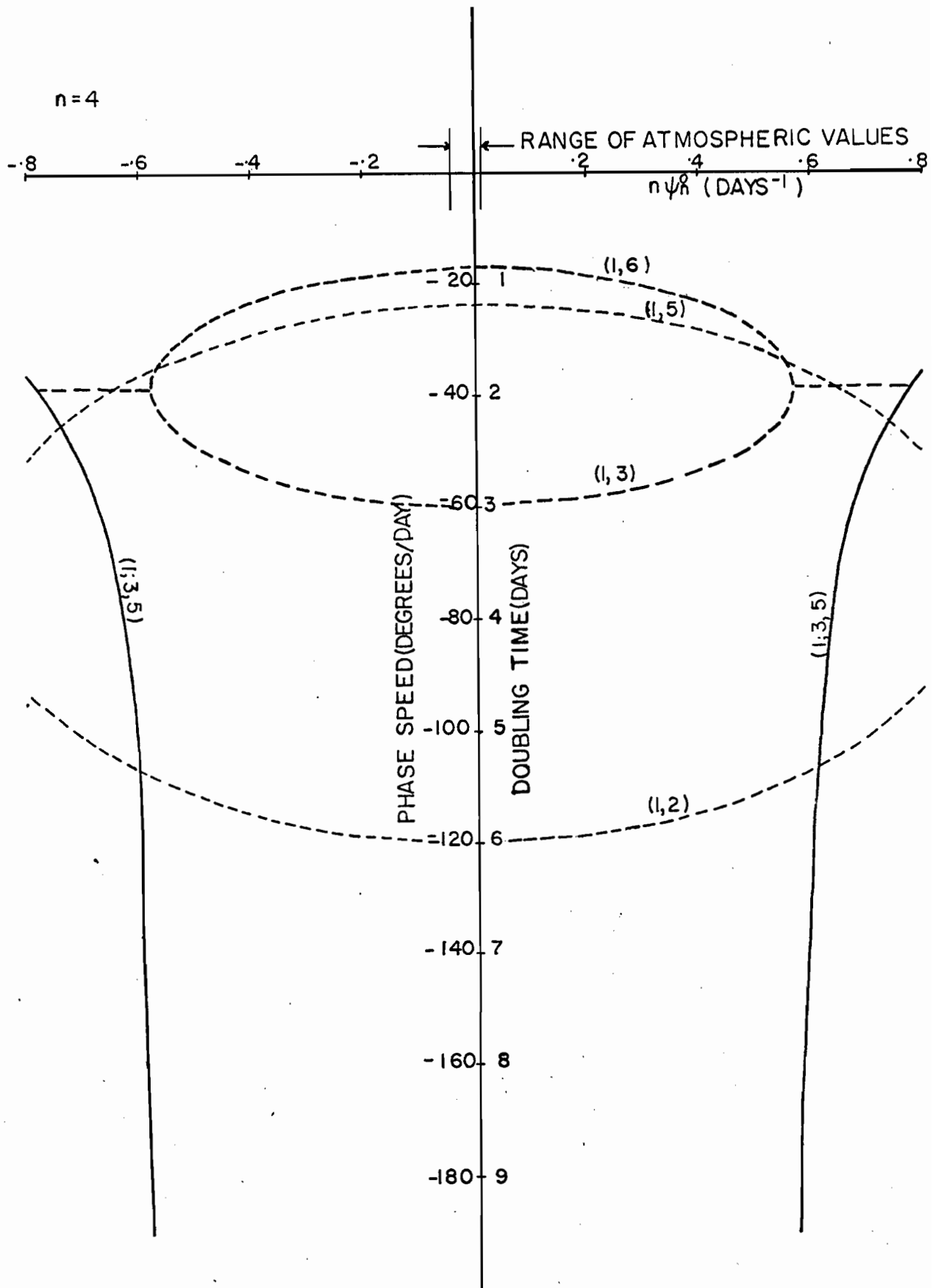


Figure 3.13: Linear phase speeds and growth rates of waves in Model 3. Abscissa is  $n$  times the amplitude of the zonal current. The curves are labelled such that the first index is the east-west wave number, the second is the total wave number.

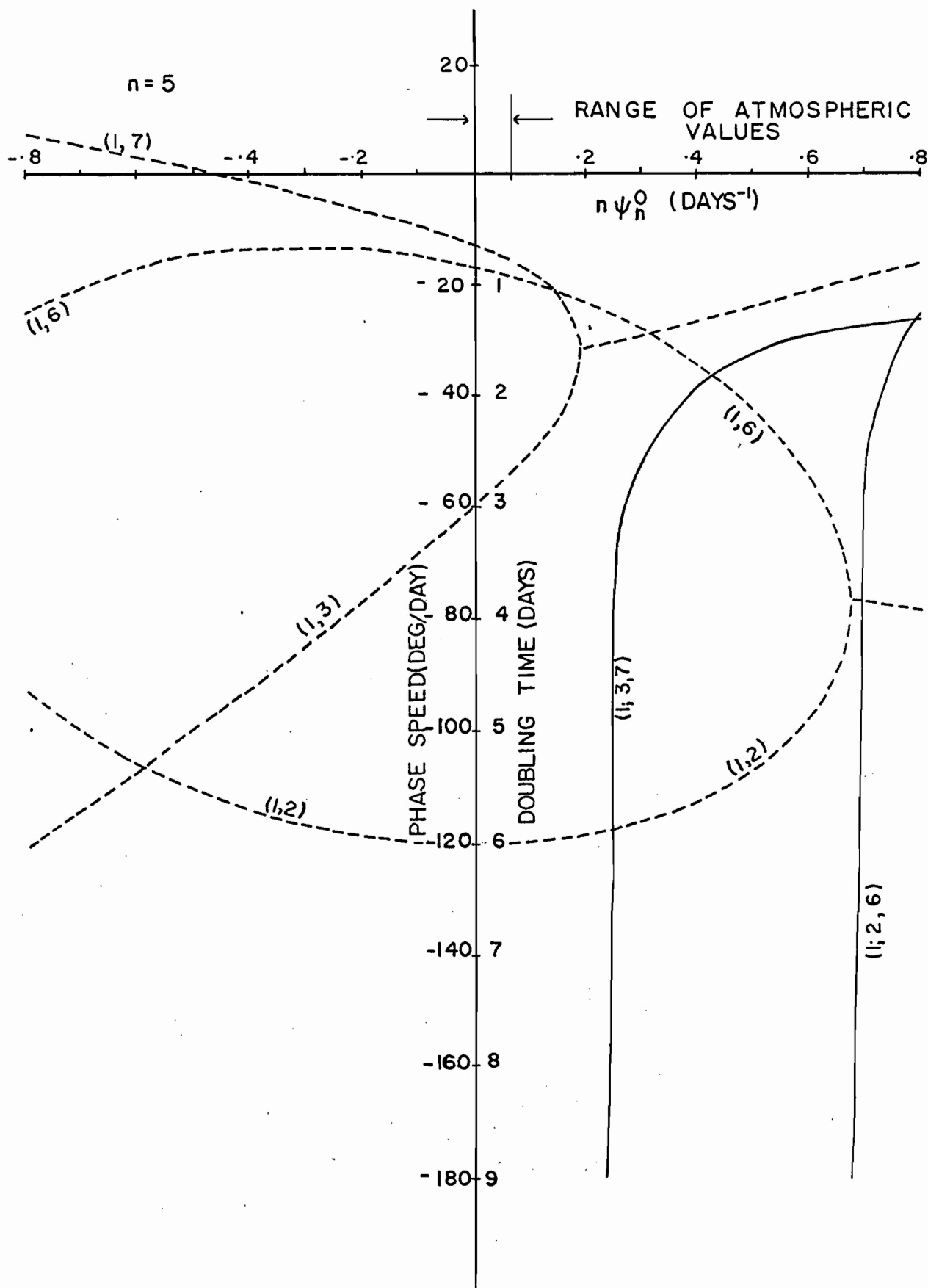


Figure 3.14: Linear phase speeds and growth rates of waves in Model 3. Abscissa is  $n$  times the amplitude of the zonal current. The curves are labelled such that the first index is the east-west wave number, the second is the total wave number.

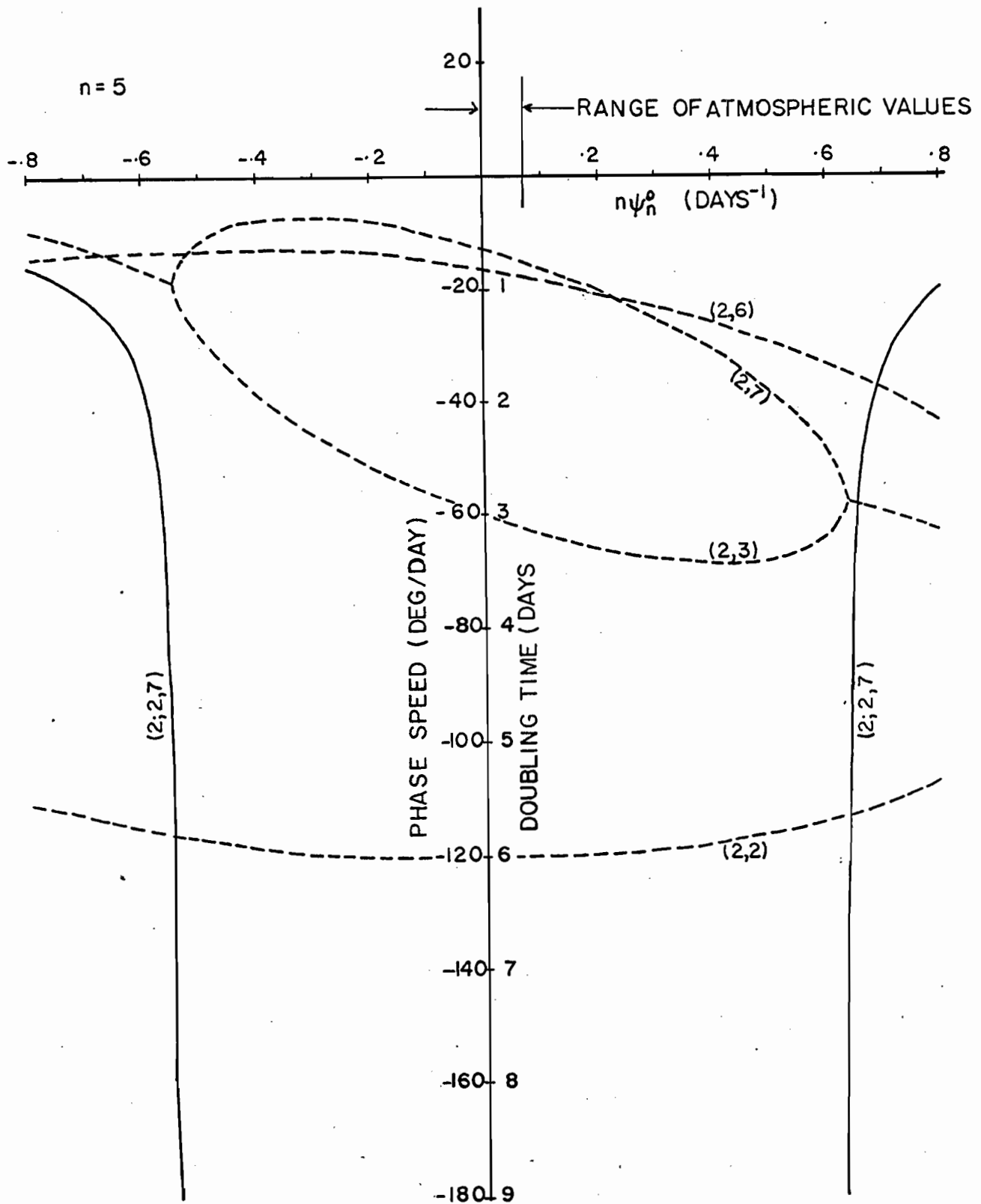


Figure 3.15: Linear phase speeds and growth rates of waves in Model 3. Abscissa is  $n$  times the amplitude of the zonal current. The curves are labelled such that the first index is the east-west wave number, the second is the total wave number.

added to the sinusoidal profile since the  $\beta$ -plane approximation was employed.

In Model 3 the importance of the difference in the Rossby-Haurwitz phase speeds ( $\gamma_s, \gamma_k$ ) in determining the stability of the system is much more explicit. In Figures 3.12 to 3.15 the results of the computation of phase speeds and doubling time for zonal currents with  $n = 3$  to 5 for some possibly unstable combinations of  $(s, k)$ . The abscissae represent  $n$  times the amplitude of the zonal components in units of  $\text{day}^{-1}$ . If  $n \psi_n^0$  is the same for different  $n$ 's then the maximum values of the zonal wind they represent are approximately equal. In anticipation of the results of the spherical harmonic analysis of the 500 mb surface the range of values of  $n \psi_n^0$  for the month of September 1957 have been indicated on the stability diagrams.

The picture presented is similar to Model 2. In the stable regime the phase speeds are widely different, as one approaches the neutral point the phase speeds become more nearly equal. While this result would occur in any quadratic frequency equation of this type the physical interpretation of the difference in linear phase speeds in terms of horizontal momentum convergence makes it more meaningful (see Model 2).

These diagrams show that, at least as far as this model describes the situation, the zonal components as observed at 500 mb during September 1957 are well into the stable regime. (No zonal components up to  $n = 7$  ever during the month has an amplitude

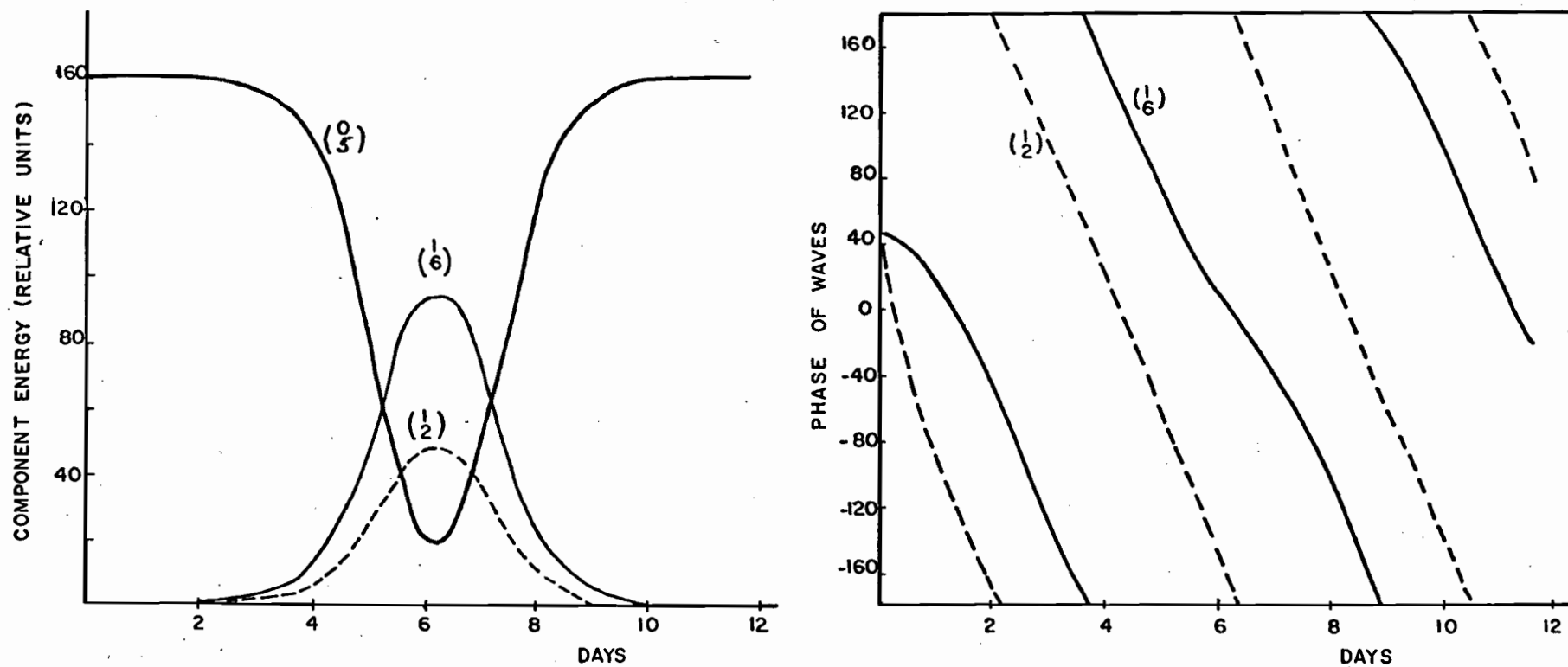


Figure 3.16: The fluctuation of energy and variation of phase lineals of components in degrees for Model 3, where initial value of  $\psi_5^0$  is linearly stable. Upper index of labelling corresponds to east-west wave number; lower corresponds to total wave number.

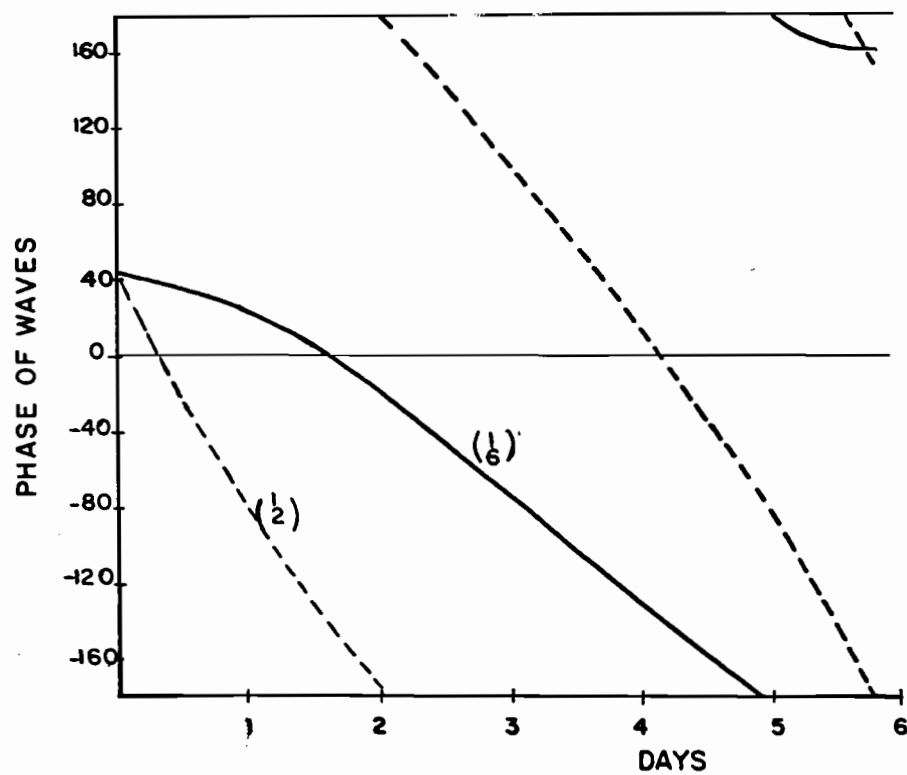
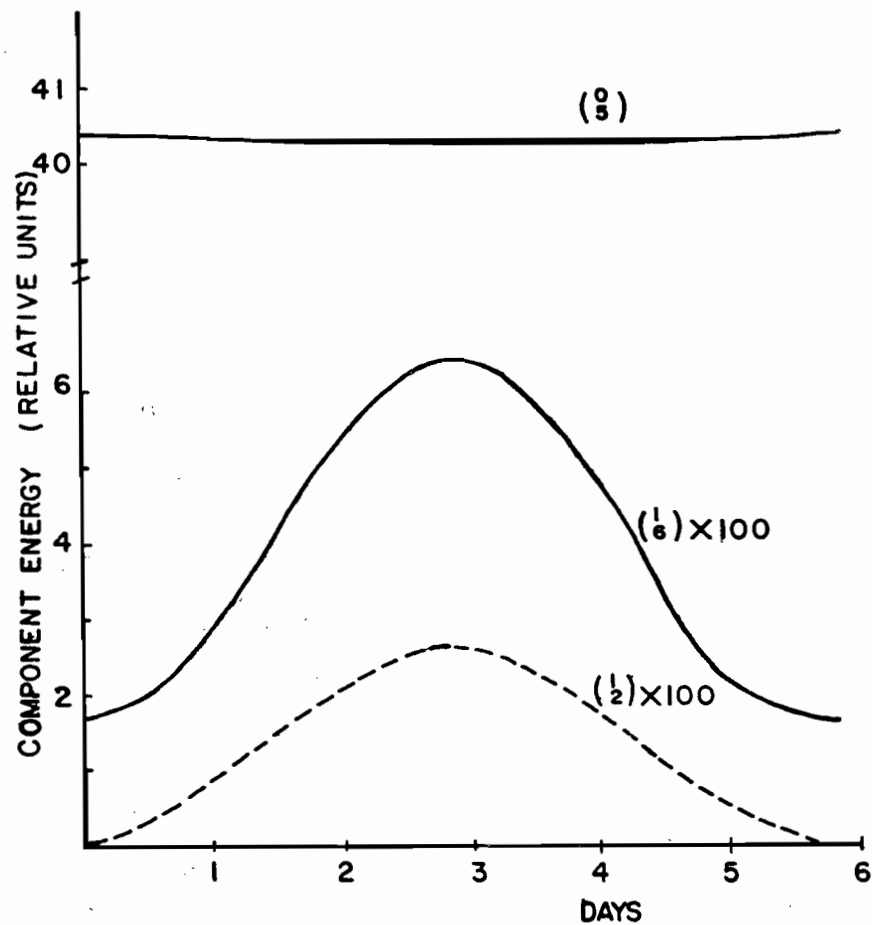


Figure 3.17: The fluctuation of energy and variation of phase lineals of components in degrees for Model 3, where initial value of  $\psi_5^0$  is unstable. Upper index of labelling corresponds to east-west wave number; lower corresponds to total wave number.

which is unstable for any combination of  $s, k \leq 10$  ). So that if the barotropic motions described by this model are to be observed they will probably be of the stable type.

The integration of equations 3.17 (because of their similarity to equations 3.8 ) produce essentially the same results as Model 2. Figures 3.16, 3.17 show the results of two cases of numerical integration of equations 3.17 . In one case (Figure 3.16) the initial value of  $\psi_5^0$  is in the unstable regime, the other (Figure 3.17) is for a stable initial value of  $\psi_5^0$  . In both cases the initial values of  $F_1, F_2, G_1, G_2$  were one hundredth of the initial values of  $\psi_5^0$  .

Thus the same interpretation of the stability diagrams and the numerical integrations in terms of horizontal momentum transport and convergence as was formulated in Model 2 apply to Model 3.

#### 4. DATA ANALYSIS IN TERMS OF SPHERICAL HARMONICS

In order to study further the application of the spherical harmonic representation of the dynamic equation we need to represent real observations in terms of these harmonics. Generally speaking, both the non-divergent and the divergent parts of the wind field as well as the temperature are required in harmonic form. Due to the limitations of the data, at least at the present time, the spectral representation of the divergent wind must be considered as unobtainable, and even the non-divergent wind must be obtained from some diagnostic equation relating it to the generally observed variable, the geopotential height field.

Given the geopotential height field of some constant pressure surface there are two ways in which the spectral representation of the non-divergent wind field (i. e. the stream function) may be obtained. The first method consists of analyzing the height field into spectral components, then solving a diagnostic equation in the spectral domain; the second consists of solving the diagnostic equation numerically, then analyzing the resulting stream function. Each is not without its problems, some of which are discussed below. In this study the first method was used with the linear balance equation. The second method is being applied by A. Robert and his associates (private communication) using the non-linear balance equation for the purpose of barotropic forecasting.

### The Analysis of the Geopotential Height Field

The geopotential height  $Z$ , expanded in a series of spherical harmonics, has the form

$$\begin{aligned} Z(\theta, \lambda) &= \sum_{m=0}^{\infty} (A^m(\theta) \cos m\lambda + B^m(\theta) \sin m\lambda) \\ &= \sum_{m=0}^{\infty} \sum_{n=m}^{\infty} (A_n^m \cos m\lambda + B_n^m \sin m\lambda) P_n^m \end{aligned} \quad 4.1$$

where  $\theta$  is colatitude,  $\lambda$  is longitude and  $P_n^m$  denotes the normalized associated Legendre function of the first kind as defined previously. The first series represents a simple Fourier analysis around latitude circles and thus it follows that

$$\begin{aligned} A^m(\theta) &= \sum_{n=m}^{\infty} A_n^m P_n^m \\ B^m(\theta) &= \sum_{n=m}^{\infty} B_n^m P_n^m \end{aligned} \quad 4.2$$

The above expansions are based on the following orthogonality condition

$$\int_0^{\pi} P_n^m P_k^m \sin \theta d\theta = \delta_{nk} \quad 4.3$$

In accordance with equation 4.1 and 4.2 the analysis usually proceeds in two stages. Firstly, Fourier analyses are performed at latitude circles; then these Fourier amplitudes are analyzed in terms of the Legendre functions. The properties of one-dimensional Fourier analysis of grid point data around latitude

circles has been fully discussed elsewhere (Godson, 1959, Boville, 1959). Here, the problem of transforming the Fourier amplitudes into spherical harmonical amplitudes will be considered.

Applying the orthogonality condition 4.3 to equation we can determine  $A_n^m$  and  $B_n^m$  by the following integrals

$$A_n^m = \int_0^\pi A^m(\theta) P_n^m \sin \theta d\theta \quad 4.4$$

$$B_n^m = \int_0^\pi B^m(\theta) P_n^m \sin \theta d\theta$$

In order to evaluate these integrals Fourier amplitudes from latitudes extending from the north pole to the south pole must be available. Failing this, the representation must be restricted to either even or odd functions for a hemisphere of data or to some scheme of a statistical "best fit" to the data (Haurwitz and Craig 1952). Even if the data are available over the entire range of latitude the integrals on the right hand side of 4.4 must still be evaluated by numerical quadrature.

#### Properties of Numerical Quadrature

Suppose that Fourier analyses have been performed at a set of colatitude circles  $\theta_i$ ; one may define a numerical quadrature scheme so that the integral  $\int_0^\pi f(\theta) d\theta$  is approximated by

$$\int_0^\pi f(\theta) d\theta \approx \sum_i f(\theta_i) w(\theta_i) \equiv \overline{f(\theta)} \quad 4.5$$

where  $w(\theta_i)$  is a weighting function which may correspond to Simpson's rule etc.,  $i$  is summed over the data latitudes and the bar represents the entire quadrature procedure.

In order to preserve as much as possible the integrity of the original data fields especially when regenerating grid point data fields from the analyzed components, it is necessary that the numerical errors introduced by the analysis scheme be as small as possible. Ideally the orthonormality condition (4.3) in the integral domain should be satisfied in the quadrature domain (4.5) as well. Practically speaking, quadrature schemes may be judged on how closely they approximate this ideal condition. This question will now be considered.

Assume that the data, i. e. the Fourier amplitudes, are exactly represented by the series

$$A^m(\theta) = \sum_{k=m}^{\infty} A_k^m P_k^m \quad 4.6$$

If 4.6 is multiplied by  $P_n^m \sin \theta$  and the quadrature scheme 4.5 is applied the result is

$$\tilde{A}_n^m = \overline{A^m(\theta) P_n^m \sin \theta} = \sum_k A_k^m \overline{P_k^m P_n^m \sin \theta} \quad 4.7$$

where  $\tilde{A}_n^m$  is the estimate of the true amplitude  $A_n^m$ , for if orthonormality is preserved the quadrature part of equals 1 if  $k=n$  and zero for  $k \neq n$ .

If a matrix  $G_{nk}^m$  is defined such that

$$G_{nk}^m = \frac{P_n^m P_k^m \sin \theta}{P_n^m P_k^m \sin \theta} - 1 \quad 4.8$$

then 4.7 becomes

$$\tilde{A}_n^m - A_n^m = \sum_k G_{nk}^m A_k^m \quad 4.9$$

If the orthonormality is preserved in the quadrature scheme then  $G_{nk}^m$  will be identically zero.

Thus the error introduced in the estimate of the amplitude  $A_n^m$  depends on the quadrature scheme and the distribution of the true amplitudes,  $A_k^m$ .

The form of the data used in this study is Fourier amplitudes at  $5^\circ$  latitude intervals from north pole to south pole. To study the effect of the quadrature scheme, the matrices were evaluated over this grid. Three quadrature schemes were tested; trapezoidal, Simpson's rule and Gaussian of order 40. The first two are suited to equally spaced grid points, the last requires very specifically located grid points so that some interpolation scheme must be used. Eliassen and Machenhauer (1965)

Table 4.1a: Matrix  $G_{n,k}^o$  using the trapezoidal rule (in units of  $10^{-3}$ )

k <sup>n</sup>	1	2	3	4	5	6	7	8	9	10	11	12	13	14	15	16	17
1	-1.9	0 <sup>+</sup>	-2.9	0	-3.7	0	-4.3	0	-4.9	0	-5.4	0	-5.9	0	-6.4	0	-6.9
2		-3.2	0	-4.3	0	-5.2	0	-5.9	0	-6.7	0	-7.3	0	-8.0	0	-8.6	0
3			-4.5	0	-5.6	0	-6.6	0	-7.5	0	-8.3	0	-9.1	0	-9.8	0	-11
4				-5.8	0	-6.9	0	-8.0	0	-9.0	0	-9.9	0	-11	0	-12	0
5					-7.1	0	-8.3	0	-9.4	0	-10	0	-11	0	-12	0	-13
6						-8.4	0	-9.6	0	-11	0	-12	0	-13	0	-14	0
7							-9.7	0	-11	0	-12	0	-13	0	-15	0	-16
8								-11	0	-12	0	-14	0	-15	0	-16	0
9									-13	0	-14	0	-15	0	-16	0	-18
10										-14	0	-15	0	-17	0	-18	0
11											-15	0	-17	0	-18	0	-20
12												-17	0	-18	0	-20	0
13													-19	0	-20	0	-22
14														-20	0	-22	0
15															-22	0	-24
16																-24	0
17																	-26

+ Values given as zero are less than  $10^{-7}$ .

Table 4. 1b: Matrix  $G_{n,k}^4$  using the trapezoidal rule (in units of  $10^{-5}$ ).

$k \ n$	4	5	6	7	8	9	10	11	12	13	14	15	16	17	18	19	20	
4	-0.3	0+	0	0	0	0	0	0	0	0	0	0	0	0	0	0	0	
5		-0.3	0	0	0	0	0	0	0	0	0	0	0	0	0	0	0	
6			-0.3	0	0	0	0	0	0	0	0	0	0	0	0	0	0	
7				-0.3	0	0	0	0	0	0	0	0	0	0	0	0	0	
8					-0.4	0	0	0	0	0	0	0	0	0	0	0	0	
9						-0.4	0	-0.1	0	0	0	0	0	0	0	-0.1	0	
10							-0.5	0	-0.1	0	-0.1	0	-0.1	0	-0.2	0	-0.2	
11								-0.5	0	-0.2	0	-0.2	0	-0.2	0	-0.2	0	
12									-0.6	0	-0.2	0	-0.3	0	-0.3	0	-0.4	
13										-0.7	0	-0.4	0	-0.4	0	-0.5	0	
14											-0.8	0	-0.5	0	-0.6	0	-0.9	
15												-0.9	0	-0.7	0	-.10	0	
16													-.12	0	-.11	0	-.17	
17														-.16	0	-.18	0	
18															-.23	0	-.29	
19																-.34	0	
20																		-.54

+ Values given as zero are less than  $10^{-7}$ .

Table 4. 2a: Matrix  $G_{nk}^{\circ}$  using Simpson's rule (in units of  $10^{-5}$ )

k \ n	1	2	3	4	5	6	7	8	9	10	11	12	13	14	15	16	17	
1	.67	0+	3.3	0	9.5	0	20	0	38	0	64	0	100	0	150	0	230	
2		3.1	0	9.0	0	20	0	39	0	67	0	110	0	170	0	250	0	
3			8.7	0	19	0	38	0	66	0	110	0	170	0	260	0	380	
4				19	0	36	0	64	0	110	0	170	0	260	0	380	0	
5					36	0	63	0	100	0	160	0	250	0	380	0	560	
6						62	0	100	0	160	0	250	0	370	0	550	0	
7							100	0	160	0	240	0	360	0	540	0	800	
8								160	0	240	0	360	0	530	0	790	0	
9									240	-0.1	350	0	520	0	780	0	1200	
10										350	-0.1	520	0	770	0	1200	0	
11											520	-0.1	770	0	1200	0	1800	
12												770	-0.1	1200	0	1800	0	
13													1200	-0.1	1800	0	3000	
14														1800	-0.1	3000	0	
15															3000	-0.1	5800	
16																5800	-0.1	
17																		20000

+ Values given as zero are less than  $10^{-7}$ .

Table 4.2b: Matrix  $G_{n,k}^4$  using Simpson's rule (in units of  $10^{-5}$ )

$k^n$	4	5	6	7	8	9	10	11	12	13	14	15	16	17	18	19	20
4	-.03	0 <sup>+</sup>	0	0	0	0	0	0	0	0	-.02	0	-.04	0	-.11	0	-.29
5		-.03	0	0	0	0	0	-.01	0	-.04	0	-.10	0	-.25	0	-.66	0
6			-.03	0	0	0	-.02	0	-.06	0	-.16	0	-.42	0	-1.1	0	-3.0
7				-.04	0	-.03	0	-.09	0	-.23	0	-.59	0	-1.6	0	-4.3	0
8					-.06	0	-.10	0	-.29	0	-.75	0	-2.0	0	-5.5	0	-16
9						-.15	0	-.32	0	-.89	0	-2.4	0	-6.7	0	-20	0
10							-.37	0	-.97	0	-2.7	0	-7.7	0	-23	0	-77
11								-1.0	0	-2.9	0	-8.4	0	-25	0	-85	0
12									-3.0	0	-8.9	0	-27	0	-92	0	-400
13										-9.1	0	-28	0	-97	0	-420	0
14											-29	0	-99	0	-440	0	-4100
15												-100	0	-450	0	-4200	0
16													-450	0	-4200	0	24000
17														-4300	0	24000	0
18															24000	0	-13000
19																-13000	0
20																	-12000

+ Values given as zero are less than  $10^{-7}$ .

Table 4.3a: Matrix  $G_{nk}^0$  -40 point Gaussian\* and 6 point interpolation (in units of  $10^{-5}$ )

k <sup>n</sup>	1	2	3	4	5	6	7	8	9	10	11	12	13	14	15	16	17	
1	0	0	0	0	0	0	0	0	0	0	0	0	0	0	0	0	0	
2	0	0	0	0	0	0	0	0	0	0	0	0	0	0	0	0	-.01	0
3	0	0	0	0	0	0	0	0	0	0	0	0	0	0	0	-.01	0	-.01
4	0	0	0	0	0	0	0	0	0	0	0	-.01	0	-.01	0	-.01	0	0
5	0	0	0	0	0	0	0	0	0	0	-.01	0	-.01	0	-.01	0	0	-.02
6	0	-1.8	0	.84	0	-.68	0	.88	0	-.81	0	.38	0	-.03	0	-.20	0	0
7	5.9	0	-6.5	0	-1.3	0	1.1	0	.96	0	-3.1	0	2.7	0	-1.4	0	.22	0
8	0	10	0	-26	0	14	0	2.2	0	-2.2	0	-4.9	0	5.9	0	-3.3	0	0
9	36	0	-13	0	-43	0	42	0	-4.2	0	-5.0	0	-12	0	15	0	-6.6	0
10	0	21	0	-36	0	-60	0	85	0	-13	0	-21	0	-16	0	36	0	0
11	78	0	10	0	-65	0	-86	0	168	0	-56	0	-43	0	-12	0	64	0
12	0	115	0	3.5	0	-122	0	-85	0	260	0	-130	0	-61	0	-7.6	0	0
13	32	0	173	0	-60	0	-152	0	-119	0	385	0	-233	0	-96	0	43	0
14	0	88	0	194	0	-74	0	-257	0	-163	0	570	0	-415	0	-78	0	0
15	152	0	90	0	314	0	-198	0	-412	0	-187	0	768	0	-588	0	-50	0
16	0	197	0	239	0	319	0	-409	0	-584	0	-272	0	1133	0	-830	0	0
17	292	0	465	0	247	0	236	0	-673	0	-903	0	-210	0	1593	0	-1159	0

Values given as zero are less than  $10^{-7}$

\*NOTE  $k$  index corresponds to the interpolated function

Table 4.3b: Matrix  $G_{n,k}^4$  -40 point Gaussian and 6 point interpolation (in units of  $10^{-5}$ )

$k^n$	4	5	6	7	8	9	10	11	12	13	14	15	16	17	18	19	20
4	0+	0	0	0	0	0	0	0	0	0	0	0	0	0	0	0	0
5	0	-.01	0	0	0	0	0	0	0	0	0	0	0	0	0	0	0
6	.79	0	-.20	0	.21	0	-.25	0	.15	0	-.03	0	-.04	0	.06	0	-.04
7	0	2.9	0	.16	0	-.21	0	-.87	0	1.0	0	-.57	0	.15	0	.14	0
8	-2.4	0	13	0	-2.7	0	-1.2	0	-1.4	0	2.6	0	-1.4	0	.49	0	0
9	0	3.8	0	25	0	-9.9	0	-1.4	0	-4.7	0	8.8	0	-4.1	0	.56	0
10	16	0	-4.4	0	50	0	-21	0	-7.9	0	-4.7	0	21	0	-13	0	4.0
11	0	-4.3	0	-16	0	102	0	-54	0	-9.6	0	-2.4	0	38	0	-23	0
12	-55	0	-28	0	-12	0	164	0	-96	0	-10	0	-2.6	0	77	0	-54
13	0	-91	0	-32	0	-38	0	284	0	-162	0	-22	0	23	0	118	0
14	36	0	-94	0	-94	0	-24	0	464	0	-284	0	-11	0	37	0	177
15	0	123	0	-190	0	-114	0	21	0	683	0	-411	0	-9.1	0	64	0
16	47	0	94	0	-227	0	-114	0	54	0	1049	0	-653	0	-15	0	136
17	0	-76	0	189	0	-247	0	-167	0	225	0	1441	0	-988	0	25	0
18	-151	0	-15	0	327	0	-356	0	-73	0	359	0	1920	0	-1379	0	-21
19	0	-11	0	78	0	370	0	-298	0	-76	0	533	0	2571	0	-2029	0
20	237	0	104	0	31	0	653	0	-398	0	-82	0	862	0	3161	0	-2654

+ Values given as zero are less than  $10^{-7}$

\* NOTE  $k$  index corresponds to the interpolated function

used a five point interpolation formula, here a six-point Lagrangian interpolation was used.

Because of the interpolation necessary in Gaussian quadrature the expression for the G-matrix must be modified to include the interpolation scheme. So that the  $G_{nk}^m$  for Gaussian quadrature is given by

$$G_{nk}^m = \sum_j \left( \sum_i P_n^m(x_i) g_{ij} \right) P_k^m(x_j) w_j - 1 \quad 4.10$$

where  $g_{ij}$  are the interpolation weights to convert the field to be analyzed from the data latitudes  $x_i$  to the Gaussian latitudes  $x_j$  and  $w_j$  are the appropriate Gaussian weights

In Tables 4.1, 4.2, 4.3 the G matrices are given for the zonal components ( $m = 0$ ) and for a typical set of wave components ( $m = 4$ ). With the exception of the G matrices for Gaussian quadrature plus interpolation, the matrices are symmetric in  $n, k$ ; so that in these cases only half the matrix is presented.

The first thing to notice about the matrices is that there is no parity mixing. That is, for a symmetric component only symmetric components produce non-zero effects, and vice versa. This is understandable because the set of latitudes used is symmetric with respect to the equator, and the numbers obtained for these elements, if non-zero, are just a measure of the truncation and round-off error in using 29 bit precision. As well, quite generally,

Table 4.4a: Matrix  $G_{nk}^{\circ}$  using Gaussian quadrature of order 40 over Gaussian latitudes (in units of  $10^{-7}$ )

$k^n$	1	2	3	4	5	6	7	8	9	10	11	12	13	14	15	16	17
1	.93	-.48	-.02	-.04	-.02	-.02	-.14	-.01	-.27	0 <sup>+</sup>	-.38	0	-.57	0	-.89	-.01	-.96
2		.59	-.40	-.07	0 <sup>+</sup>	-.04	0	-.27	0	-.42	0	-.72	0	-.97	0	-1.1	0
3			.33	-.41	-.10	-.05	-.15	0	-.44	0	-.75	0	-1.1	0	-1.2	0	-1.3
4				.30	-.45	-.16	-.05	-.32	0	-.75	0	-1.1	0	-1.3	0	-1.4	0
5					.04	-.42	-.30	-.04	-.62	0	-1.1	0	-1.3	0	-1.5	0	-1.6
6						-.24	-.30	-.63	-.04	-.93	-.02	-1.3	0	-1.5	0	-1.7	0
7							-.72	-.41	-.86	-.07	-1.2	-.01	-1.5	0	-1.8	0	-1.6
8								-1.0	-.44	-1.2	-.03	-1.4	-.03	-1.8	-.01	-1.7	0
9									-1.4	-.41	-1.4	-.02	-1.7	-.01	-1.7	0	-1.5
10										-1.6	-.42	-1.6	-.04	-1.7	-.03	-1.6	0
11											-2.4	-.46	-1.6	-.03	-1.7	-.03	-1.9
12												-2.7	-.42	-1.4	-.06	-1.9	0
13													-2.5	-.45	-1.8	-.05	-2.3
14														-2.9	-.41	-2.3	-.05
15															-3.6	-.43	-2.6
16																-4.1	-.46
17																	-4.6

+ Values given as zero are less than  $10^{-9}$ .

Table 4.4b: Matrix  $G_{nk}^4$  using Gaussian quadrature of order 40 over Gaussian latitudes (in units of  $10^{-7}$ )

$k \ n$	4	5	6	7	8	9	10	11	12	13	14	15	16	17	18	19	20
4	-.57	-.18	-.07	0+	-.16	0	-.07	0	-.01	0	-.01	0	-.03	0	-.02	0	-.20
5		-.44	-.27	-.16	-.02	-.09	0	-.03	0	-.04	0	-.01	0	-.14	0	-.29	0
6			-.96	-.35	-.26	0	-.20	-.01	-.03	0	-.06	0	-.18	0	.18	0	.07
7				-1.2	-.27	-.41	-.02	-.24	0	0	0	-.25	0	.17	0	.09	0
8					-1.5	-.34	-.53	-.01	-.37	0	-.21	0	-.04	0	.08	0	-.30
9						-1.7	-.33	-.75	-.04	-.67	0	.01	0	-.06	0	-.33	0
10							-2.1	-.38	-1.1	-.02	-.49	0	-.02	0	-.50	-.01	-.25
11								-2.6	-.36	-.96	-.04	-.66	0	-.51	0	-.46	0
12									-2.5	-.42	-1.1	-.03	-1.2	0	-.56	0	-.13
13										-2.9	-.38	-1.7	-.02	-1.3	0	-.27	0
14											-3.6	-.36	-1.9	-.02	-1.1	0	-.49
15												-3.9	-.40	-1.7	-.04	-1.3	0
16													-4.0	-.36	-2.1	-.04	-1.8
17														-4.2	-.45	-2.6	-.05
18															-5.1	-.43	-2.4
19																-5.3	-.43
20																	-5.4

+ Values given as zero are less than  $10^{-9}$ .

the higher the order of the function to be integrated the larger the element of the G matrix. As far as the zonal components are concerned, the Gaussian plus interpolation G matrix is closest to zero, whereas for the wave components the trapezoidal G matrix is closest to zero. Another feature of the Gaussian plus interpolation is that it is very accurate as long as the function to be integrated is of a lower order than the interpolation scheme. This illustrates how the interpolation scheme degenerates the Gaussian quadrature. Table 4.4 shows the G matrices for Gaussian integration over Gaussian latitudes and the difference is striking. These results also show that if one wishes to minimize the purely numerical errors introduced into an analysis the data should be obtained at Gaussian latitudes. However, if the data are at regularly spaced intervals of latitude, then Gaussian plus interpolation should be used for the zonal components, and trapezoidal integration for the wave components.

Thus far only the numerical properties of different quadrature schemes has been considered; the data has been considered precise and independent at each data point required. This of course is not true. In fact the data in original form are full of errors, both systematic and random. As well, in order to obtain the data at the grid points, interpolations over at least  $5^{\circ}$  latitude are performed either by a numerical process in the case of objectively analyzed fields or by eye in the case of subjectively

analyzed fields. In view of this, discussion of the merits of various quadrature schemes becomes questionable. However, one may take the attitude that any numerical operation performed on the data fields which has internal errors only serves to degenerate the information content in the data and thus one should be as careful as possible about any numerical operation, i. e. minimize sources of error which are controllable.

The Linear Balance Equation.

The linear or geostrophic balance equation is

$$f \nabla^2 \psi + \frac{1}{a^2} \frac{\partial f}{\partial \theta} \frac{\partial \psi}{\partial \theta} = g \nabla^2 Z \quad 4.11$$

where  $\psi$  is a stream function,  $Z$  is the geopotential height field,  $f$  is the Coriolis parameter  $2\Omega \cos \theta$ ,  $\Omega$  is the angular velocity of the earth's rotation,  $g$  is the acceleration due to gravity. Equation 4.11 may be rewritten to the following form

$$\cos \theta \nabla^2 \psi - \sin \theta \frac{\partial \psi}{\partial \theta} = \frac{g}{2\Omega} \nabla^2 Z \quad 4.12$$

where  $\nabla^2 = a^2 \nabla^2$ . If  $\psi$  is expanded in terms of spherical harmonics

$$\psi = \frac{g}{2\Omega} \sum_{m=0}^{\infty} \sum_{n=m}^{\infty} (\alpha_n^m \cos m\lambda + \beta_n^m \sin m\lambda) P_n^m$$

and this expansion, as well as the expansion for the height field is inserted into the balance equation, the following recurrence relation is obtained

$$n(n+2)\epsilon_{n+1}^m \begin{Bmatrix} \alpha_{n+1}^m \\ \beta_{n+1}^m \end{Bmatrix} + (n-1)(n+1)\epsilon_n^m \begin{Bmatrix} \alpha_{n-1}^m \\ \beta_{n-1}^m \end{Bmatrix} = n(n+1) \begin{Bmatrix} A_n^m \\ B_n^m \end{Bmatrix} \quad 4.13$$

$$\text{where } \epsilon_n^{m^2} = \frac{(n-m)(n+m)}{(2n-1)(2n+1)}$$

Equation 4.13 is the same (apart from constants) as obtained by Eliassen and Machenhauer (1965).

In practice the representation of the height field must be truncated at some point. In this study the truncation was such that each set of waves corresponding to a given value of  $m$  contained 17 components. So that for  $m=0$ ,  $n$  ranges from 1 to 17; for  $m \neq 0$ ,  $n$  ranges from  $m$  to  $m+16$ . For anti-symmetric non-zonal components ( $n-m = \text{odd}$ ) and symmetric zonal components ( $n = \text{even}, m=0$ ) of the stream function, the recurrence relation is self-starting and the only problem is the truncation. For symmetric non-zonal components ( $n-m = \text{even}$ ) and antisymmetric zonal components ( $n = \text{odd}, m=0$ ) some condition must be applied to obtain a solution.

There are two physical properties of horizontal stream flow that are easily expressed in terms of the spherical harmonic

Table 4.5: Solution of linear balance equation in the spectral domain.

TYPE	MODE	BOUNDARY CONDITION	RECURRENCE RELATION AND RANGE OF INDEX	IMPLIED CONDITION ON HEIGHT FIELD
Zonal	Symmetric	$3\epsilon_2^{\circ}\alpha_2^{\circ} = 2A_1^{\circ}$	$n(n+2)\epsilon_{n+1}^{\circ}\alpha_{n+1}^{\circ} = n(n+1)A_n^{\circ}$ $-(n-1)(n+1)\epsilon_n^{\circ}\alpha_{n-1}^{\circ}$ for $n=3,5,\dots,15$	$17A_{17}^{\circ} = 6\epsilon_{17}^{\circ}\alpha_{16}^{\circ}$
Zonal	Anti-symmetric	$\alpha_{17}^{\circ} = 0$	$(n-1)(n+1)\epsilon_n^{\circ}\alpha_{n-1}^{\circ} = n(n+1)A_n^{\circ}$ $-n(n+2)\epsilon_{n+1}^{\circ}\alpha_{n+1}^{\circ}$ for $n=16,14,\dots,2$	
Non-zonal	Symmetric	$\begin{Bmatrix} \alpha_{m+16}^m \\ \beta_{m+16}^m \end{Bmatrix} = 0$	$(n-1)(n+1)\epsilon_n^m \begin{Bmatrix} \alpha_{n-1}^m \\ \beta_{n-1}^m \end{Bmatrix} = n(n+1) \begin{Bmatrix} A_n^m \\ B_n^m \end{Bmatrix}$ $-n(n+2)\epsilon_{n+1}^m \begin{Bmatrix} \alpha_{n+1}^m \\ \beta_{n+1}^m \end{Bmatrix}$ for $n=m+15 \dots m+1$	
Non-zonal	Anti-symmetric	$\begin{Bmatrix} \alpha_{m+1}^m \\ \beta_{m+1}^m \end{Bmatrix} =$ $\frac{m+1}{(m+2)\epsilon_{m+1}^m} \begin{Bmatrix} A_m^m \\ B_m^m \end{Bmatrix}$	$n(n+2)\epsilon_{n+1}^m \begin{Bmatrix} \alpha_{n+1}^m \\ \beta_{n+1}^m \end{Bmatrix} = n(n+1) \begin{Bmatrix} A_n^m \\ B_n^m \end{Bmatrix}$ $-(n-1)(n+1)\epsilon_n^m \begin{Bmatrix} \alpha_{n-1}^m \\ \beta_{n-1}^m \end{Bmatrix}$ for $n=m+2 \dots m+14$	$\begin{Bmatrix} A_{m+16}^m \\ B_{m+16}^m \end{Bmatrix} =$ $\frac{m+15}{(m+16)\epsilon_{m+16}^m} \begin{Bmatrix} \alpha_{m+15}^m \\ \beta_{m+15}^m \end{Bmatrix}$

amplitudes of the stream function. They are the mean horizontal kinetic energy  $\bar{E}$  and the mean square vorticity  $\bar{\zeta}^2$

$$\bar{E} = \frac{1}{4\pi} \int_S \frac{1}{2} (\mathbf{V} \cdot \mathbf{V}) dS = \frac{1}{4} \left( \frac{g}{2\Omega a} \right)^2 \sum_{n=1}^{\infty} \sum_{m=0}^n n(n+1) \frac{(\alpha_n^{m^2} + \beta_n^{m^2})}{2} (1 + \delta_0^m)$$

4.14

$$\bar{\zeta}^2 = \frac{1}{4\pi} \int_S (\nabla^2 \psi)^2 dS = \frac{1}{2} \left( \frac{g}{2\Omega a^2} \right)^2 \sum_{n=1}^{\infty} \sum_{m=0}^n [n(n+1)]^2 \frac{(\alpha_n^{m^2} + \beta_n^{m^2})}{2} (1 + \delta_0^m)$$

where  $\delta_0^m = 1$  if  $m = 0$ ;  $\delta_0^m = 0$  otherwise, and  $\beta_n^0 \equiv 0$  where  $a$  is the radius of the earth.

In barotropic flow both these quantities are conserved. It seems reasonable to expect that, in any representation of the horizontal wind field, these quantities should be well defined. It can be shown that neither the series for  $\bar{E}$  nor the series for  $\bar{\zeta}^2$  (4.14) converges without a zero in the recurrence relation beyond the last of the height components. This then gives us a condition that may be applied to the non-starting recurrence set and a modification that must be made (implicitly or explicitly) to the height field in the self-starting recurrence set.

The system and the boundary condition are summed up in Table 4.5. The system is reversible in the sense that once having modified the last component of the height field (for a given value of  $m$ ), then to solve the balance equation for  $\bar{Z}$  from the computed stream function components regenerates the initial height field components.

The system and boundary conditions have a simple physical interpretation for the zonal components. For symmetric zonal components the condition imposed on the height field is that  $\frac{d\bar{z}}{d\theta} = 0$  at the equator (where  $\bar{z}$  denotes the longitudinal mean at a given latitude), so that geostrophy for the zonal current can be applied everywhere. For antisymmetric zonal components the boundary condition can be shown to be equivalent to requiring that the mean angular momentum of the zonal current (measured by  $\alpha'_j$ ) be equal to the mean angular momentum of the geostrophically computed zonal current. (This condition was used by Eliassen and Machenhauer in an explicit manner for the northern hemisphere). Presumably equivalent conditions hold for non-zonal components but their precise nature has not yet been determined.

There is another feature of the solution to the linear balance equation which can cause difficulty; error propagation from smaller scales to larger scales during the determination of symmetric non-zonal components and antisymmetrical zonal components. Say the balance equation has been solved for a given set of height field components. One may consider any one value of  $m$ , as the argument still holds. Consider  $m$  equal to 1. Then  $(\alpha'_n, \beta'_n)$  are the stream functions corresponding to the set  $(A'_n, B'_n)$  of height components and they are related by the recurrence relations given in Table 4.5. If a small change,  $\Delta$ , is made in  $A'_{i7}$  (or  $B'_{i7}$ ), then the stream functions amplitudes  $\alpha'_n$  (or  $\beta'_n$ ) will be

changed. If  $d'_n$  denotes the change in  $\alpha'_n$  we have

$$d'_{15} = \frac{16}{15} \frac{\Delta}{\epsilon'_{15}} ; \quad d'_{13} = -\frac{14 \cdot 16}{15 \cdot 13} \frac{\epsilon'_{15}}{\epsilon'_{14}} d'_{15}, \text{ etc.}$$

or in general 
$$d'_{n-1} = \frac{-n(n+2)}{(n-1)(n+1)} \frac{\epsilon'_{n+1}}{\epsilon'_n} d'_{n+1}$$

Now 
$$\frac{\epsilon'_{n+1}}{\epsilon'_n} = \left[ \frac{n(n+2)(2n-1)}{(n+1)(n-1)(2n+3)} \right]^{\frac{1}{2}} > 1 \quad \text{for all } n$$

Thus 
$$\frac{d'_{n-1}}{d'_{n+1}} > 1 \quad \text{for all } n$$

so that a change in the last component of the height field is propagated to the larger scale components and amplified. In the case of the total amplification to component  $\alpha'_1$  is approximately by a factor 25. In simpler terms it means that each of the stream functions so computed is just a linear combination of the height field components of a smaller scale, but that the weight that a particular height field component has in determining the stream component increases for an increasing difference in scale (as represented by the index  $n$ ). In contrast; for antisymmetric stream fields components, an error in one of the height field components is damped in the iteration.

## Hemispheric Analyses

The above methods which apply to global analysis may be easily specialized to perform hemispheric analyses. The simplest way to modify the analysis is to assume that the height field is either symmetric or antisymmetric with respect to the equator. This may be done explicitly in a general analysis programme or implicitly in a purely hemispheric analysis programme. If the symmetric mode is chosen there are no difficulties. If the antisymmetric mode is chosen, Gibbs phenomenon can arise because antisymmetry implies the vanishing of all Fourier components at the equator. This may be avoided by subtracting the equatorial value of  $A^0$  from the  $A^0/5$  at the rest of the latitudes and setting  $A^m$  and  $B^m$  equal to zero at the equator. The Fourier amplitudes are small in the equatorial regions and thus this process does not generate much error. Indeed, one may interpolate the Fourier amplitudes linearly to zero from some higher latitude without seriously affecting the results.

## The Details of the Method Used

The data points were spaced at every five degrees of latitude (except latitudes  $\pm 85^\circ$ ) including the equator and every ten degrees longitude including the Greenwich meridian. The data consisted of geopotential height values in decametres at each of the grid points of the 500 millibar surface for the month of September

1957. The data source and methods of synoptic analysis and extraction are described by Lui stro (1964) and Steinberg (1965).

Fourier analyses were performed at all data latitudes; the amplitudes at  $\pm 85$  degrees latitude were obtained by averaging those at the poles and  $\pm 80$  degrees. These Fourier amplitudes were then analyzed into coefficients of the associated Legendre functions using the trapezoidal rule for  $m \neq 0$  and Simpson's rule for  $m = 0$ . The Legendre functions were generated at the data latitudes using the following set of recursion formulae.

$$P_{m+1}^{m+1} = (2m+3)^{\frac{1}{2}} \sin \theta P_m^m$$

$$P_{n+1}^m = \left[ \frac{(2n+1)(2n+3)}{(n+1)^2 - m^2} \right]^{\frac{1}{2}} \left\{ \cos \theta P_n^m - \left[ \frac{n^2 - m^2}{4n^2 - 1} \right]^{\frac{1}{2}} P_{n-1}^m \right\} \quad 4.15$$

where  $P_0^0 = \frac{1}{\sqrt{2}}$ ;  $P_n^m \equiv 0$   $m > n$

The Fourier analysis (for this data grid) permits the definition of seventeen waves and a mean height around a latitude circle. Since there are 37 data latitudes (35 for non-zonal components because the values at the poles are identically zero) the system permits a maximum of 37 zonal components and 35 non-zonal components to be defined for each Fourier wave number. In this study each wave was analyzed into seventeen coefficients of the Legendre functions. All of these waves are not, of course, significantly above the noise level; but presumably a complete

Table 4.6: The distribution of the variance of the mean of a height analysis of 100 sets of random fields.  
 Theoretical variance of the mean = 0. ; values have been multiplied by  $10^4$ .

j \ m	0	1	2	3	4	5	6	7	8	9	10	11	12	13	14	15	16	17
1	3	7	12	5	1	16	1	1	5	4	6	12	14	16	4	2	16	4
2	12	10	5	4	10	6	4	32	9	4	5	2	0	4	2	5	13	11
3	3	20	3	5	1	7	10	5	4	2	0	9	17	21	1	0	10	7
4	4	5	4	11	7	2	34	4	6	11	1	8	7	30	2	12	3	12
5	6	4	1	8	16	31	3	2	7	0	8	18	10	8	7	3	13	0
6	1	32	4	3	12	9	1	2	1	6	18	5	2	7	1	9	2	1
7	10	12	11	9	6	1	8	5	2	6	3	7	1	12	3	6	3	1
8	52	10	0	5	15	6	5	8	17	12	3	2	5	1	2	5	12	12
9	10	11	12	6	12	0	7	10	1	1	7	7	6	10	6	16	5	7
10	195	0	1	1	16	5	10	9	11	13	1	7	15	25	8	9	3	1
11	2	5	2	3	13	8	2	1	3	1	9	17	15	11	18	22	8	6
12	751	0	23	1	4	10	9	3	5	8	0	8	7	8	0	7	9	5
13	31	9	1	2	2	1	7	4	3	2	6	0	1	0	2	7	1	0
14	1295	0	20	24	4	1	11	13	3	1	0	3	5	2	2	4	5	5
15	11	5	7	3	2	6	6	8	7	9	9	1	3	9	10	20	9	5
16	2542	2	1	3	1	2	10	6	1	1	9	0	4	0	33	10	6	13
17	2	7	3	2	11	4	8	4	5	7	3	5	4	21	1	2	17	20

Table 4.7: The distribution of the mean variance of a height analysis of 100 sets of random fields.

Theoretical mean variance = 39.2; values have been multiplied by  $10^4$ .

j	m	0	1	2	3	4	5	6	7	8	9	10	11	12	13	14	15	16	17
1		540	843	851	932	921	959	906	959	826	985	1015	942	884	1029	972	825	804	936
2		502	732	826	677	844	888	1009	869	941	806	919	895	949	1044	855	856	862	835
3		688	618	798	809	699	839	911	838	861	726	762	960	940	814	877	881	917	918
4		800	600	615	740	715	805	852	733	750	798	939	638	916	897	959	761	931	935
5		600	627	512	624	807	850	658	706	797	873	1034	748	840	792	757	884	836	807
6		634	571	595	679	700	782	759	795	708	734	725	788	806	766	771	795	781	846
7		624	714	695	661	605	736	661	660	770	769	711	680	879	709	873	704	908	661
8		730	647	563	629	637	819	745	708	698	665	795	800	776	649	845	828	747	1015
9		751	579	582	636	648	755	759	602	797	790	847	653	886	831	657	822	812	687
10		708	625	604	535	645	757	588	715	713	723	626	770	583	744	722	845	763	863
11		555	580	524	652	556	754	660	745	732	633	714	698	715	599	812	902	688	810
12		486	508	634	569	690	795	748	656	736	679	646	754	824	651	698	849	781	774
13		675	611	644	604	680	701	684	691	708	713	755	636	772	795	772	791	732	784
14		659	556	599	464	546	753	652	631	716	670	514	816	767	641	686	693	798	832
15		779	608	632	713	582	587	692	603	708	849	784	700	582	739	721	596	823	644
16		667	601	605	581	631	725	632	727	562	558	682	633	780	576	734	745	713	750
17		1252	593	574	583	619	553	684	682	802	640	766	826	673	593	751	665	728	739

analysis will thus aid in the determination of the noise level.

#### The Random Error Noise Level

It has been shown (Godson 1959) that random errors tend to produce a "white" spectrum when subjected to a Fourier analysis. (A "white" spectrum is one in which the variance is constant for all wave numbers). It seems reasonable that this same property should hold in the case of spherical harmonic analysis. To test this property, 100 sets of Fourier coefficients at all data latitudes were generated from a standard random number generator programme. The random numbers had a normal distribution with a standard deviation of 25/17 units. Five hundred was added to the mean values at latitude circles (i. e. the  $A^{\circ}$ ). These generated Fourier data were then analyzed into Legendre polynomials (using the same analysis scheme as was used on the real data). The variance of the mean and the mean variance of the 100 samples were computed for each wave component and are shown in Tables 4.6 and 4.7. The results indicate that the spectrum is quite closely "white". The bias to higher variances and mean values for large values of  $\eta$  is due to the increasing bias in the analysis programme for large values of  $\eta$ . This bias in the analysis is especially large for the zonal components where for some components the mean variance is smaller than the variance of the mean. Theoretically, if the spectrum is exactly white then the mean variance in any component

Table 4.8: Variance of mean values of stream function amplitudes obtained from 100 sets of random height fields. Values have been multiplied by  $10^2$ .

j	m	0	1	2	3	4	5	6	7	8	9	10	11	12	13	14	15	16	17
1		7415	255	45	76	52	7	115	28	24	6	40	3	2	7	19	18	83	32
2		0	0	0	0	0	2	0	0	1	1	1	3	3	4	1	1	5	1
3		1115	26	11	21	14	4	35	18	7	1	16	3	1	2	10	3	21	5
4		0	1	0	1	0	0	0	0	0	1	1	1	7	9	0	0	0	3
5		424	9	5	7	5	1	16	11	6	0	11	1	2	2	9	2	12	4
6		1	1	0	1	1	2	1	0	1	1	0	1	7	9	1	0	1	2
7		231	2	4	4	2	0	10	8	5	0	3	2	1	3	8	3	8	4
8		0	0	0	2	1	1	1	0	1	1	1	2	4	6	0	1	0	3
9		114	0	3	3	0	0	6	3	1	1	1	2	1	2	6	1	4	2
10		0	0	1	0	2	1	1	1	1	1	1	2	5	5	1	4	1	4
11		130	0	1	3	0	1	2	4	0	0	1	2	0	0	3	1	4	1
12		1	1	1	1	4	2	1	1	0	0	0	4	4	7	1	4	2	6
13		21	0	1	2	0	0	2	2	0	0	1	0	1	0	2	0	1	1
14		0	1	1	1	3	2	2	2	0	0	1	3	3	6	1	5	2	5
15		116	0	0	0	0	0	0	0	0	0	0	0	0	0	2	1	0	1
16		1	1	1	1	4	1	3	3	0	0	2	2	2	3	2	9	1	4
17		0	0	0	0	0	0	0	0	0	0	0	0	0	0	0	0	0	0

Table 4.9: Distribution of mean variance of stream function amplitudes obtained from 100 sets of random height fields. Values have been multiplied by 10

j	m	0	1	2	3	4	5	6	7	8	9	10	11	12	13	14	15	16	17
1		1994	2552	1072	571	490	488	404	404	393	340	317	393	357	308	393	293	415	320
2		1	2	3	5	7	9	11	13	13	17	20	20	21	26	24	27	25	31
3		289	272	224	147	142	157	134	140	138	130	108	152	121	118	149	112	156	124
4		2	3	4	6	7	9	11	12	13	15	17	20	22	24	27	26	30	30
5		106	102	95	70	72	82	71	74	75	72	58	87	68	65	86	69	85	73
6		4	4	5	6	8	10	10	11	12	15	16	18	21	20	26	27	31	25
7		53	51	47	39	43	47	41	45	48	44	36	53	44	41	55	46	50	46
8		6	6	6	7	9	11	10	12	13	14	17	18	22	20	20	22	32	24
9		30	28	26	22	27	28	27	28	28	28	23	36	29	27	34	28	31	30
10		8	7	7	8	10	13	11	12	15	16	19	18	23	22	25	20	30	26
11		17	16	14	14	16	17	17	17	16	17	14	21	19	15	22	18	21	19
12		9	8	8	8	9	13	13	15	15	17	18	17	24	23	30	22	32	29
13		10	9	7	8	8	10	8	10	9	8	8	11	12	8	11	10	12	13
14		10	9	10	9	10	15	15	16	15	19	19	16	25	24	31	23	31	29
15		3	3	3	3	3	3	3	4	3	3	4	3	4	3	4	4	4	5
16		13	11	11	11	10	16	15	17	17	22	22	16	25	26	30	23	31	32
17		0	0	0	0	0	0	0	0	0	0	0	0	0	0	0	0	0	0

should be the same, and then we can compute this value by the following consideration.

There are 37 data points entering into the analysis of each Fourier wave. For all non-zonal waves, the polar values are not considered since the representation has no degrees of freedom at the poles (i. e.  $P_n^m(0) = P_n^m(\pi) \equiv 0$  if  $m \neq 0$ ). Thus the total number of degrees of freedom in the field is  $35 \times 17 + 37 = 632$ . For a "white" spectrum then the theoretical field variance will be divided equally into each degree of freedom, so that the variance in any component should be  $= 39.2/632 = 620 \times 10^{-4}$ .

This number agrees quite well with the values given in Table 4.7. The error level in the analysis of real data can be estimated then by considering the distribution of variance in the smaller scales. This involved the estimation of the point where the spectrum becomes "white" so that the error level obtained must be considered as only an estimate.

It is also of great interest to determine the effect of random errors in the geopotential height field on the stream functions obtained through the linear balance equation. To determine this effect the sample of random height fields was put through the linear balance equation. The statistics of the stream functions obtained are given in Tables 4.8, 4.9. The zero values in the Tables for  $j = 17$  are just the boundary condition imposed on the solution of the linear balance equation. Generally the tables show that the

Table 4.10: Distribution of the variance of the mean height field in  $DM^2$ . Values have been multiplied by  $10^2$

j \ m	0	1	2	3	4	5	6	7	8	9	10	11	12	13	14	15	16	17
1	11110	102	28	1	8	0	0	0	0	0	0	0	0	0	0	0	0	0
2	52761	140	0	3	14	26	9	2	1	1	0	0	0	0	0	0	0	0
3	1194	133	57	5	30	3	6	4	1	0	1	0	0	0	0	0	0	0
4	2416	213	158	17	23	20	5	2	0	2	0	0	0	0	0	0	0	0
5	52	27	10	15	68	5	7	4	0	0	0	0	0	0	0	0	0	0
6	396	32	45	2	22	11	1	0	0	0	0	0	0	0	0	0	0	0
7	2	78	25	1	39	7	4	0	0	0	0	0	0	0	0	0	0	0
8	2	135	85	11	5	4	1	1	0	0	0	0	0	0	0	0	0	0
9	92	51	27	3	7	0	0	2	0	0	0	0	0	0	0	0	0	0
10	13	36	36	5	2	1	0	1	0	0	0	0	0	0	0	0	0	0
11	0	5	3	1	0	0	0	0	0	0	0	0	0	0	0	0	0	0
12	5	11	18	2	0	0	0	0	0	0	0	0	0	0	0	0	0	0
13	2	3	1	2	0	1	0	0	0	0	0	0	0	0	0	0	0	0
14	19	3	0	0	0	0	0	0	0	0	0	0	0	0	0	0	0	0
15	2	3	0	0	0	0	0	0	0	0	0	0	0	0	0	0	0	0
16	21	1	0	0	0	0	0	0	0	0	0	0	0	0	0	0	0	0
17	0	2	0	1	0	0	0	0	0	0	0	0	0	0	0	0	0	0

Table 4.11: Distribution of mean variance of the height field in  $DM^2$ . Values have been multiplied by  $10^2$

j	m	0	1	2	3	4	5	6	7	8	9	10	11	12	13	14	15	16	17
1		11287	135	52	17	22	15	10	8	3	1	1	0	0	0	0	0	0	0
2		52792	193	52	36	67	62	37	24	11	9	3	2	1	1	0	0	1	0
3		1283	197	130	80	120	60	47	37	15	9	7	3	3	2	1	1	0	0
4		2452	311	268	106	207	87	60	45	17	16	6	3	2	2	1	1	1	1
5		85	106	78	140	157	82	41	27	17	14	7	4	3	2	1	1	0	0
6		420	79	195	67	127	59	40	27	12	7	5	4	3	1	1	1	1	1
7		33	145	84	76	80	33	27	19	9	9	4	2	2	2	1	0	0	0
8		29	174	134	39	28	24	19	12	7	4	2	3	1	1	1	1	1	1
9		125	79	54	31	31	16	9	12	4	4	3	1	1	1	1	1	0	0
10		33	60	72	21	19	13	10	5	4	4	2	1	1	0	0	0	1	1
11		29	30	28	15	15	10	5	6	2	2	1	1	1	1	1	1	0	0
12		12	30	35	15	10	6	4	3	3	2	2	1	1	0	0	0	1	1
13		6	20	12	10	6	5	3	3	2	1	1	0	0	1	1	1	0	0
14		24	12	8	4	7	5	1	1	2	1	1	1	1	0	0	0	0	0
15		4	9	8	5	3	4	2	2	1	1	0	0	0	1	0	0	0	0
16		24	5	4	4	4	3	1	1	1	1	1	1	1	0	0	0	0	0
17		1	5	4	4	3	2	1	1	0	0	0	0	0	0	0	1	0	0

variance of the mean of the stream function is approximately 100 times greater than for the height field. However, the mean variance is also different by the same factor, so that this is consistent with the numerical values of the stream field components being on the average 10 times greater than the height amplitudes. However, the distribution of variance is quite different.

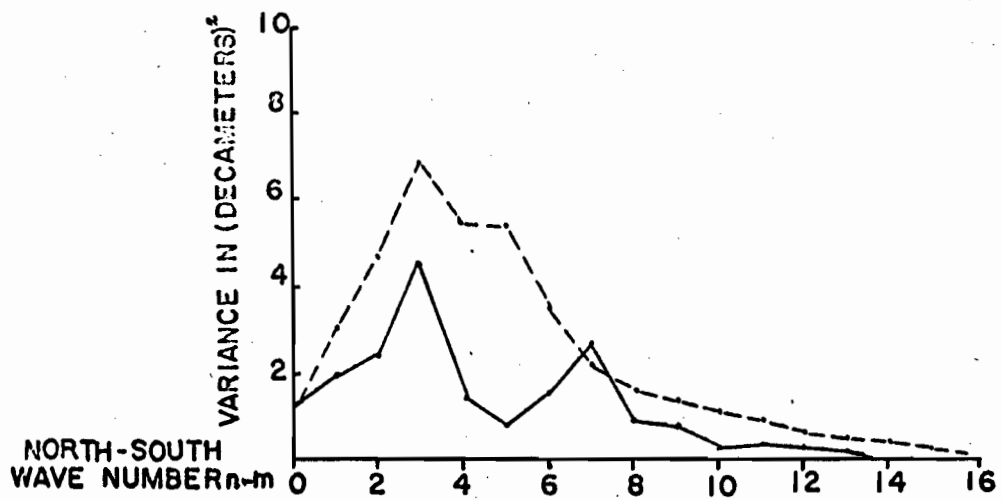
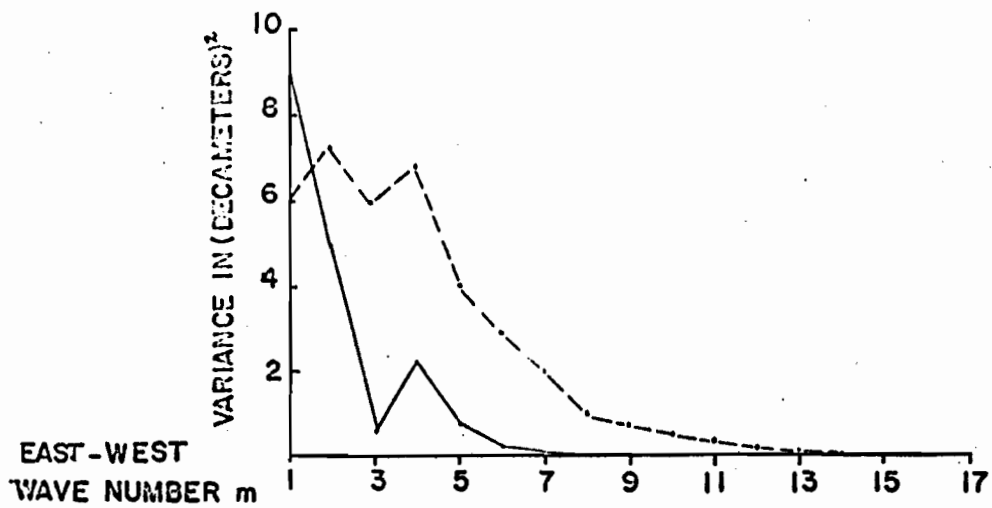
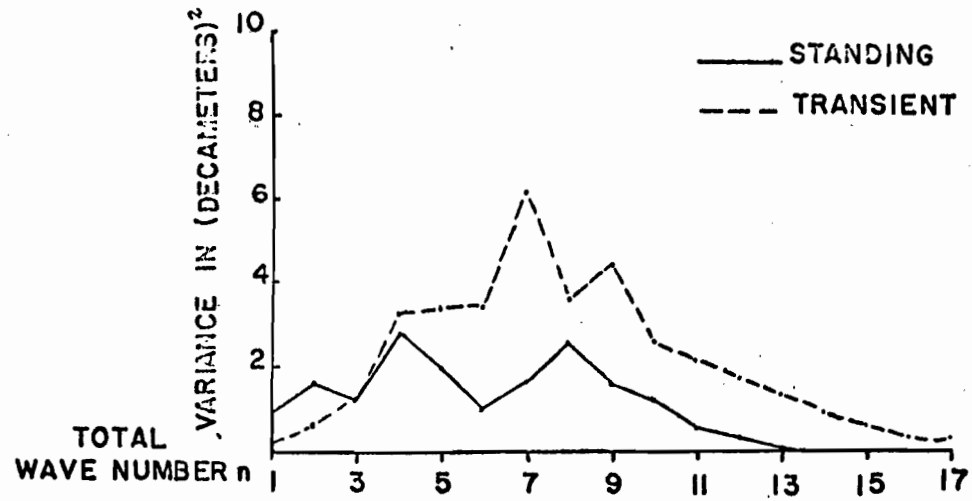
The most obvious feature is the dependence on parity. The variance in symmetric components is generally much larger than the variance in the antisymmetric components. The feature of error amplification in the symmetric components is thus well illustrated in these tables. On the basis of these tables an estimate of the noise level in each of the components may be obtained, and at the very least applied to the long term statistics of the flow.

The Statistics of the Flow at 500 mb for Sept. 1957

The Geopotential Height Field

In Tables 4.10, 4.11 the variance of the mean and the mean variance of the geopotential height field for the month of September 1957 are shown as distributed over the components. In these tables (as in others of the same type in this section) index  $j = n - m + 1$  if  $m \neq 0$  and  $j = n$  if  $m = 0$ . These tables show that the great majority of the variance is contained in the zonal components; 97% for the mean field and 91% for the mean variance. However, the zonal components contribute very little to the transient

Figure 4.1: Distribution of variance of height field for eddy components as a function of the three wave numbers (decametres)<sup>2</sup>.



part of the variance since the variance of the mean is 99% of the mean variance, and in fact the contribution of the zonal components to the transient part of the variance is only about 14%.

Disregarding the zonal components, the main contributions of variance come from the low wave numbers or large scale waves. In a spherical harmonic representation there are three wave numbers one may consider. The wave number  $n$  and its corresponding wavelength  $L^2 = \frac{4\pi^2 a^2}{n(n+1)}$  is the two dimension wavelength that enters as the dynamically significant wavelength in any analysis based on spherical harmonics. The wave number,  $m$ , measures the wavelength of a disturbance around a latitude circle, and  $n-m$  measures the wavelength in a north-south direction. For example, for a given  $n$  (i. e. two-dimensional wavelength) one may have a system which is elongated along a latitude circle (low  $m$ , high  $n-m$ ) or elongated along a meridian (low  $n-m$ , high  $m$ ). The wave number  $n-m$  also measures the symmetry or asymmetry of the flow with respect to the equator according to whether it is even or odd respectively.

In Figure 4.1 the distributions of variance for the standing (monthly mean) and the transient (mean square minus square of the mean) parts of the height field (excluding the zonal components) are shown as a function of the three wave numbers. The distribution over  $n$  shows a broad maximum in the transient part ranging from  $n = 4 - 10$  which corresponds to a wavelength range of approximately

9000 km to 4000 km. The standing part shows maxima at  $\eta = 4$  and  $\eta = 8$  and a relative minimum at  $\eta = 6$ .

The distribution over  $m$  shows that the variance of the mean field is largely contained in waves with  $m=1$  and  $2$ . There is a secondary maximum at  $m=4$ . The transient part is much more equally distributed over the first five wave numbers.

The distribution over the north-south wave number indicates that the mean field is more largely asymmetric than symmetric with respect to the equator (maxima at  $\eta-m=3$ , and  $\eta-m=7$ ). Even the transient part has its largest variances in odd components but the general picture is not one of dominance.

These results are in agreement with those of Steinberg (1965) who analyzed the same data using a different analysis technique.

#### Noise Level in the Height Field Analysis

In accordance with the experiment described in the previous section one may expect that random errors will contribute equally to the mean variance of each component in the system. Thus if one can determine where the variance approaches some constant value, then an estimate of the random noise level may be made. An inspection of Table 4.7 shows that although the mean variance shows a tendency to level off the values are still monotonically decreasing. This may indicate that the noise level from purely random errors is less than  $0.01 \text{ DM}^2$ . Indeed the random noise

level consisted with a standard deviation of an individual grid point value of  $\pm 2$  DM ( $\pm 65$  feet) is given by  $\frac{4}{632} = .006 \text{ DM}^2$ . This is not to say that these components whose variance is greater than  $.006 \text{ DM}^2$  are significant, but rather that the noise level may be determined by another cause.

Each spherical harmonic wave is in principle a global entity. Real highs and lows, especially on the smaller scale, are not global entities, but in this context localized perturbations (e. g. a hurricane). The process of analysis will misinterpret these perturbations and form global waves which when added together reproduce the localized variations. As far as the distribution of variance of the amplitudes necessary to represent a localized perturbation is concerned, one may expect that those components whose wavelengths are similar to the scale of the localized perturbation will have a large part of it, and the variance will decrease for smaller and larger scales. This process would tend then to produce a distribution of variance which decreases monotonically for decreasing wavelength since it would add little to the variance contained in the large scale waves. Thus one might expect that if the energy spectrum of the waves was obtained that the energy contained in the smaller scales of motion would be approximately equal. Thus seems to be the case as will be shown from the energy spectrum derived through the linear balance equation.

A determination of the noise level on this basis is

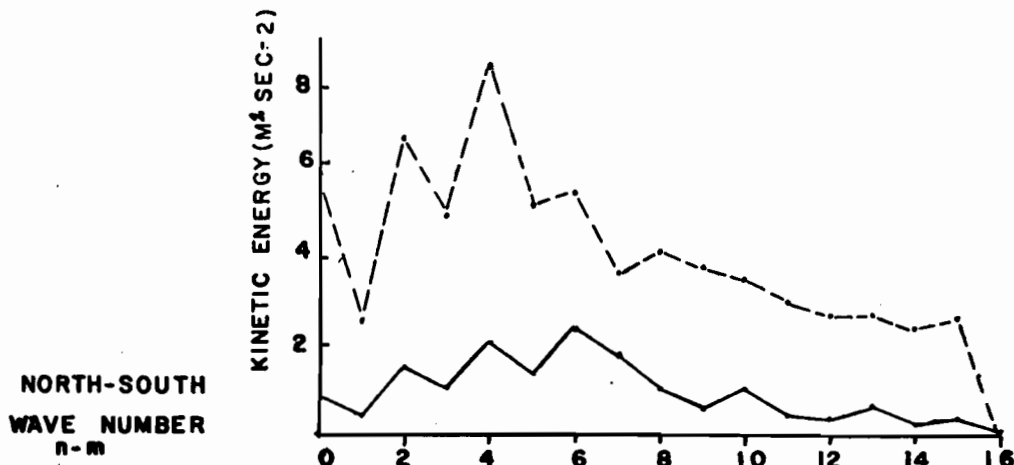
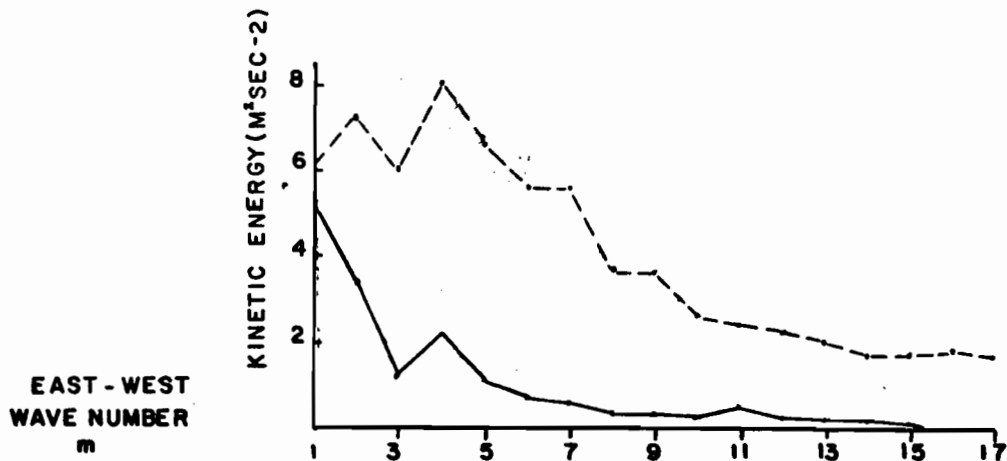
Table 4.12: Distribution of kinetic energy of the mean (metres/sec)<sup>2</sup>; zonal values X10<sup>2</sup>; other X10<sup>3</sup>

j <sup>m</sup>	0	1	2	3	4	5	6	7	8	9	10	11	12	13	14	15	16	17
1	1555	212	33	73	336	116	20	11	4	19	35	25	28	0	5	7	7	4
2	619	76	76	6	100	11	8	5	10	6	40	5	4	28	2	7	7	13
3	2595	83	27	130	271	329	208	100	70	117	67	38	26	15	5	4	21	13
4	37	237	115	38	274	29	132	120	48	46	16	15	18	47	17	9	0	1
5	295	824	920	93	44	41	0	1	12	11	21	90	15	12	2	6	2	2
6	0	27	341	73	503	207	23	112	7	20	3	49	10	8	4	1	2	0
7	5	1310	413	100	277	150	74	2	8	8	1	25	6	5	1	1	1	4
8	2	1060	145	188	139	60	78	8	35	0	5	36	1	21	10	3	5	1
9	0	163	549	79	68	14	3	86	32	3	1	14	9	12	12	4	0	3
10	228	8	201	92	31	17	58	73	13	8	2	35	8	25	3	23	3	9
11	39	569	320	24	9	26	2	10	0	5	11	10	1	4	4	4	0	2
12	238	150	28	15	22	10	37	44	7	8	2	17	0	11	0	13	8	4
13	4	30	89	90	13	4	7	18	13	6	1	8	5	1	0	1	4	4
14	159	389	88	104	7	20	50	18	1	1	1	17	3	10	10	11	1	1
15	132	53	10	28	49	4	14	10	6	2	10	9	2	2	1	0	2	5
16	251	73	55	90	2	7	60	42	8	4	0	23	1	10	4	3	1	6
17	0	0	0	0	0	0	0	0	0	0	0	0	0	0	0	0	0	0

Table 4.13: Distribution of mean energy (metres/sec)<sup>2</sup>; zonal values X 10<sup>2</sup>; other X 10<sup>3</sup>

j <sup>m</sup>	0	1	2	3	4	5	6	7	8	9	10	11	12	13	14	15	16	17
1	1590	622	403	371	865	521	399	519	355	412	308	363	314	275	241	227	247	277
2	629	100	137	113	277	344	381	394	243	141	194	128	117	96	71	54	95	99
3	2626	442	420	459	1110	1096	987	823	543	642	294	284	244	237	213	200	171	161
4	53	354	341	474	1007	676	601	634	404	391	267	207	188	177	126	92	80	85
5	346	1571	1862	904	1662	808	780	678	403	386	340	306	305	208	165	156	145	116
6	18	352	891	779	1076	947	456	465	309	342	255	215	126	134	97	65	100	101
7	35	1758	1371	559	928	708	569	441	279	237	172	260	136	142	117	125	136	120
8	14	1338	489	634	629	335	396	392	234	174	131	154	125	133	96	77	116	86
9	27	724	884	441	452	415	396	426	256	184	130	181	134	113	117	138	93	122
10	270	524	656	465	411	379	309	308	168	188	124	115	124	142	104	125	134	119
11	64	974	1193	297	387	253	192	167	124	158	145	141	72	80	86	105	86	83
12	257	591	452	253	256	255	177	310	184	133	115	106	82	90	74	87	83	90
13	18	380	391	434	325	249	157	197	135	125	101	104	83	80	75	100	71	58
14	171	732	475	376	235	227	214	187	165	123	102	84	99	109	83	89	107	89
15	146	307	294	303	359	232	139	130	117	85	68	75	57	54	41	82	55	61
16	260	463	366	422	186	174	202	165	123	136	85	128	96	136	96	96	105	92
17	0	0	0	0	0	0	0	0	0	0	0	0	0	0	0	0	0	0

Figure 4.2: Distribution of the horizontal mean kinetic energy per unit mass over the three wave numbers (metres/sec)<sup>2</sup>.

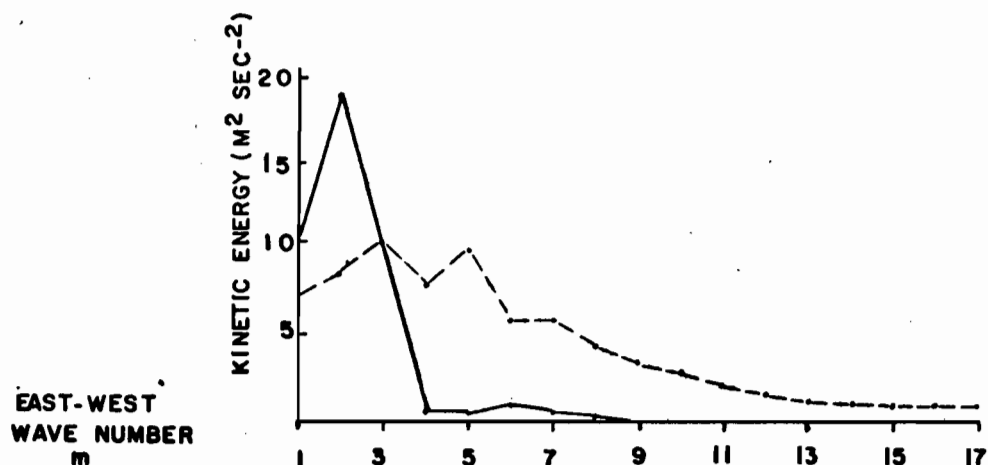
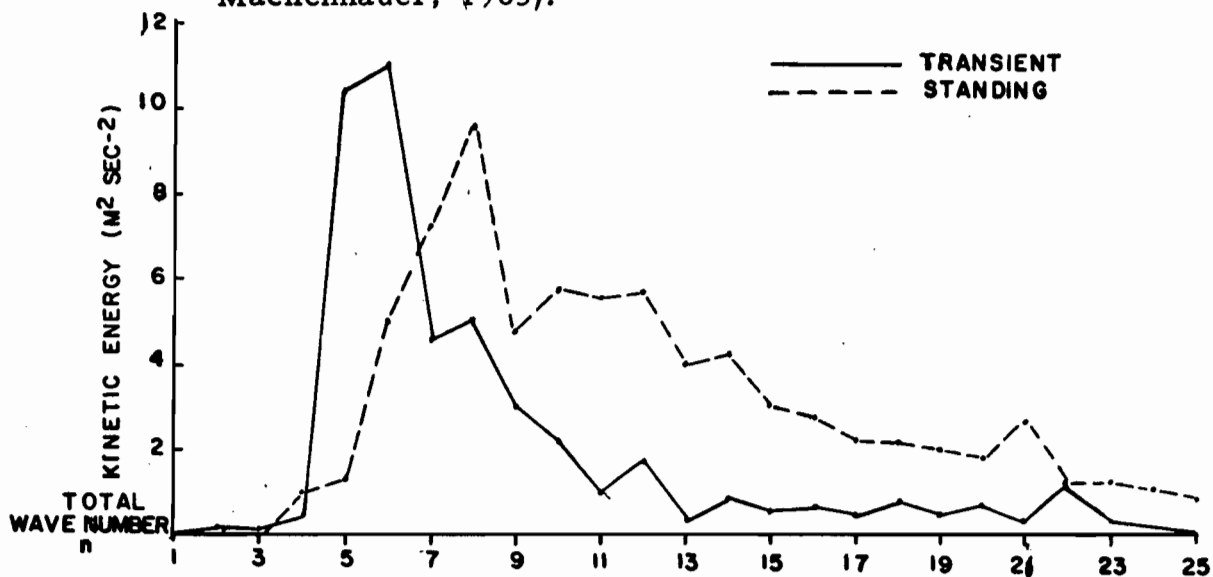


essentially equivalent to deciding on a noise level by requiring continuity in time. Steinberg (1965) used continuity in time to estimate the noise level at  $0.6 \text{ DM}^2$  which is consistent with a random error with a standard deviation of  $\pm 6 \text{ DM}$  or  $\pm 200 \text{ feet}$ ! This hardly seems reasonable; so that some process similar to that described above must occur in the analysis.

#### The Stream Function

In Tables 4.12, 4.13 the horizontal mean kinetic energies per unit mass are shown as distributed over the components. Table 4.12 gives the kinetic energy of the mean and Table 4.13 mean kinetic energy in  $\text{metres}^2 \text{ sec}^{-2}$ . In the mean flow the energy is split between zonal flow and eddies in the ratio of 4 to 1 while in the total flow (i. e. mean energy) the ratio is 3 to 4 respectively. The bulk of the energy of the zonal flow (94%) is contained in the mean flow. Figure 4.2 illustrates the distribution of kinetic energy for the standing and transient parts of the eddies over the three wave numbers  $\eta$ ,  $\mathfrak{m}$ , and  $\eta - \mathfrak{m}$ . The distributions are not too different in shape from the distributions of the variance of the height field, but the maxima are shifted to higher wave numbers. In particular the absolute maximum shifts from  $\eta = 7$  in the case of the height field to  $\eta = 8$ . As well, the distribution over  $\mathfrak{m}$  of the transient kinetic energy shifts the absolute maximum from  $\mathfrak{m} = 1$  to  $\mathfrak{m} = 4$ .

Figure 4.3: Distribution of the horizontal mean kinetic energy per unit mass over wave number (metres/sec)<sup>2</sup>. (From Eliassen and Machenhauer, 1965).



The distribution of kinetic energy over  $n-m$  shows relative maxima for even values of  $n-m$ , which indicates that the circulation is asymmetric with respect to the equator from an energetic point of view as well.

The tails of these distribution indicate (as can be seen in the Table of mean kinetic energy) that for large wave numbers each component has approximately the same energy. (This appears as a horizontal line for the distribution of  $m$  and  $n-m$  since each  $m$  and  $n-m$  has 17 components. In the distribution over  $n$  however it will appear as a line sloping negatively towards zero at  $n = 35$  ).

Eliassen and Machenhauer have performed similar calculations for the northern hemisphere (assuming a symmetric southern hemisphere) for the month of January 1957. From their published results the distributions of kinetic energy were calculated and are presented in Figure 4.3. (The distribution over  $n-m$  was not calculated since the only permitted values in their scheme are the odd values). The main features of the distributions of the transient component compare quite closely, except that the January values are about twice as large as those for September. However, the standing eddies have quite a different distribution of kinetic energy over wave length. In particular, in January the energy in components  $m=2$  and  $3$  is five or six times that in September. Also the distribution over  $n$  shows a large maximum at  $n = 5, 6$

Figure 4.4: Distribution of horizontal mean kinetic energy per unit mass corrected for an equal energy noise level (metres/sec)<sup>2</sup>.

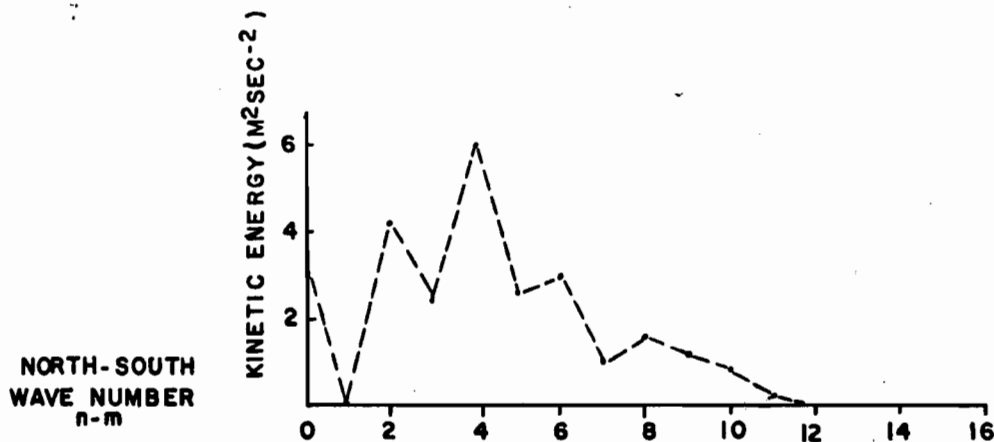
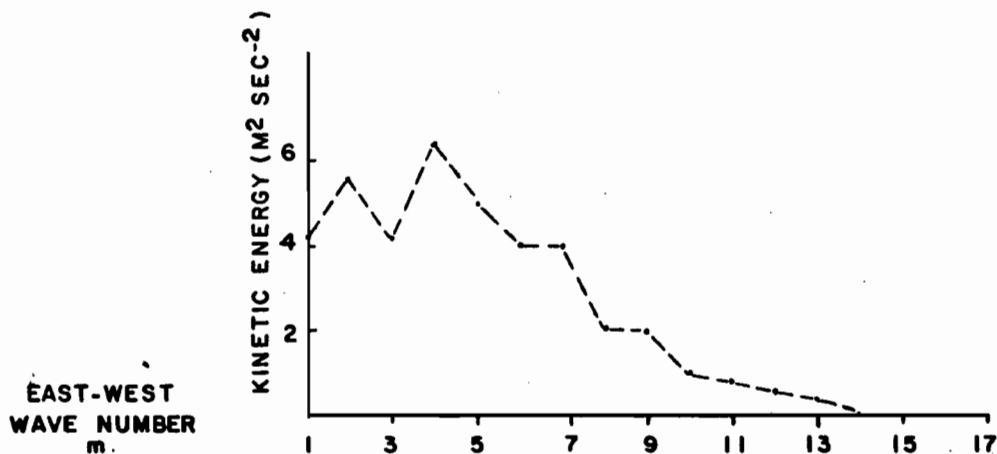
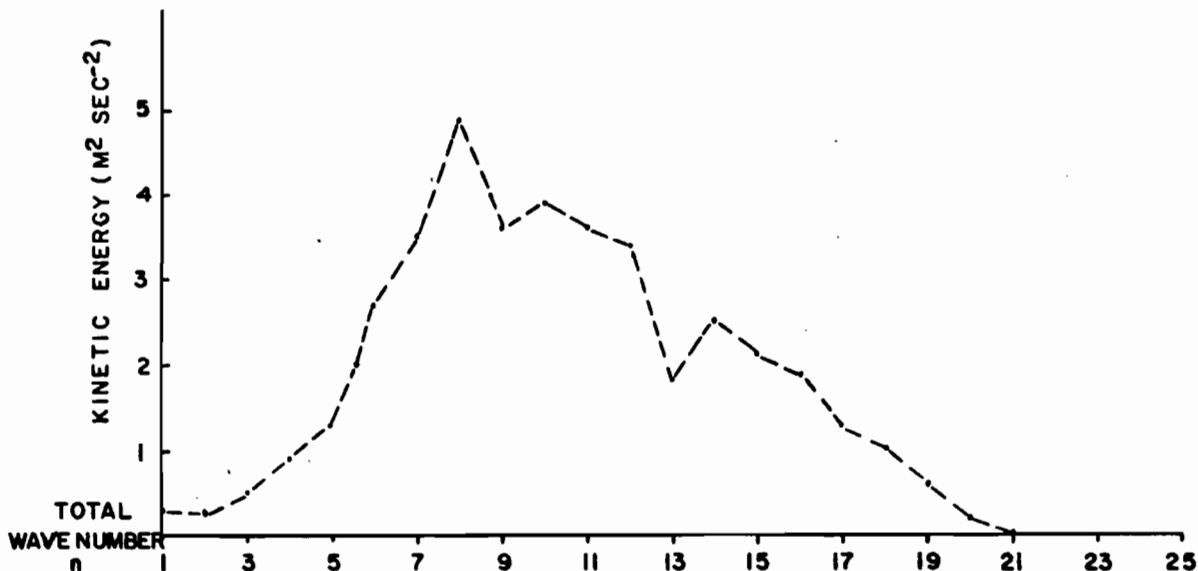
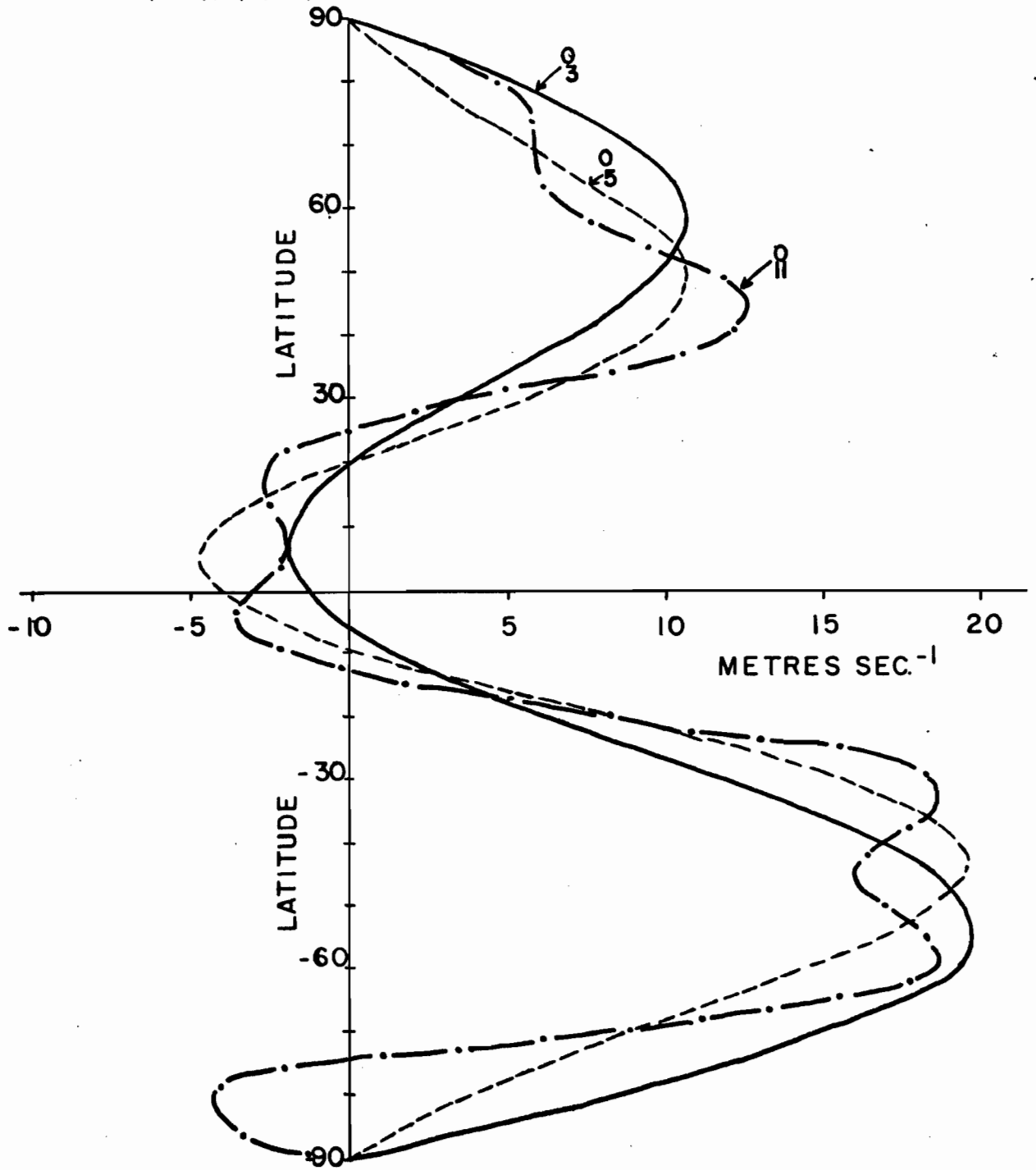


Table 4.14: Mean zonal wind profiles (metres/sec) including components up to the indicated wave number.

n	1	2	3	4	5	6	7	8	9	10	11	12	13	14	15	16
Lat																
90	0	0	0	0	0	0	0	0	0	0	0	0	0	0	0	0
80	1.19	-0.46	5.06	5.90	2.55	2.54	1.88	1.42	1.58	7.29	4.83	-1.28	-0.54	4.18	0.19	-4.76
70	2.34	-0.76	8.88	10.35	5.63	5.61	5.02	4.72	4.78	5.47	5.77	7.88	7.48	4.24	7.39	11.52
60	3.41	-0.76	10.59	11.99	8.81	8.80	8.85	9.03	8.94	5.51	6.70	8.29	8.31	9.85	7.55	3.96
50	4.39	-0.35	9.91	10.69	10.66	10.67	11.12	11.37	11.34	12.24	11.19	8.14	8.39	8.54	9.90	12.98
40	5.23	0.49	7.23	7.15	9.68	9.69	9.89	9.79	9.87	12.21	12.05	13.91	13.57	12.12	11.72	9.18
30	5.91	1.74	3.53	2.75	5.59	5.59	5.30	5.06	5.08	3.21	4.24	4.89	5.12	7.20	6.72	8.67
20	6.42	3.32	0.10	-0.91	0.00	-0.01	-0.33	-0.28	-0.36	-1.57	-2.25	-4.63	-4.63	-6.59	-5.39	-6.71
10	6.73	5.08	-1.82	-2.51	-4.13	-4.14	-4.04	-3.81	-3.81	-1.46	-1.88	0.16	-0.05	1.12	-0.55	0.12
0	6.83	6.83	-1.42	-1.42	-4.18	-4.18	-3.81	-3.81	-3.74	-3.74	-2.74	-2.74	-2.44	-2.44	-0.61	-0.61
-10	6.73	8.37	1.47	2.16	0.54	0.54	0.64	0.41	0.41	-1.95	-2.37	-4.41	-4.62	-5.79	-7.47	-8.14
-20	6.42	9.51	6.29	7.30	8.21	8.22	7.89	7.85	7.78	8.99	8.32	10.70	10.70	12.66	13.86	15.18
-30	5.91	10.09	11.87	12.65	15.49	15.48	15.20	15.43	15.45	17.33	18.36	17.72	17.95	15.87	15.38	13.43
-40	5.23	9.98	16.71	16.79	19.32	19.31	19.51	19.61	19.68	17.34	17.17	15.30	14.96	16.40	16.00	18.53
-50	4.39	9.13	19.39	18.61	18.58	18.57	19.02	18.77	18.74	17.83	16.78	19.84	20.09	19.95	21.32	18.24
-60	3.41	7.59	18.93	17.53	14.35	14.35	14.40	14.21	14.12	17.54	18.73	17.14	17.16	15.62	13.32	16.90
-70	2.34	5.43	15.07	13.60	8.88	8.89	8.30	8.60	8.66	7.97	8.27	6.17	5.77	9.01	12.17	8.04
-80	1.19	2.83	8.35	7.42	3.98	4.00	3.34	3.81	3.97	-1.74	-4.19	1.91	2.65	-2.07	-6.06	-1.12
-90	0	0	0	0	0	0	0	0	0	0	0	0	0	0	0	0

Figure 4.5: Comparison of mean zonal wind profiles (metres/sec) obtained by successive inclusion of components of the stream function from the linear balance equation. Curves include components up to  $(0, 3)$ ,  $(0, 5)$ ,  $(0, 11)$ .



which is absent in the September curves. The January distributions also appear to have constant energy in the large wave numbers but at a somewhat lower value.

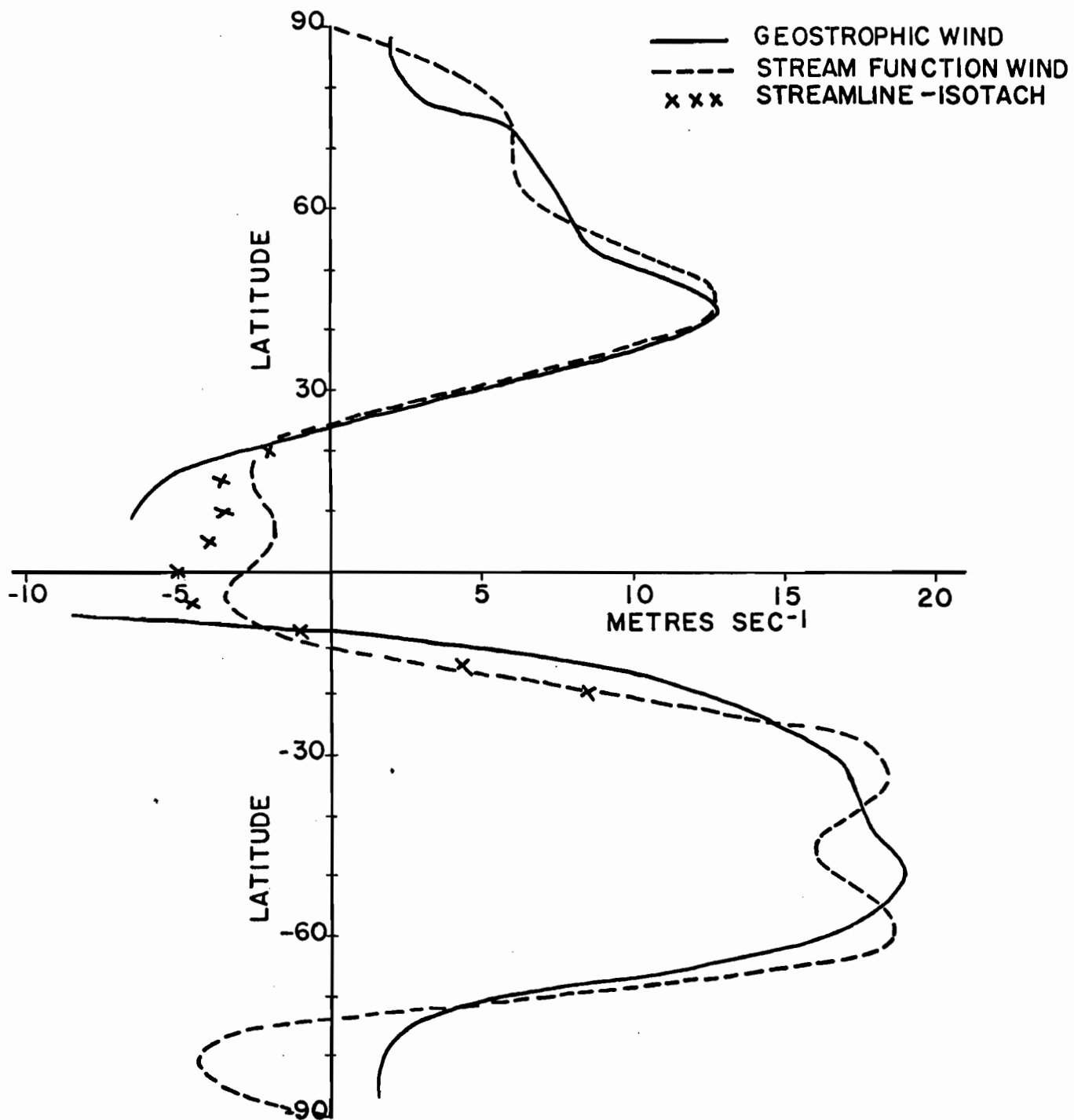
This last observation appears to be confirmed in Table 4.13 where the components of even symmetry appear generally to have higher energies. This is consistent with the error propagating feature of the solution of the linear balance equation (pp 97, 98) so that the jagged appearance of Figure 4.2 may be somewhat spurious. (This does not imply that the conclusion about the anti-symmetry of the height field is invalid).

Considering the equal energy distribution as a "noise level" on the remainder of the distributions, corrections were made, and the final distributions of the transient part are shown in Figure 4.4. The shape of the distributions hardly changes, but the absolute values are reduced by 1 to 2 metres<sup>2</sup>/sec<sup>2</sup>.

#### Representation of the Mean Zonal Flow

The mean zonal flow for the month was calculated from the mean values of the zonal components of the stream function. The calculation was performed for each component separately, then these results were added successively to see the effect of each term of the resulting profile (Table 4.14). In Figure 4.5 the profiles of zonal wind obtained by adding components up to and including the indicated number are presented. The two jet structure, with a

Fig 4. 6: Comparison of mean zonal winds for the month of September 1957. Stream function winds include components up to and including (0, 11). Tropical zonal wind values obtained from De Las Alas (1966).



stronger jet in the southern hemisphere, is determined mainly by components up to  $n = 3$ . The jet maxima are too far north and south however, and thus components  $\psi_4^{\circ}$ ,  $\psi_5^{\circ}$  take care of this by shifting the maxima towards the equator without affecting the maximum values. Components with  $n = 6, 7, 8, 9$  add very little to this profile because their mean values are very small. Components  $\psi_{10}^{\circ}$ ,  $\psi_{11}^{\circ}$  add detail to the jet maxima, actually producing two maxima in the southern hemisphere and a secondary maximum in the northern hemisphere. They also add structure to the profile in the tropical regions.

The mean geostrophic zonal wind profile was calculated by finite differences over  $5^{\circ}$  of latitude from the mean height profile. Figure 4.6 shows the comparison between the geostrophically computed winds and the stream function winds (for  $n \leq 11$ ). The agreement between the two is very good north and south of  $20^{\circ}$  latitude. The stream winds give a small region of easterlies near the south pole, but since the analysis gives equal weights to equal area this is probably spurious. As might be expected the geostrophic winds behave rather badly near the equator, being  $-40$  metres per second at  $2.5^{\circ}\text{S}$  and  $+8.5$  metres per second at  $2.5^{\circ}\text{N}$ . The stream function winds are well behaved near the equator, and agree fairly well with the observed mean zonal winds in this region. (The observed zonal winds were taken from a study by De Las Alas (1966) of the tropical region for the same period.) This is not too surprising because one of the conditions for solution of the linear balance equation is that the derivative of the zonal height

Figure 4.7:

Daily values of zonal stream function components for the month of September 1957.

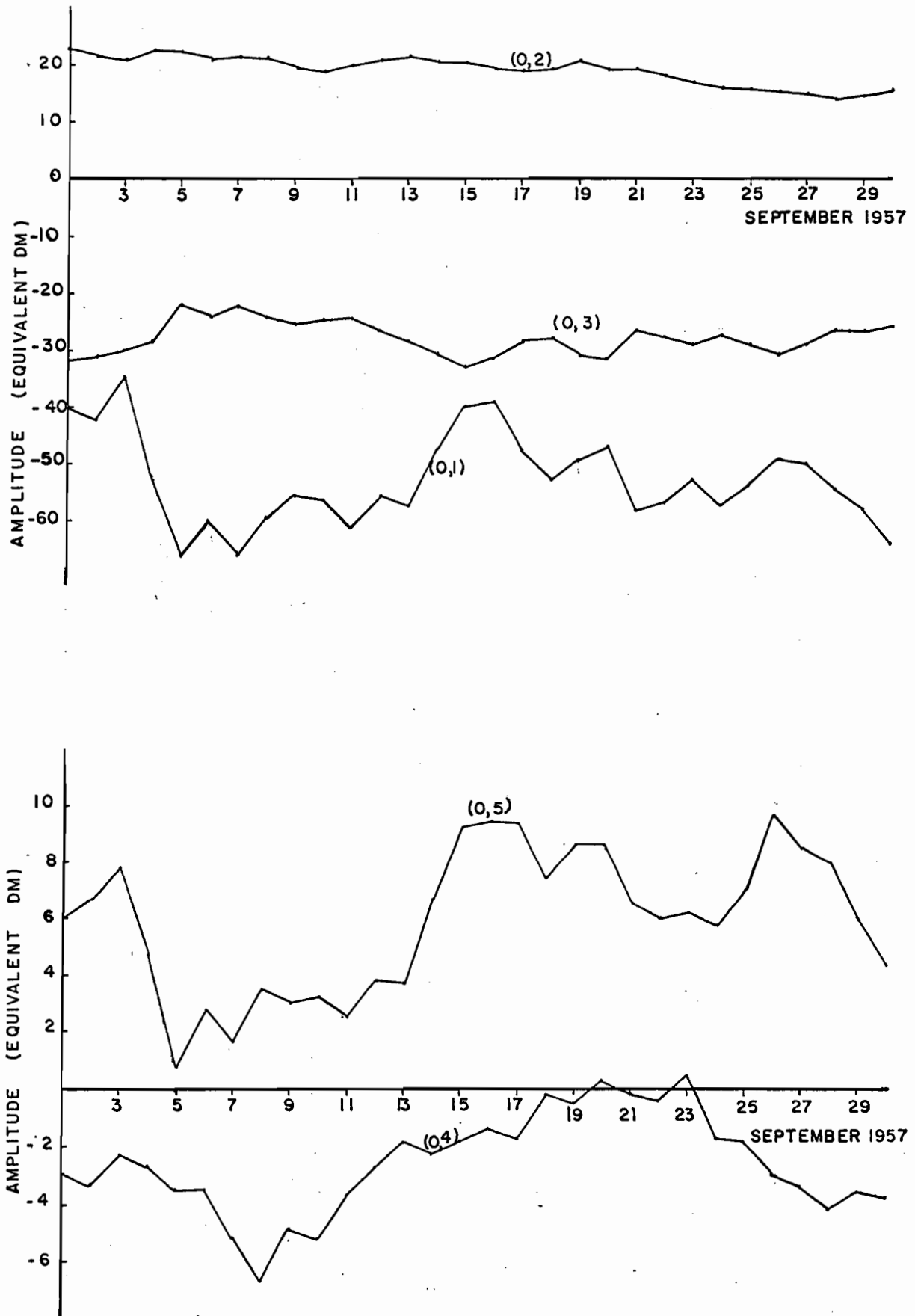
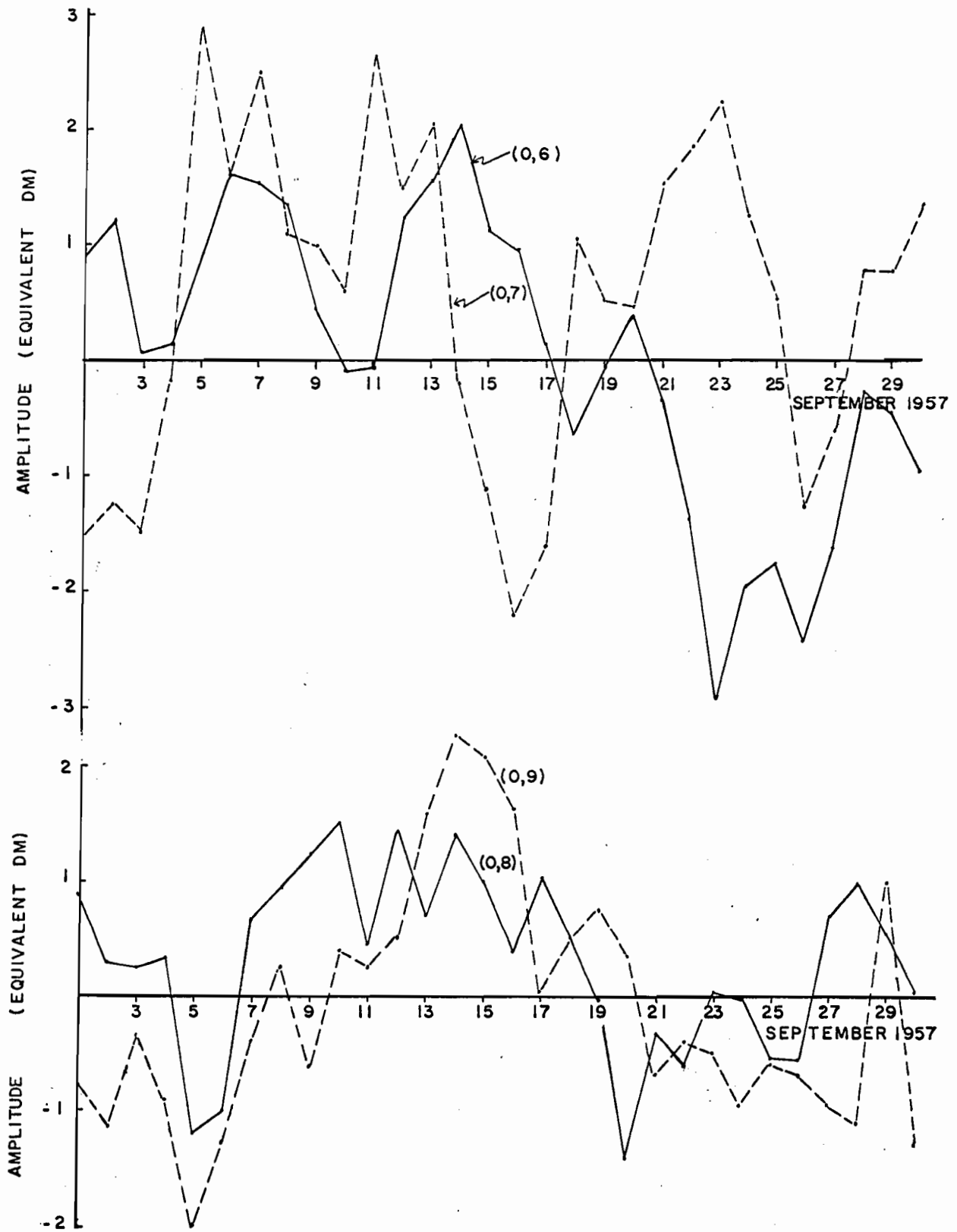


Figure 4.8:

Daily values of zonal stream function component for month of September 1957.



field be zero at the equator. Since the height field is implicitly modified to reach this condition, geostrophy could be applied everywhere. It was found that the best agreement was obtained by only including zonal components of the stream function up to  $n = 11$ . The remaining components seemed to just add noise to the profile.

### The Fluctuations of Large Scale Components of the Stream Field.

#### Zonal Components

The variation of the largest scale zonal components ( $n = 1, 2, 3$ ) as a function of time is shown in Figure 4.7. These components determine to a large extent the total structure of the zonal flow, and thus do not change very much over the month. The symmetric component  $\psi_2^0$  (giving a stronger jet in the southern hemisphere) does show a tendency to decrease during the course of the month in accordance with increasing zonal flow in the northern hemisphere and decreasing in the southern hemisphere. Any secular changes in  $\psi_1^0$  and  $\psi_3^0$  are masked by what appears to be a high noise level in these components.

The components  $\psi_4^0$ ,  $\psi_5^0$  (Figure 4.7), undergo fluctuations at least as large as their mean values with a dominant period of the order of a month. Their values are predominantly of one sign however,  $\psi_4^0$  being negative for 28 days and  $\psi_5^0$  positive for the 30 days. The smaller scale components  $\psi_6^0, \psi_7^0, \psi_8^0, \psi_9^0$ , (Fig. 4.8)

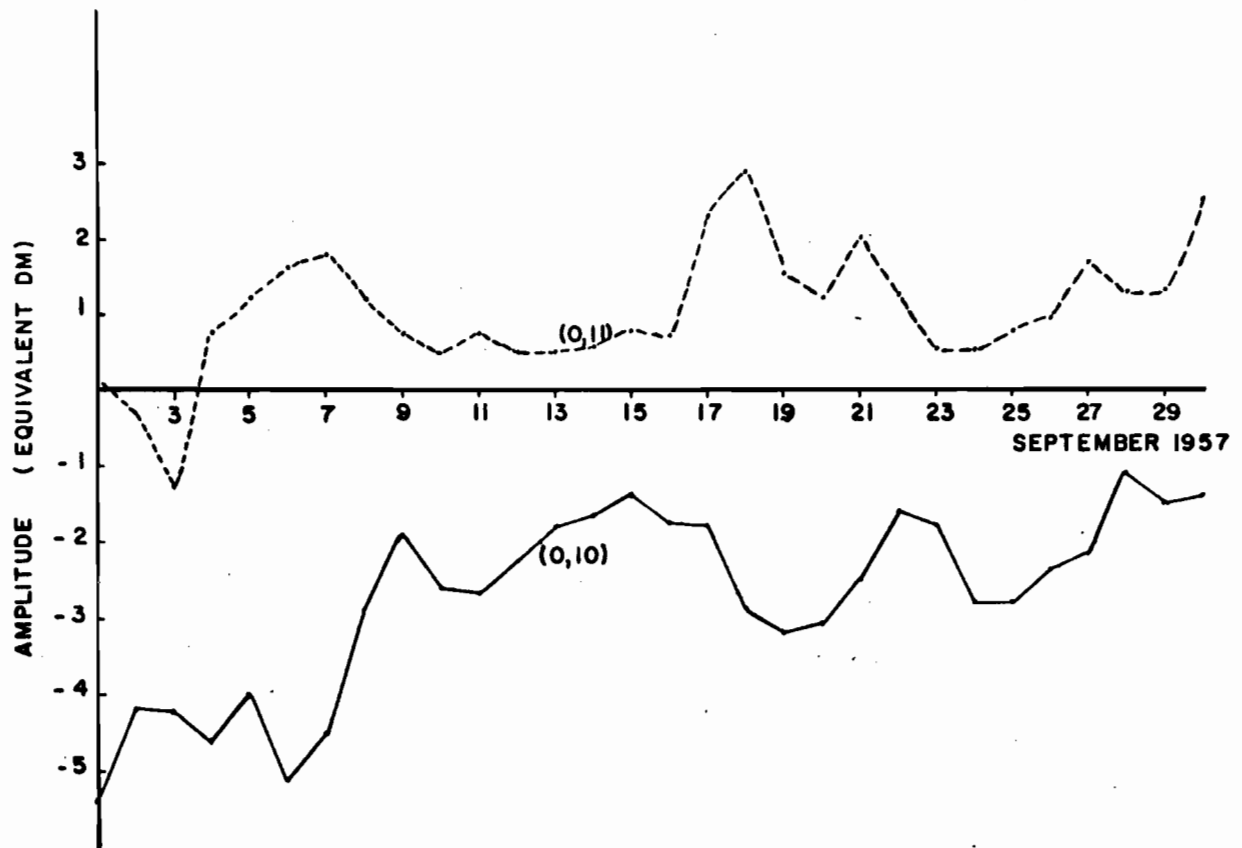


Figure 4.9: Daily values of zonal stream function components for month of September 1957.

essentially fluctuate about zero with amplitudes of the order of 1 - 3 equivalent decametres.\* The components  $\psi_{10}^{\circ}$ ,  $\psi_{11}^{\circ}$  (Fig. 4.9) behave in the same manner as  $\psi_4^{\circ}$ ,  $\psi_5^{\circ}$  undergoing relatively large fluctuations but remaining predominantly of the same sign.

The components with  $n > 11$  have not been considered for two reasons. Firstly the analysis program is such that numerical errors of the order of the mean amplitudes of the components with  $n > 11$  can be produced; secondly these components add nothing but noise to the computed mean zonal wind profile.

#### Non-zonal or wave components

In their studies of the fluctuations of the planetary scale waves both Eliassen and Machenhauer (1965) and Deland (1965) have demonstrated (using spherical harmonic analysis over the northern hemisphere) that there is a component of barotropic, or more precisely equivalent barotropic, motion on this scale. These planetary waves are composed of a relatively stationary component plus a moving component which moves westward with phase speeds of up to 40 degrees longitude per day for the largest scale. Recent evidence indicates that these fast moving components extend to great heights. Hemispheric analysis in terms of spherical harmonics at

---

\* Equivalent decametre - the stream function has been reduced to approximate geopotential height in decametres. For proper units of  $m^2 \text{sec}^{-1}$  multiply by the constant  $5g/\Omega$  in M. K. S. units.

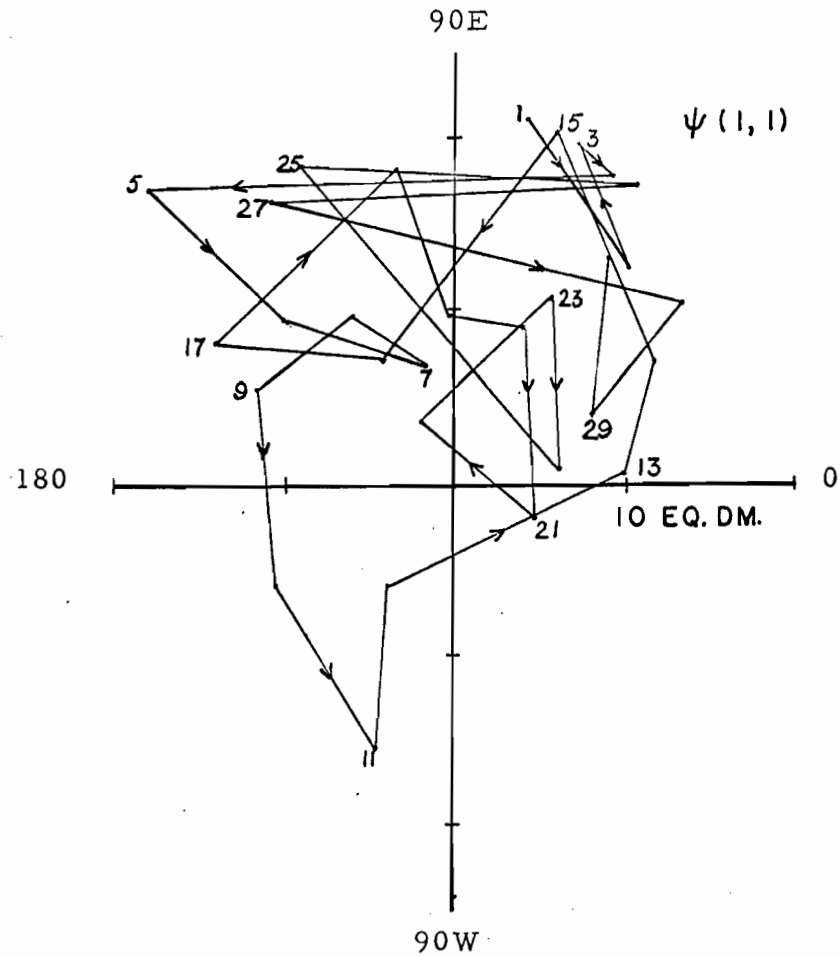


Fig. 4.10: Daily values of amplitudes and relative phase angle of stream function component (1,1) for month of September 1957. Amplitude in equivalent decameters.

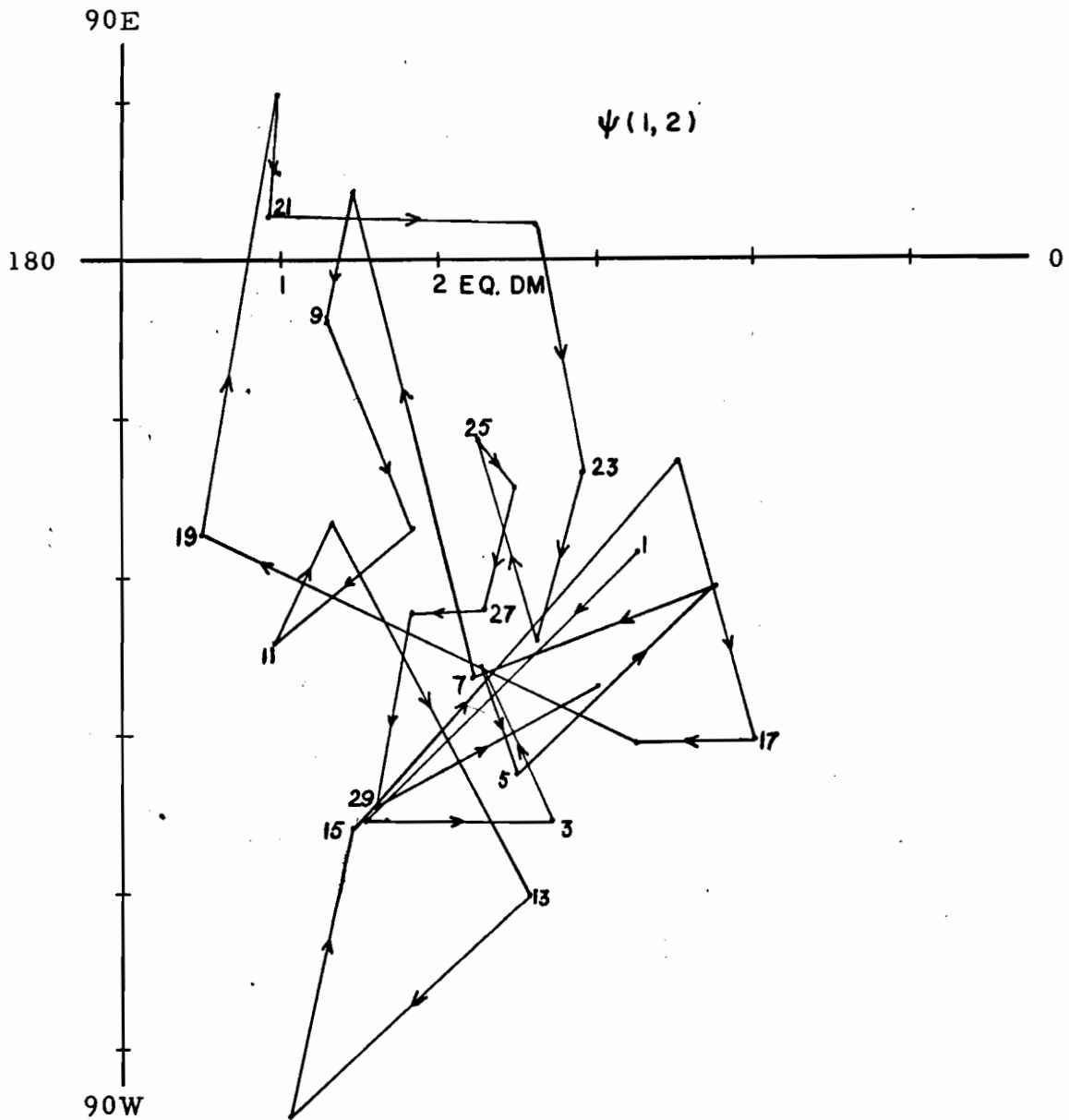


Fig. 4.11: Daily values of amplitudes and relative phase angle of stream function component (1, 2) for month of September 1957. Amplitude in equivalent decimeters.

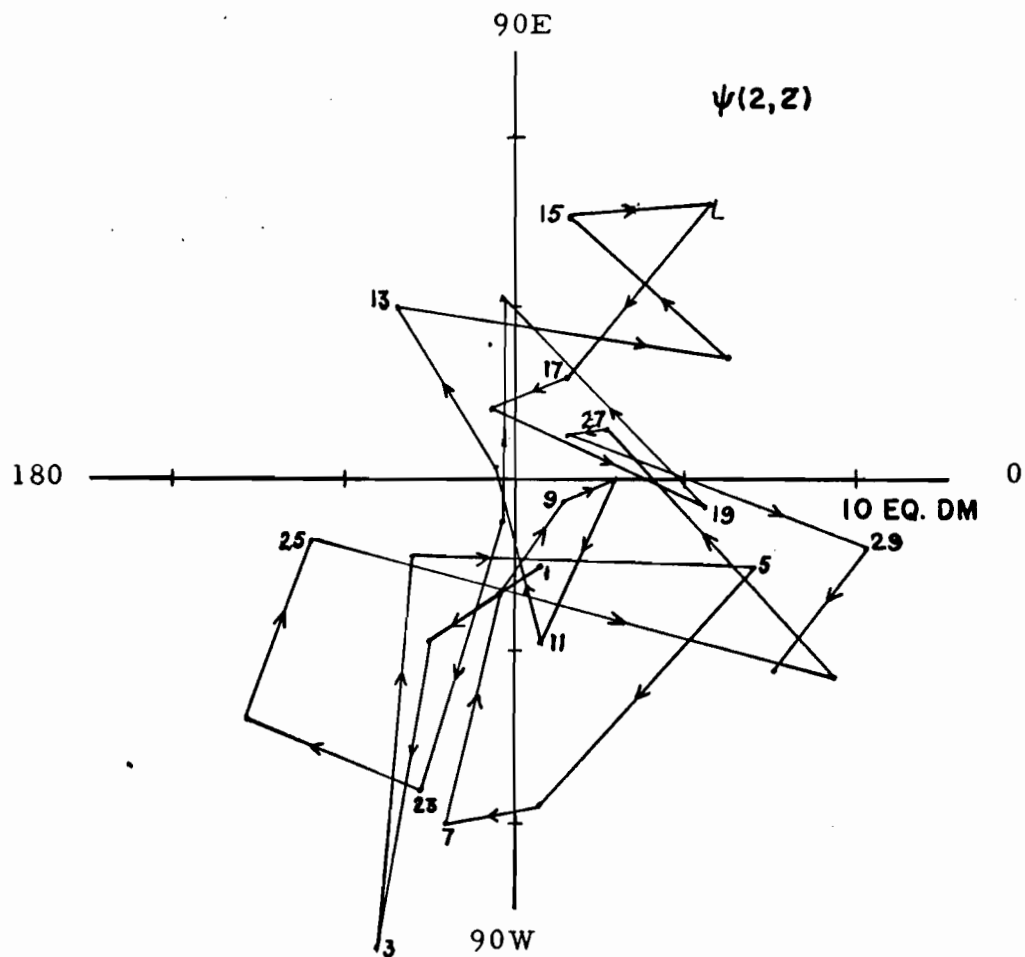


Fig. 4.12: Daily values of amplitudes and relative phase angle of stream function component (2, 2) for month of September 1957. Amplitude in equivalent decameters.

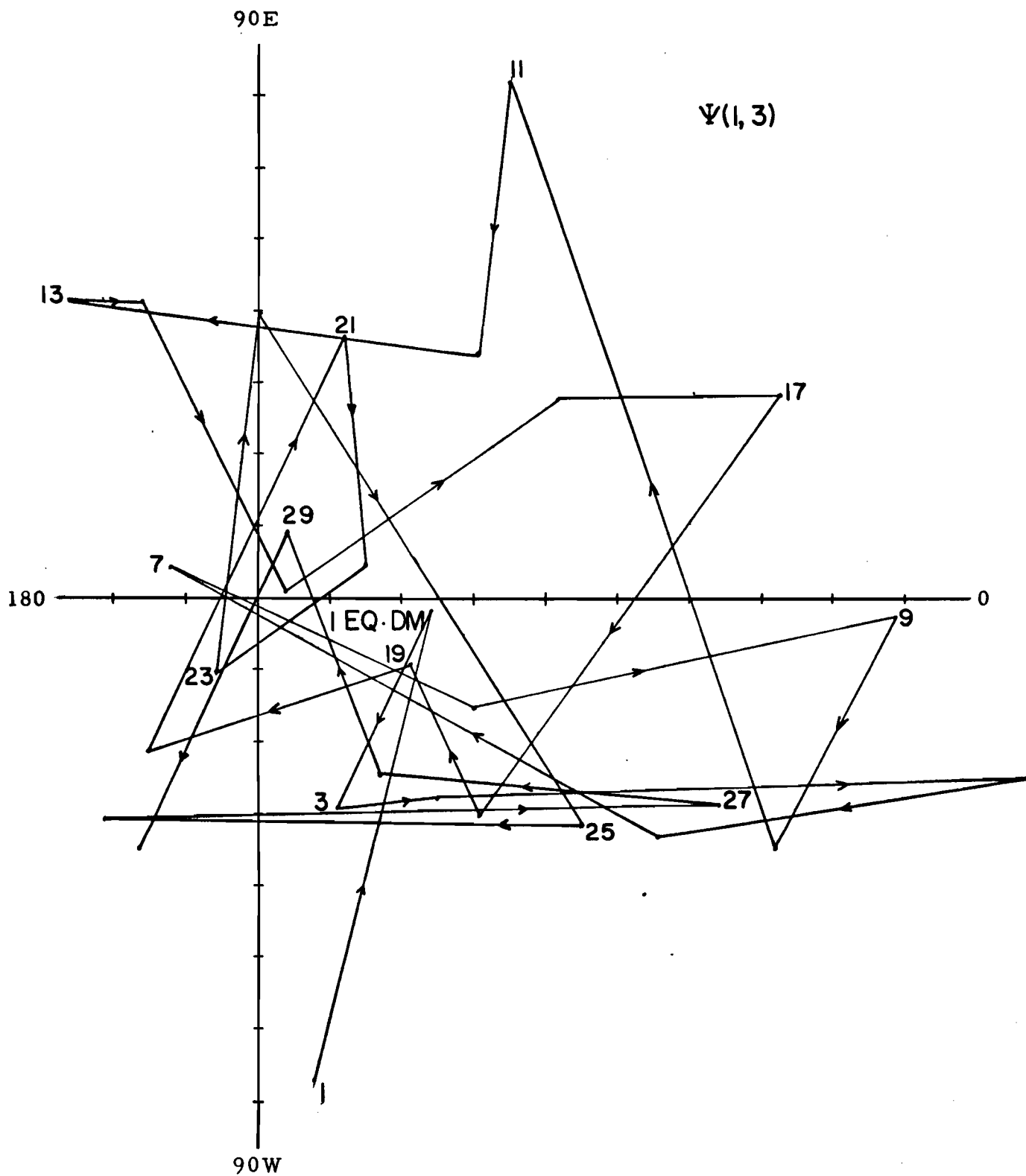
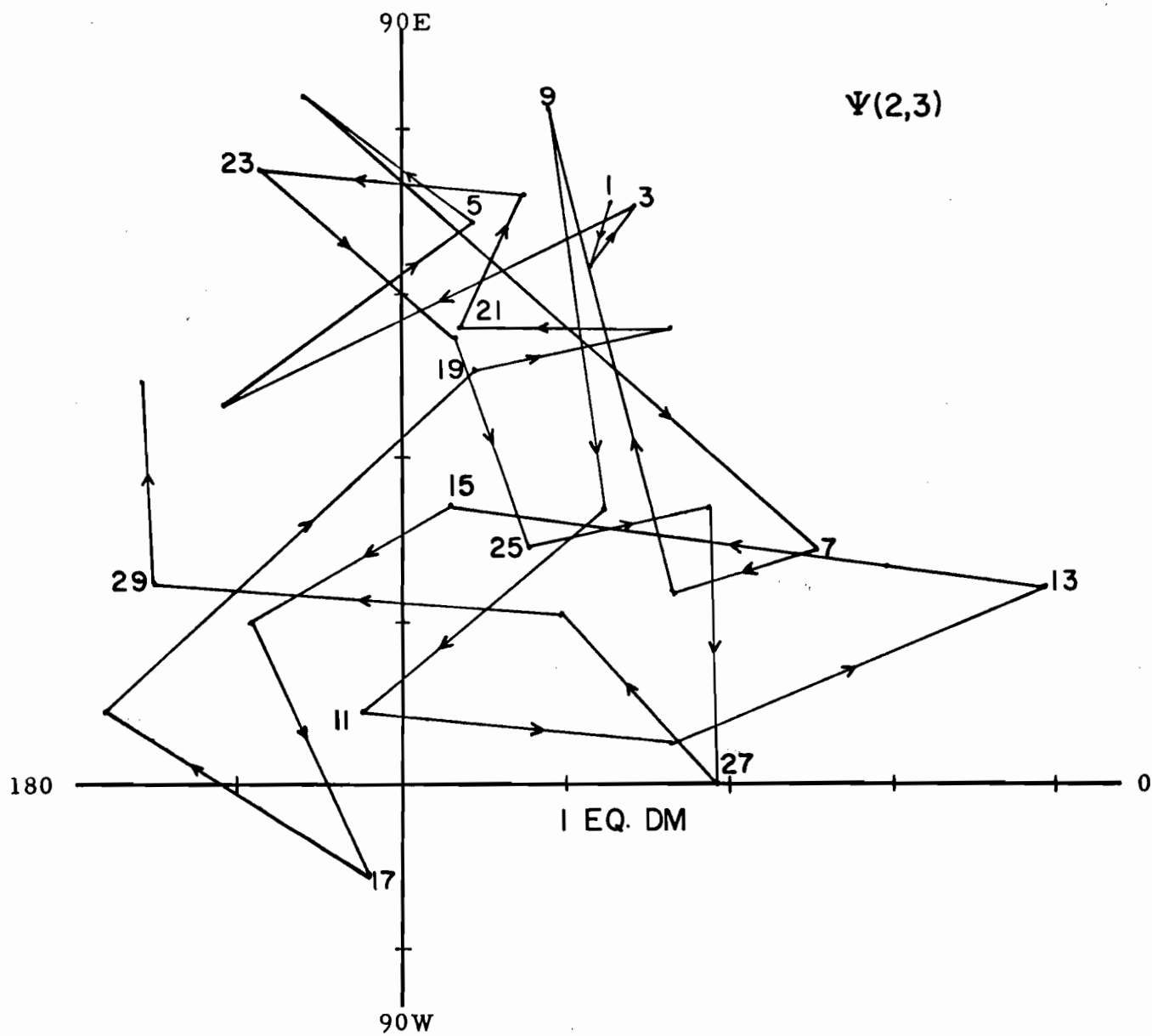


Figure 4.13: Daily values of amplitude and relative phase angle of stream function component (1, 3) for month of September 1957. Amplitude in equivalent decameters.



**Figure 4.14:** Daily values of amplitude and relative phase angle of stream function component (2, 3) for month of September 1957. Amplitude in equivalent decameters.

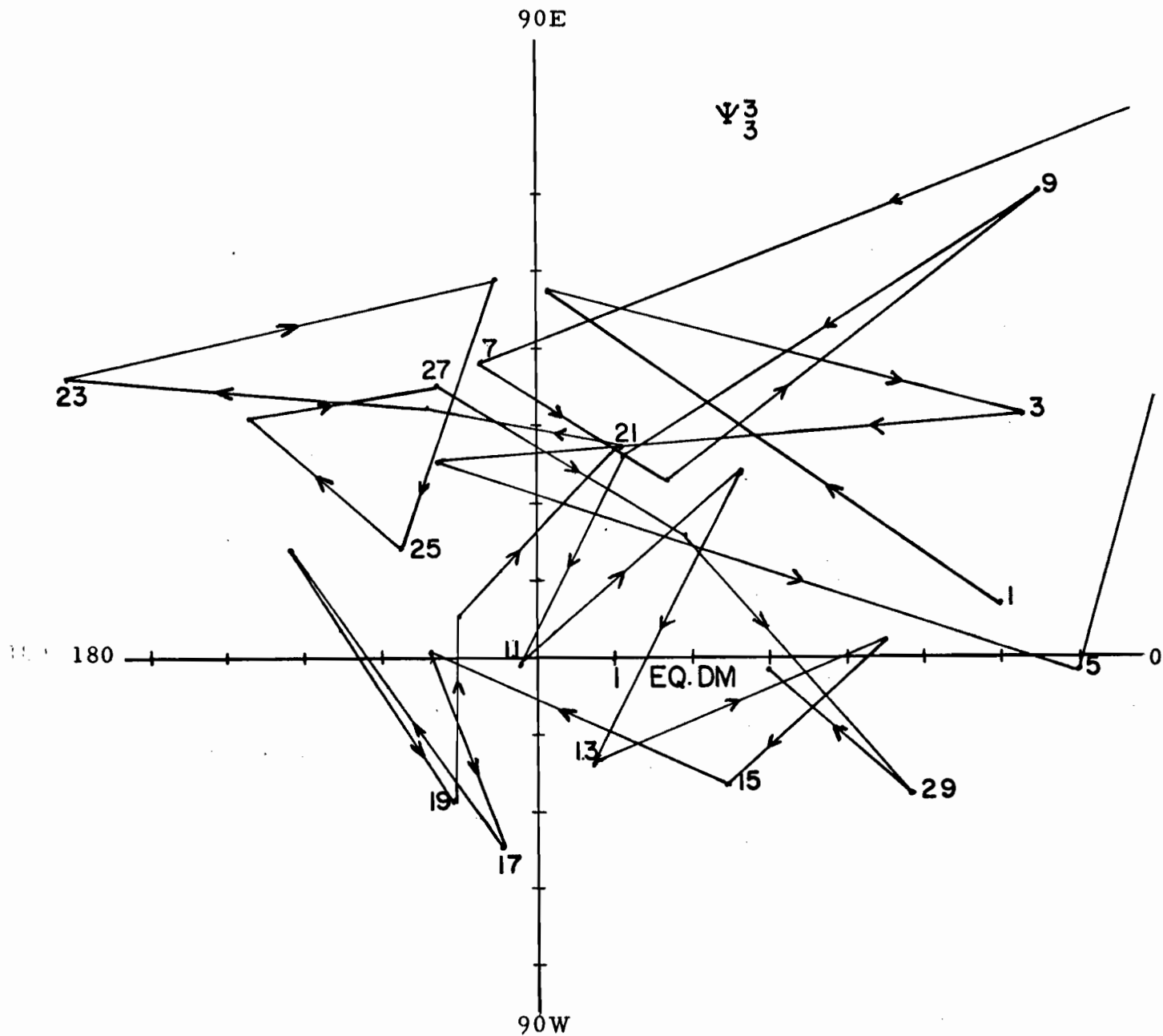


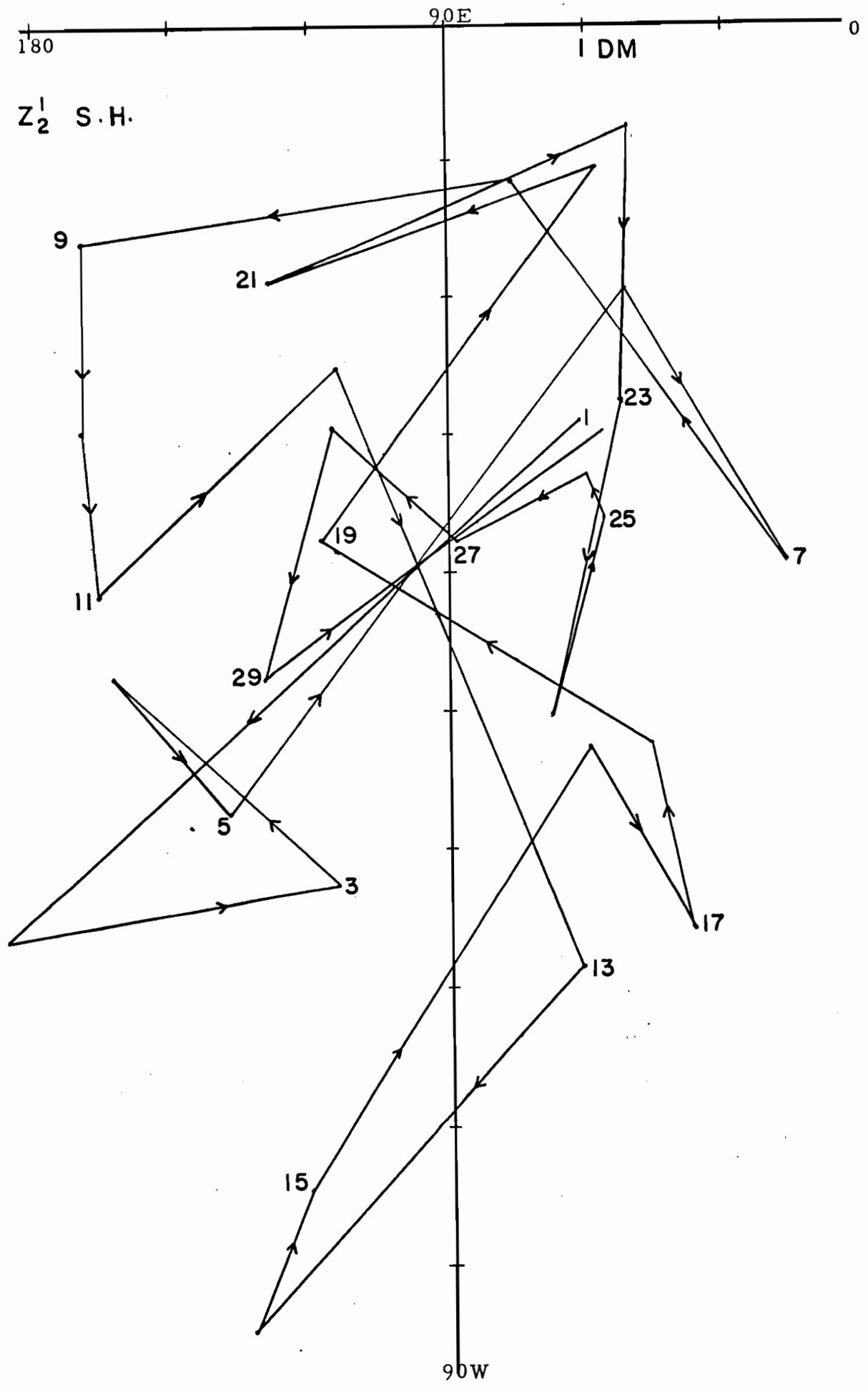
Figure 4.15: Daily values of amplitude and relative phase angle of stream function component (3, 3) for month of September 1957. Amplitude in equivalent decameters.

three levels, 500 mb, 100 mb, 25 mb, indicate that the moving parts are consistent in the vertical. (Boville, to be published). One of the most striking ways of illustrating this behaviour is on a phase diagram. This is a plot of the amplitude and phase on a polar diagram, each point representing the wave at a given time. If a wave behaves according to the model above, the trajectory of the point representing it will tend to be circular about some mean value. This trajectory may or may not enclose the origin depending on the relative magnitudes of the moving part and the stationary part.

In the phase diagrams to follow the positive abscissae is the Greenwich meridian; motion from east to west is in a clockwise sense. As well, the plotted points represent the amplitude and relative phase of the waves so that to determine angular phase speeds, the relative phase changes must be divided by the zonal wave number  $m$ .

Figures 4.10 to 4.15 are the phase diagrams (in equivalent decametres) for the very largest scale waves ( $n \leq 3$ ) in the stream field at 500 mb for September 1957. These diagrams indicate that there is little if any coherence in the time variations of the amplitudes and phase of these components. (This is not primarily due to the properties of the linear balance equation because the same incoherence in time is observed for the height field components for the globe). Certainly there appears to be no evidence of any retrogressive barotropic mode.

Figure 4.16: Daily values of amplitude and relative phase angle of southern hemispheric height field component (1, 2) for month of September 1957. Antisymmetry with respect to the equator is assumed. Amplitude in decameters.



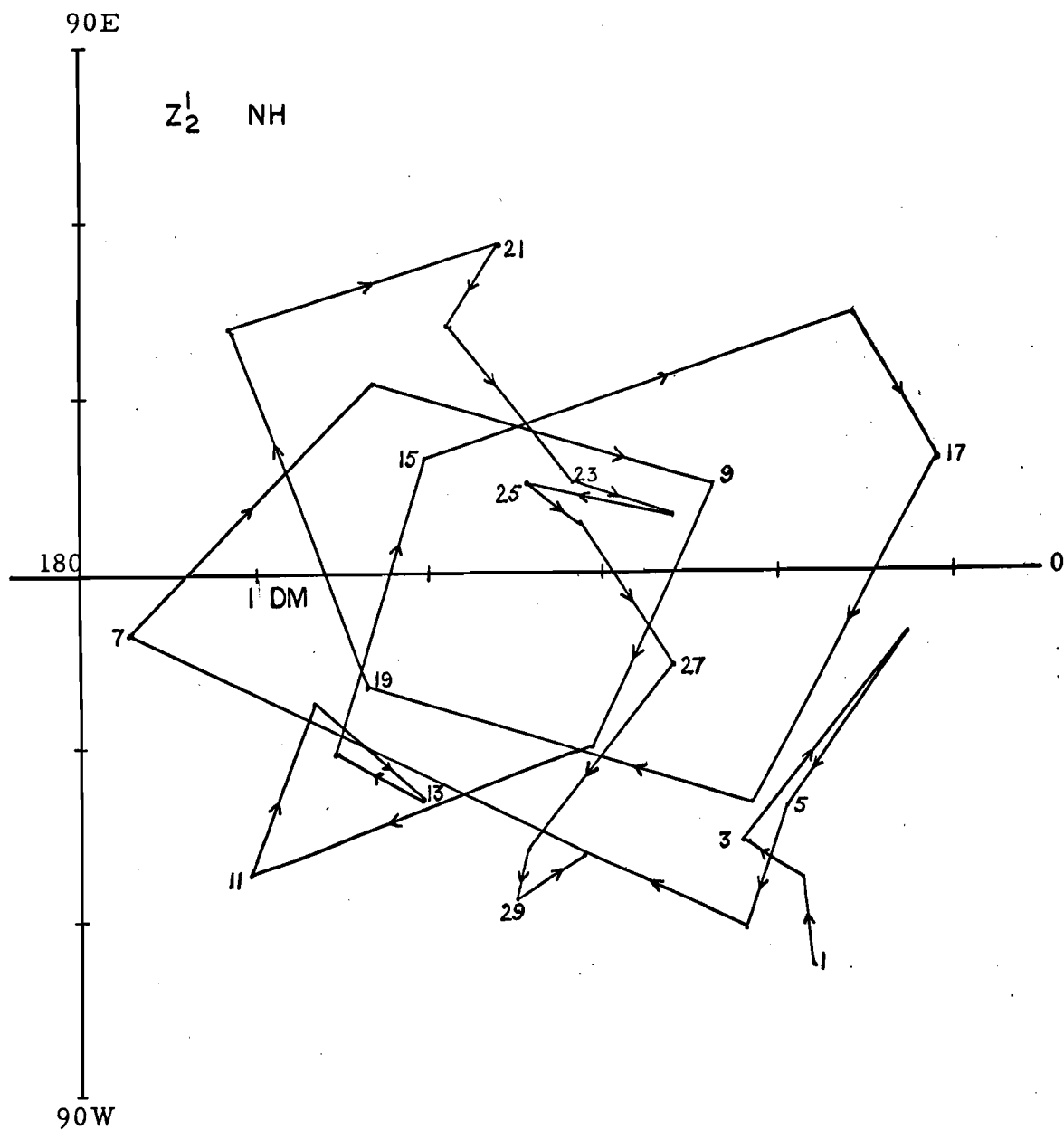


Figure 4.17: Daily values of amplitude and relative phase angle of northern hemispheric height field component (1, 2) for month of September 1957. Antisymmetry with respect to the equator is assumed. Amplitude in decameters.

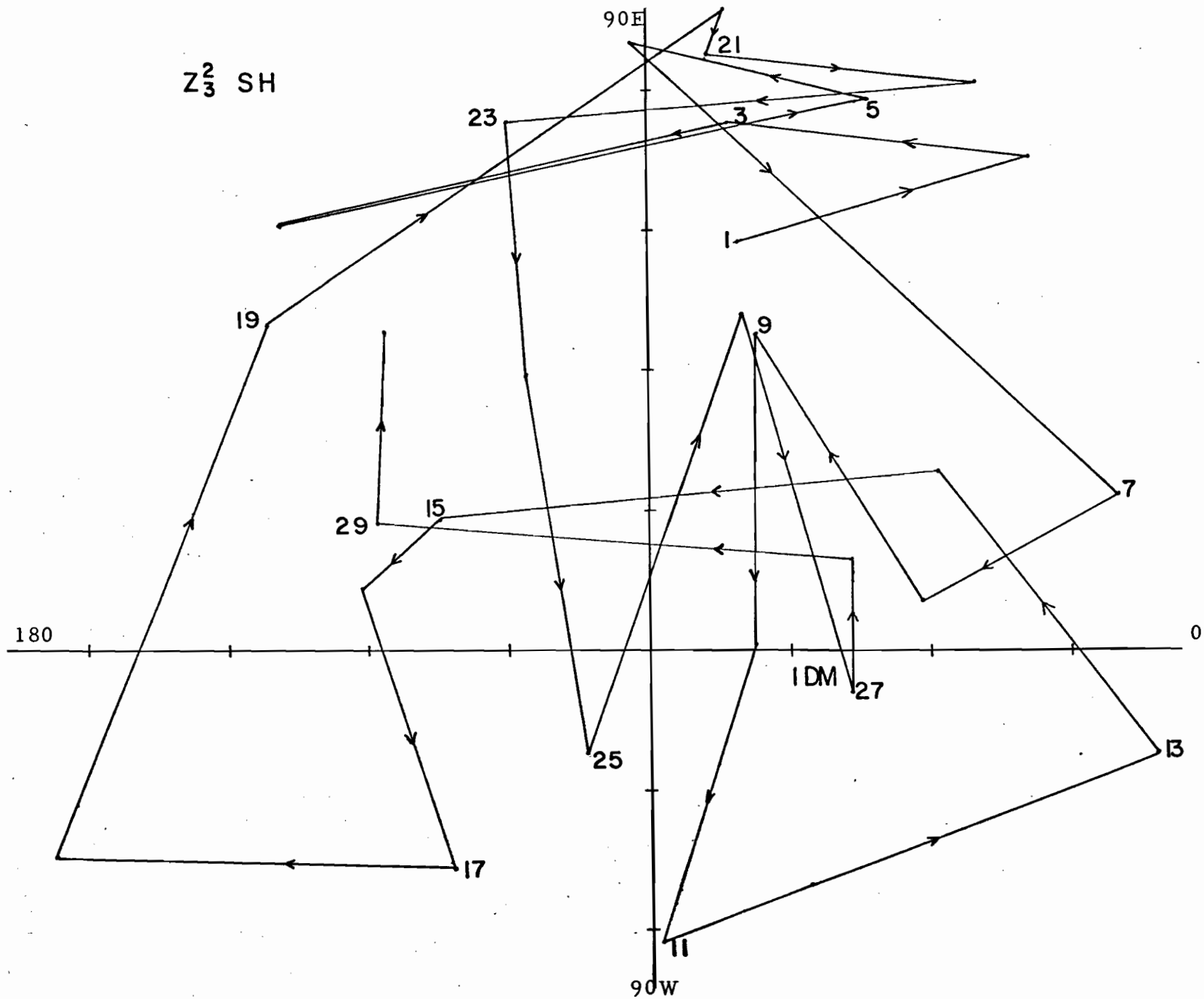


Figure 4.18: Daily values of amplitude and relative phase angle of southern hemispheric height field component (2, 3) for month of September 1957. Antisymmetry with respect to the equator is assumed. Amplitude in dm.

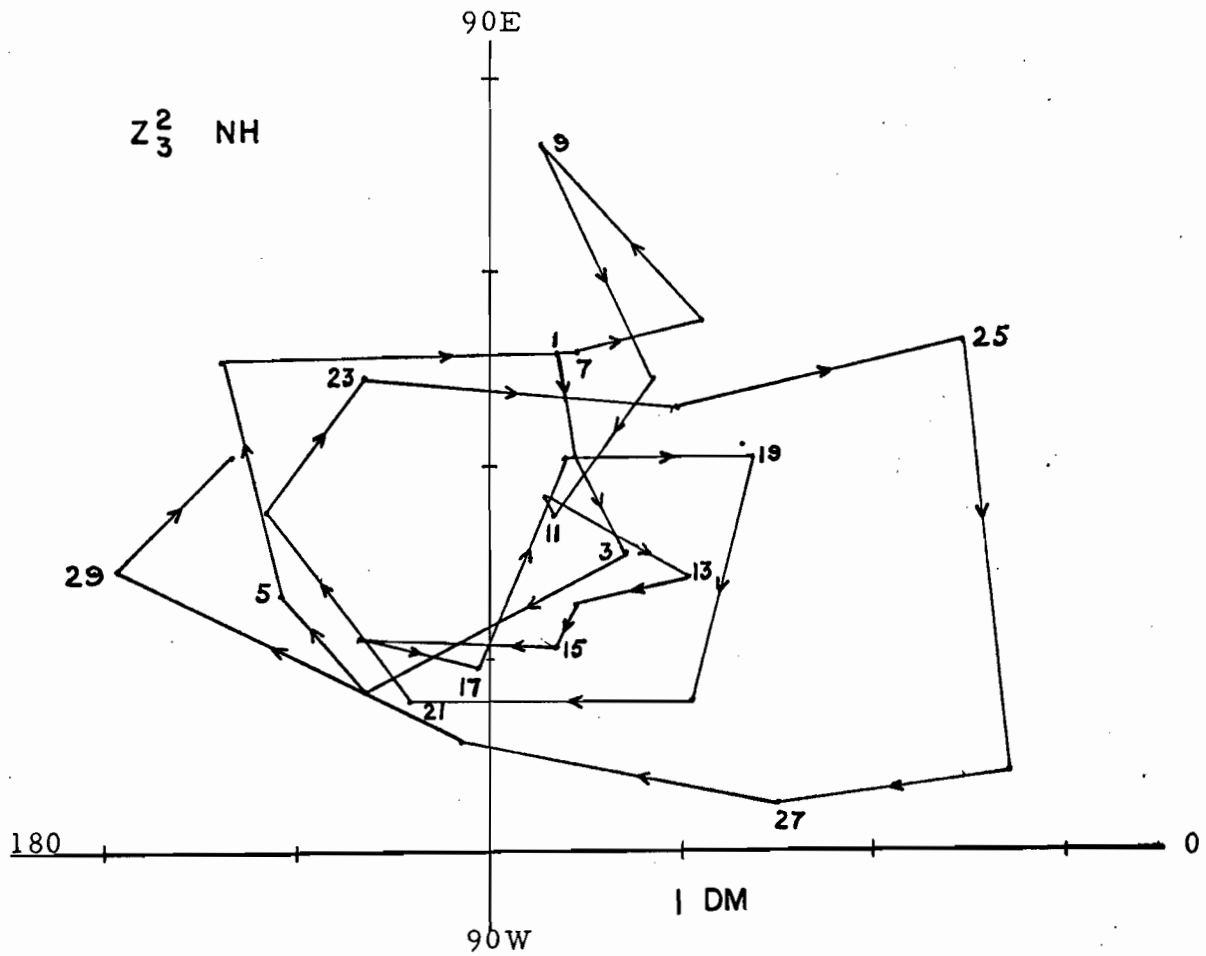


Figure 4.19. Daily values of amplitude and relative phase angle of northern hemispheric height field component (2, 3) for month of September 1957. Antisymmetry with respect to the equator is assumed. Amplitude in decameters.

In order to account for this rather incoherent behaviour the original global height field was split into two hemispheres and analyzed separately assuming antisymmetry. Figures 4.16, 4.17, 4.18, 4.19 are the phase diagram (in decametres) for the largest components ( $\kappa \leq 3$ ) for the northern hemisphere and the southern hemisphere. The difference between their behaviour in the two hemispheres is quite striking. The waves in the northern hemisphere follow quite closely the model of a standing perturbation plus a rapidly retrogressing component, whereas those in the southern hemisphere show little consistency from day to day. As well the stationary parts of these waves have different amplitudes and widely different phase positions in the two hemispheres. This points up a serious difficulty that occurs when one is trying to define the behaviour of waves on a global scale. If in fact the stationary parts of the waves are generated by friction and/or heating, then there is every reason to expect these components to be unrelated in the two hemispheres. Thus even if there exist oscillations which are planet-wide, when they are superimposed on the standing parts they will be extremely difficult to detect. This may well be a factor in the time variation of the stream components. However, the large scale southern hemisphere height field components themselves behave in an erratic manner which indicates that the fluctuations of these waves are poorly defined by the data.

Generally speaking, the smaller scale waves are more

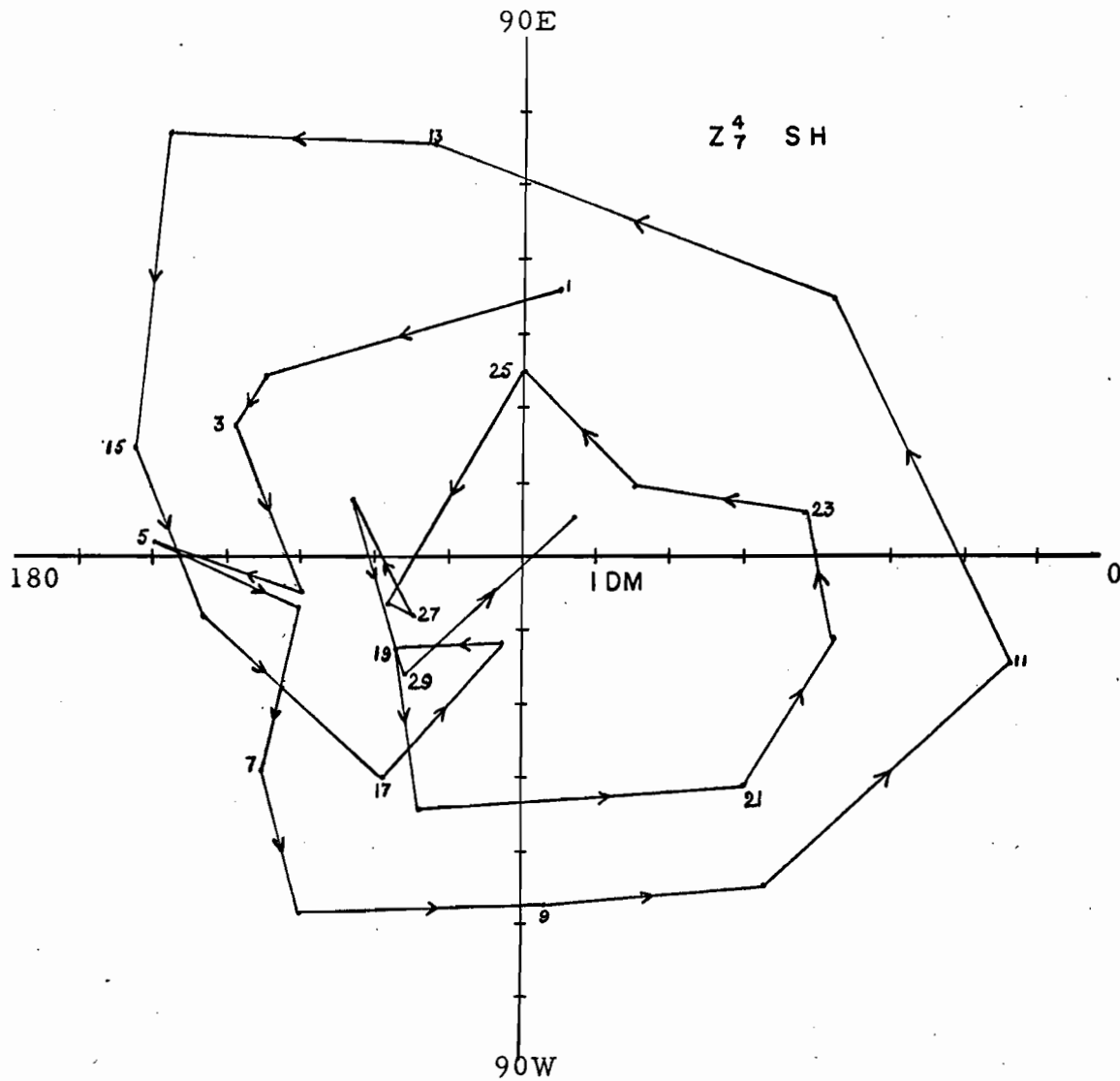


Figure 4.20: Daily values of amplitude and relative phase angle of southern hemispheric height field component (4, 7) for the month of September 1957. Antisymmetry with respect to the equator is assumed. Amplitude in decameters.

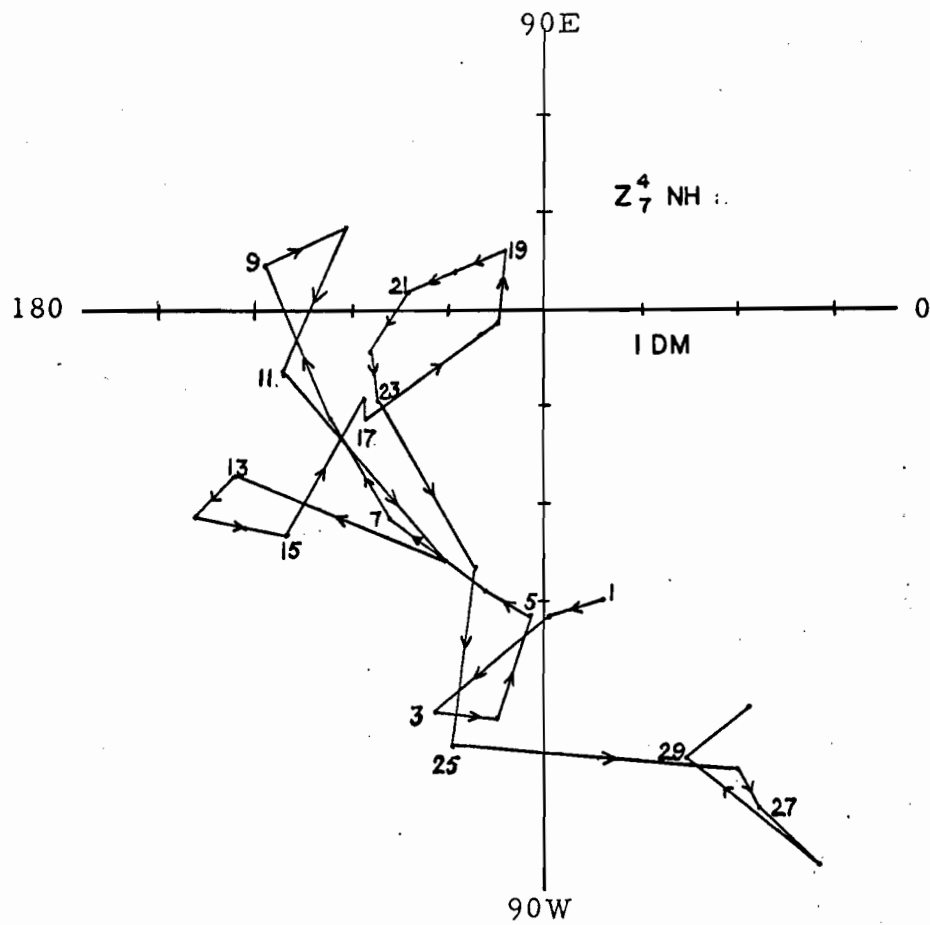


Figure 4. 21: Daily values of amplitude and relative phase angle of northern hemispheric height field component (4, 7) for month of September 1957. Antisymmetry with respect to the equator is assumed. Amplitude in decameters.

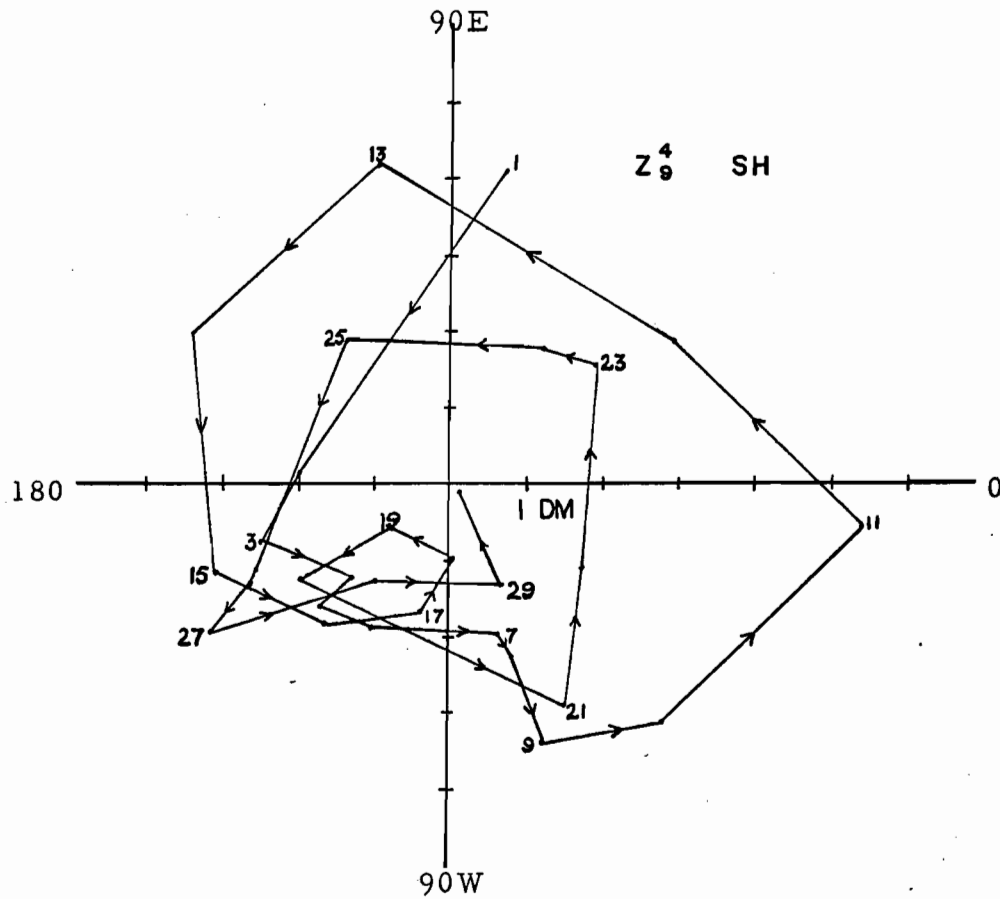


Figure 4. 22: Daily values of amplitude and relative phase angle of southern hemispheric height field component (4, 9) for month of September 1957. Antisymmetry with respect to the equator is assumed. Amplitude in decameters.

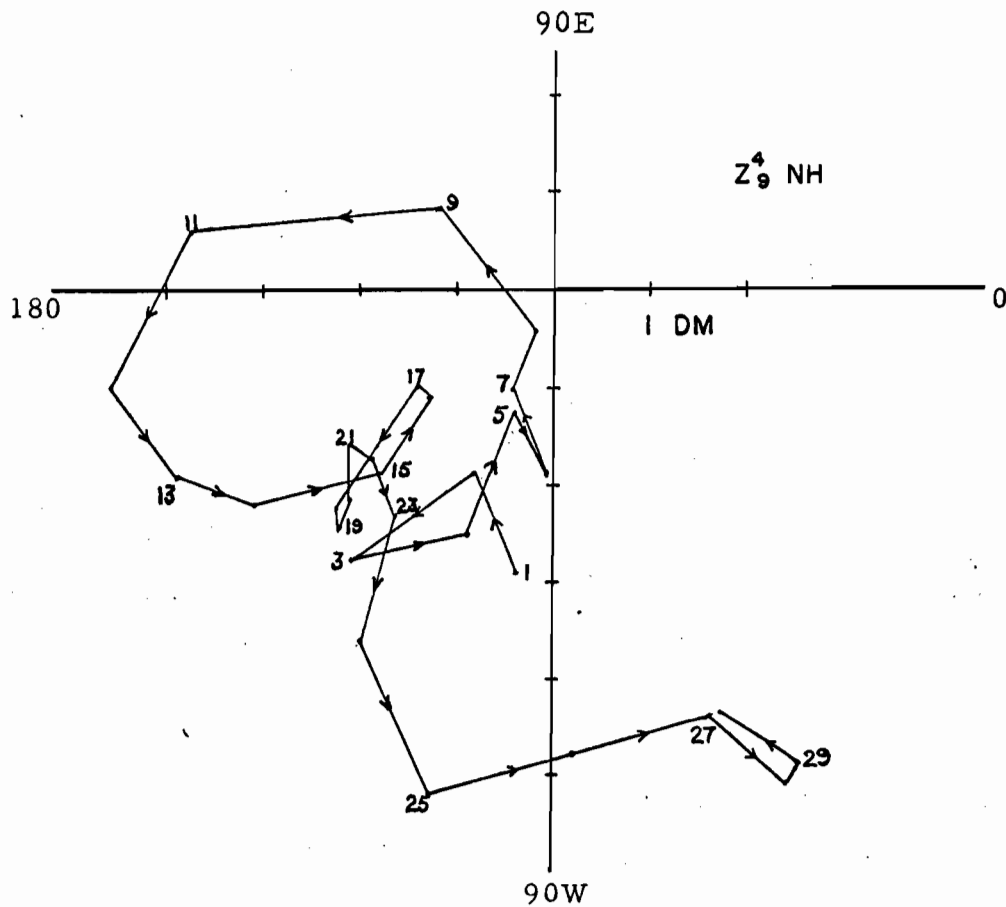


Figure 4.23: Daily values of amplitude and relative phase angle of northern hemispheric height field component (4, 9) for month of September 1957. Antisymmetry with respect to the equator is assumed. Amplitude in decameters.

well defined than the large scale waves in the southern hemisphere (at least in the sense that their time behaviour is reasonably coherent). Figures 4.20, 4.22 show the phase diagrams for the largest components of zonal wave number 4 i.e.  $Z_7^4$  and  $Z_9^4$ . Both the waves move from west to east throughout the month with fairly constant phase speeds, and smoothly varying amplitudes. It can be argued that this regularity has been forced on the data through its distribution, and the use of time continuity for its analysis. However, as can be seen from the phase diagrams, the phase goes through almost three cycles; which means that a fair part of the system will be in good data areas at least three times during the month. This rather strange idea that the short scale waves are more well defined than the large scale waves can perhaps be supported by the following argument. In order to detect a fairly rapid retrogressive component superimposed on a stationary one the phase position must be determined very accurately. Notice in Figure 4.17 that the range of phase angles for  $Z_2^1$  in the northern hemisphere is only  $\pm 45^\circ$  for the entire month. The smaller the amplitude of the moving part relative to the stationary part the more accurate must be the phase determination. The synoptic analyst in the southern hemisphere must resort to a combination of time continuity and what he can determine about 500 mb from the surface observations when working in poor data areas. The very large scale waves (such as zonal wave number one which measure the eccentricity of the flow about the pole) are not obviously apparent

on a synoptic chart. As well, their vertical structure is most probably such that they have very low amplitudes near the surface. Thus one may expect that fluctuations of the type observed in the northern hemisphere for the very large scale waves would be lost through lack of definition in the southern hemisphere.

Broadly speaking, the behaviour of the waves in the two hemispheres (even if well-defined individually) is different. (Compare Figures 4. 20, 4. 21, 4. 22, 4. 23 ). When the two hemispheres are combined then the time behaviour of the waves becomes less coherent. For example (as was shown by Steinberg (1965) for zonal wave number 4) if there exist two independent perturbations of the same zonal wave number in the northern and southern hemispheres which are imbedded in zonal currents of different speeds, then variance (or energy) will be shifted from even Legendre components to odd Legendre components of that wave as the two independent perturbations come into and go out of phase. This may be interpreted as a non-linear interaction of waves with an odd zonal flow, but this appears to add little to the understanding of the system.

Because of the variability of the phase changes from day to day of a large number of the components it was decided that computations and comparison of phase speeds of the components in general would be meaningful only as regards to sign (i. e. whether a particular component's motion was dominantly retrogressive, progressive or neither). For those components which do have well-

Table 4.15: CHARACTER OF THE FLUCTUATIONS OF SPHERICAL HARMONIC WAVES

R = RETROGRESSIVE P = PROGRESSIVE X = NOT DOMINANTLY ONE OR THE OTHER

m →	1			2			3			4			5			6		
n ↓	NH	SH	GLO-BAL	NH	SH	GLO-BAL	NH	SH	GLO-BAL	NH	SH	GLO-BAL	NH	SH	GLO-BAL	NH	SH	GLO-BAL
1	-	-	X															
2	-72	X	X	-	-	R												
3	-	-	R	-25	R	X	-	-										
4	R	X	X	-	-	R	R	X	X	-	-	X						
5	-	-	P	R	R	R	-	-	X	R	+9	X	-	-	X			
6	X	P	R	-	-	R	P	P	P	-	-	P	R	P	P	-	-	X
7	-	-	R	R	P	P	-	-	P	X	+9	P	-	-	P	P	P	P
8	R	P	X	-	-	X	P	P	P	-	-	P	X	P	P	-	-	P
9	-	-	X	X	P	X	-	-	P	P	+9	P	-	-	P	+5	P	P
10	X	P	X	-	-	X	P	P	P	-	-	P	P	P	P	-	-	P

defined and consistent phase variations over the period of the month phase speeds in degrees longitude per day were computed. These determinations were made for the three sets of components; i. e. the global stream function; the northern and southern hemisphere height components; and are presented in Table 4.15. No distinction was made between those components which had little coherent behaviour (such as  $\psi_2'$ ) and those which were progressive for one part of the month and retrogressive for the other.

The stream function components even under this very rough classification do not show any pattern save that short waves are progressive. On the other hand the northern and southern hemisphere components do show a pattern of long retrogressive waves, intermediate quasi-stationary components and short progressive waves. The wavelength of the quasi-stationary waves appears to be longer in the southern hemisphere, which is consistent with a stronger zonal flow.

Components  $Z_2^1$  and  $Z_3^2$  in the northern hemisphere retrogress very rapidly during this period (September 1957) at speeds which are approximately twice as large as those obtained by Deland for January 1957. It is noteworthy that components  $Z_5^4$ ,  $Z_7^4$ ,  $Z_9^4$  in the southern hemisphere all appear to progress at the same speed, approximately  $9^\circ$  per day.

This last observation may shed some light on the meaning of the time variations of the components, especially for the smaller

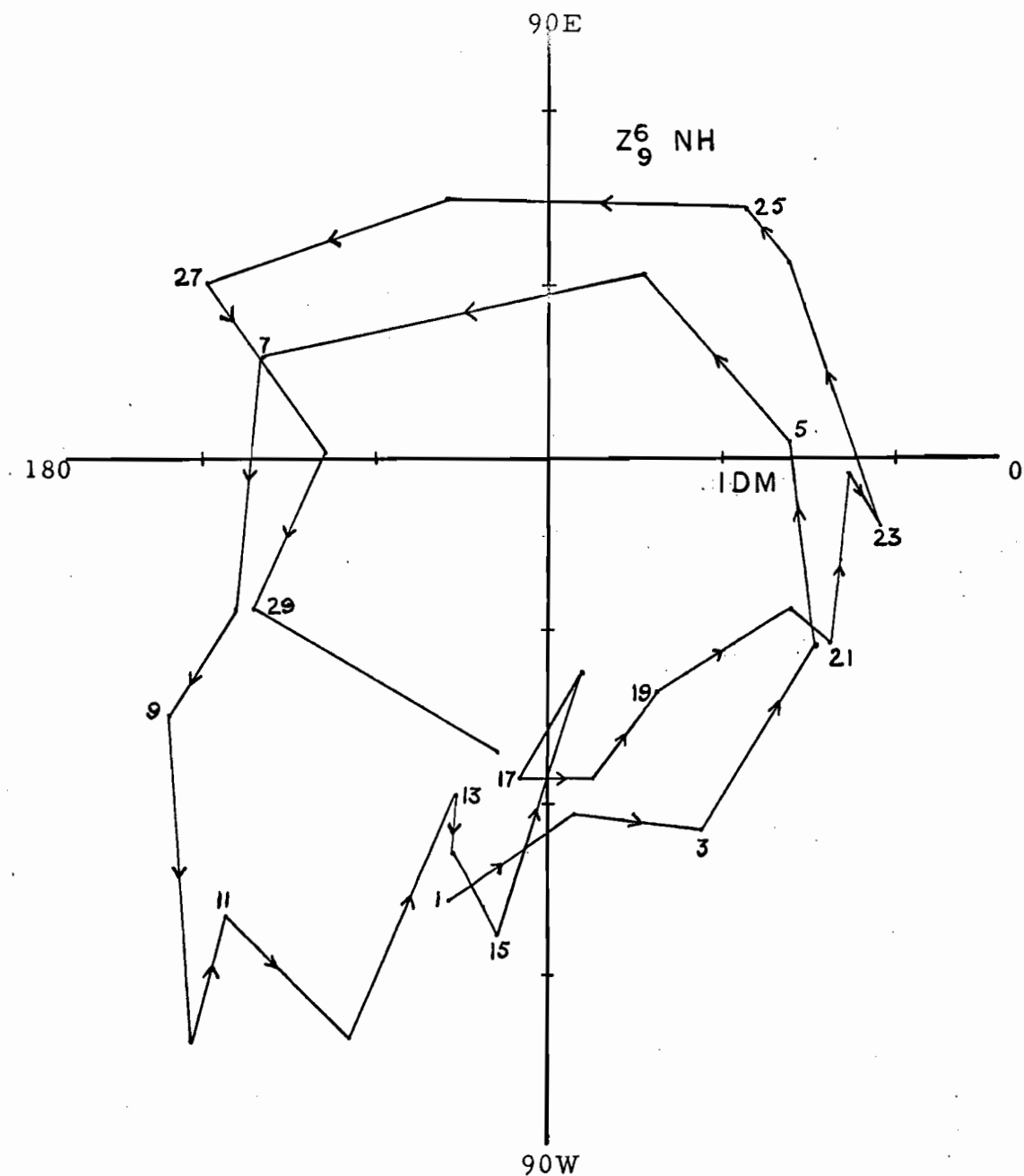


Figure 4. 24: Daily values of amplitude and relative phase angle of northern hemispheric height field component (6, 9) for month of September 1957. Antisymmetry with respect to the equator is assumed. Amplitude in decameters.



scale components. If a particular perturbation with a given zonal wave number (e. g.  $m = 4$  or  $6$ ) has a latitudinal shape which is characteristic to itself and is largely maintained as the wave is advected by the zonal flow, then the Legendre components representing the latitudinal structure of the wave may be expected to maintain their relative phase positions as the perturbation is advected. This appears to be well-illustrated by wave number four in the southern hemisphere and wave number six in the northern hemisphere (Figures 4. 20, 4. 21, 4. 24, 4. 25).

On this basis one can account for the results of Deland (1961). He found that the waves without exception "showed greater eastward, or less rapid westward, motion than would be predicted from the Rossby-Haurwitz wave speed".

For the large scale retrogressive components this result can be explained by a very small amount of divergence as illustrated by Eliassen and Machenhauer (1965). If the smaller scale waves correspond to the model above, then being largely located in the region of strong westerlies, their phase speeds and thus the observed phase speeds of the Legendre components representing their latitudinal profile will be much larger than the corresponding Rossby-Haurwitz phase speeds of Legendre components. This indicates that for small scale perturbations the Legendre components individually have little meaning in terms of the dynamic equations and linear phase speeds. This is presumably what Deland means when he says "it is possible

they are all carried along by the faster-moving smaller-scale waves, by means of non-linear interactions".

## 5. SUMMARY AND CONCLUSIONS

The broad aim of this investigation was to study the application of spectral techniques (primarily in terms of spherical harmonics) to the dynamical equations in general, to highly truncated systems in particular, and then to observed motions in the atmosphere with the view of delineating the non-linear behaviour of waves.

On this basis the following conclusions can be drawn:

1. The full dynamical equations transform straightforwardly into the spectral domain; the non-linear terms appearing as sums of products of amplitudes modified by interaction coefficients.
2. The main advantage of the spectral forms is that they conserve energy under only mildly restrictive truncation; the main disadvantage is the necessity of computing large numbers of interaction coefficients in the application of the spectral forms to models with many degrees of freedom.
3. Highly truncated spectral forms of the dynamical equation may be studied in a quasi-analytic manner with fruitful results. In particular, the results of previous stability analysis of barotropic motion can be interpreted in terms of the non-linear behaviour of the waves in simplified models.
4. In a non-linear system the distinction between stability and instability is not as clearly defined as in a linear system. In fact, zonal current systems which are linearly stable may undergo

large fluctuations if subjected to finite perturbations.

5. The comparative study of simplified barotropic motion on the  $\beta$ -plane and on a sphere indicates that they are essentially equivalent.
6. There is no evidence in the September 1957 data at 500 mb that fluctuations in the large-scale vorticity patterns are global in character, but rather that the two hemispheres behave independently. This means that although the statistics derived from a global analysis (such as the distribution of kinetic energy over wavelength) are probably meaningful, the individual behaviour of the waves is not. On the other hand, hemispheric analysis produces a reasonable picture of the fluctuations of the large-scale components.
7. There is little evidence of non-linear behaviour of the type discussed in terms of three component systems. This fact is not inconsistent with the following observations. Firstly, as was indicated previously, the large-scale zonal components are well into the stable regime. Since the zonal components are large compared to the perturbations, the large-scale waves may be expected to behave linearly. That is, they undergo little energy exchange with the zonal flow. Secondly, the existence of a quasi-stationary part of a wave (which is presumably thermally or frictionally forced) violates the basic of the truncated model. Thirdly, for shorter wavelengths the large number of possible

interactions limits the possibility of any three component exchange being dominant and thus observable. Fourthly, the behaviour of the shorter waves indicates that they may have latitudinal structures which are characteristic to themselves and not related to the spherical harmonics.

This last observation, coupled with (5), suggests that the study of smaller scale motions may be more profitable and more simply done on the  $\beta$ -plane.

The definition of the large-scale motions in the atmosphere is far from being complete. However, as this work suggests (in agreement with Deland (1965), Eliassen and Machenhauer (1965) ), the use of spherical harmonics to specify these large-scale motions seems promising. The discovery that the large-scale waves do behave approximately in accordance with the Rossby idea is significant, not only for the understanding of these motions but also for the purpose of extended range forecasting. If spherical harmonic analysis is able to separate out significant motions, then the study of the spectral forms of the dynamic equations becomes very important. Here only extremely simple barotropic motion has been studied. This work should be extended to more complicated physical systems which are able to convert potential to kinetic energy and also respond to the forcing produced by large-scale heating and friction.

## BIBLIOGRAPHY

- Baer, F., 1964: Integration with the spectral vorticity equation. *J. atmos. Sci.* 21, 260-286.
- Bilinova, E.N., 1943: A hydrodynamical theory of pressure and temperature waves and of centres of action. *C.R. Acad. Sci. U.R.S.S.*, 39, 257.
- Boville, B. W., and M. Kwizak, 1959: Fourier analysis applied to hemispheric waves of the atmosphere. Meteorological Branch, Canada, TEC-292.
- Boville, B. W., 1961: A dynamical study of the 1958-59 stratospheric polar vortex, A. M. R. G. Publication in Meteorology No. 9, McGill University.
- Bryan, K., Jr., 1959: A numerical investigation of certain features of the general circulation. *Tellus*, 11, 163-174.
- Charney, J. G., R. Fjortoft and J. von Neumann, 1950: Numerical integration of the barotropic vorticity equation. *Tellus*, 2, 237-254.
- Charney, J. G., 1947: The dynamics of long waves in a baroclinic westerly current. *J. Meteor.*, 4, 135-163.
- Charney, J. G. and A. Eliassen, 1949: A numerical method for predicting the perturbations of the middle-latitude westerlies. *Tellus*, 1, 38-54.

- Craig, R. A., 1945: A solution of the non-linear vorticity equation for atmospheric motion. *J. Meteor.*, 2, 175-178.
- Deland, R. J., 1965: Some observations of the behaviour of spherical harmonic waves. *Mon. Wea. Rev.*, 93, 307-312.
- De Las Alas, J., 1966: Kinetic energy and momentum transport at 500 mb in the tropics. M.Sc. Thesis, McGill University.
- Eady, E. T., 1949: Long waves and cyclone waves. *Tellus* 1, 33-52.
- Eliassen, E., and B. Machenhauer, 1965: A study of fluctuations of the atmospheric planetary flow patterns represented by spherical harmonics. *Tellus*, 17, 220-238.
- Eliassen, E., 1958: A study of the long atmospheric waves on the basis of zonal harmonic analysis. *Tellus* 10, 206-215.
- Ellsaesser, H. W., 1965: Expansion of hemispheric meteorological data in antisymmetric surface spherical harmonic (Laplace) series. UCRL-7617-T-REV.1.
- Fjortoft, R., 1950: Application of integral theorems in deriving criteria for laminar flows and for the baroclinic circular vortex. *Geofys. Publikasjoner, Norske Videnskaps-Akad.* Oslo, 17.
- Fjortoft, R., 1963: On the changes in the spectral distribution of kinetic energy for two-dimensional, non-divergent flow. *Tellus*, 5, 225-230.
- Fultz, D., et al., 1959: Studies of thermal convection in a rotating cylinder with some implications for large-scale atmospheric motions. *Meteor. Monographs*, 4 (21), 104 pp.

- Godson, W.L., 1959: The application of Fourier analysis to meteorological data. Meteorological Branch, Canada, TEC-295.
- Haurwitz, B., 1940: The motion of atmospheric disturbances on a spherical earth. *J. Marine Res.*, 3, 254-267.
- Haurwitz, B., and R.A. Craig, 1952: Atmospheric flow patterns and their representation by spherical surface harmonics, U.S.A.F. Cambridge Res. Cntr., Geophys. Res. Paper Non 14, 78 pp.
- Kubota, S., 1960: Surface spherical harmonic representation of systems of equations for analysis. *Papers in Meteorology and Geophysics, Met. Res. Inst. of Japan*, Vol.10, 145-166.
- Kuo, H.L., 1949: Dynamic instability of two-dimensional non-divergent flow in a barotropic atmosphere. *J. Meteor.*, 6, 105-122.
- Lorenz, E.N., 1960a: Maximum simplification of the dynamic equations. *Tellus*, 12, 243-254.
- Lorenz, E.N., 1960b: Energy and numerical weather prediction. *Tellus*, 12, 264-373.
- Lorenz, E.N., 1962: Simplified dynamic equations applied to the rotating basin experiments. *J. atmos. Sci.*, 19, 39-51.
- Luistro, F.M., 1964: Atmospheric kinetic energy at 500 mb. AMRG Publication in Meteorology No. 73, McGill University.
- Neamtan, S.M., 1946: The motion of harmonic waves in the atmosphere. *J. Meteor.*, 3, 53-56.

- Peng, L., 1965: A modelling study of the meridional temperature profile and energy transformations in the lower stratosphere. M.I.T. Planetary Circulations Project, No. 13.
- Phillips, N.A., 1963: Geostrophic motion. *Rev. Geophysics*, 1 (12), 123-176.
- Platzman, G.W., 1960: The spectral form of the vorticity equation. *J. Meteor.*, 17, 635-644.
- Platzman, G.W., 1962: The analytical dynamics of the spectral vorticity equation. *J. atmos. Sci.*, 19, 313-328.
- Robert, A.J., 1965: The behaviour of planetary waves in an atmospheric model based on spherical harmonics, AMRG Publication in Meteorology No. 77, McGill University.
- Rojanski, V., 1938: Introductory quantum mechanics, Prentice-Hall, p. 352.
- Rossby, C. -G., and collaborators, 1939: Relation between variations in the intensity of the zonal circulation of the atmosphere and the displacement of the semi-permanent centres of action. *J. Marine Res.*, 2, 38-55.
- Silberman, I., 1954: Planetary waves in the atmosphere. *J. Meteor.*, 11, 27-34.
- Steinberg, L., 1965: A spherical harmonic specification of the global 500 mb surface. M.Sc. Thesis, McGill University.

## APPENDIX A

The functions

$$P_n^m = \frac{1}{2^n n!} \left( \frac{2n+1}{2} \cdot \frac{(n-m)!}{(n+m)!} \right)^{\frac{1}{2}} (1-\mu^2)^{\frac{1}{2}m} \frac{d^{n+m}}{d\mu^{n+m}} (\mu^2-1)^n; m \geq 0 \quad \text{A.1}$$

$$P_n^{-m} = (-1)^m P_n^m$$

where  $\mu = \cos \theta$ ,  $n = 0, 1, 2, \dots$ ,  $m = 0, \pm 1, \dots, \pm n$ , are orthonormal in  $\theta$  over the range  $(0, \pi)$  and satisfy the equations (Rojanski, p 532)

$$\cos \theta P_n^m = A_n^m P_{n+1}^m + B_n^m P_{n-1}^m \quad \text{A.2}$$

$$\sin \theta P_n^m = C_n^m P_{n+1}^{m+1} - D_n^m P_{n-1}^{m+1} \quad \text{A.3}$$

$$\sin \theta P_n^m = -E_n^m P_{n+1}^{m-1} - F_n^m P_{n-1}^{m-1} \quad \text{A.4}$$

$$\frac{dP_n^m}{d\theta} = -\frac{1}{2} G_n^m P_n^{m+1} + \frac{1}{2} H_n^m P_n^{m-1} \quad \text{A.5}$$

$$\sin \theta \frac{dP_n^m}{d\theta} = n A_n^m P_{n+1}^m - (n+1) B_n^m P_{n-1}^m \quad \text{A.6}$$

$$m \cot \theta P_n^m = \frac{1}{2} G_n^m P_n^{m+1} + \frac{1}{2} H_n^m P_n^{m-1} \quad \text{A.7}$$

where the expansion coefficients are

$$A_n^{m^2} = \frac{(n+m+1)(n-m+1)}{(2n+1)(2n+3)}$$

$$B_n^{m^2} = \frac{(n+m)(n-m)}{(2n-1)(2n+1)}$$

$$C_n^{m^2} = \frac{(n+m+1)(n+m+2)}{(2n+1)(2n+3)}$$

$$D_n^{m^2} = \frac{(n-m)(n-m-1)}{(2n-1)(2n+1)}$$

$$E_n^{m^2} = \frac{(n-m+1)(n-m+2)}{(2n+1)(2n+3)}$$

$$F_n^{m^2} = \frac{(n+m)(n+m-1)}{(2n-1)(2n+1)}$$

$$G_n^{m^2} = (n-m)(n+m+1)$$

$$H_n^{m^2} = (n+m)(n-m+1)$$

## APPENDIX B

In view of equation A. 5

$$\int_0^\pi P_{n_Y}^{m_Y} \sin \theta \frac{dP_{n_d}^{m_Y}}{d\theta} \sin \theta d\theta$$

$$= \int_0^\pi P_{n_Y}^{m_Y} \left( n_d A_{n_d}^{m_Y} P_{n_d+1}^{m_Y} - (n_d+1) B_{n_d}^{m_Y} P_{n_d-1}^{m_Y} \right) \sin \theta d\theta$$

which, upon application of the orthogonal relations 2.11

gives

$$\int_0^\pi P_{n_Y}^{m_Y} \sin \theta \frac{dP_{n_d}^{m_Y}}{d\theta} \sin \theta d\theta = n_d A_{n_d}^{m_Y} \delta_{n_d+1}^{n_Y} - (n_d+1) B_{n_d}^{m_Y} \delta_{n_d-1}^{n_Y} \quad \text{B.1}$$

Thus equation 2.25 may be written as

$$\sum_{\alpha} \chi_{\alpha} \int_0^\pi P_Y \sin \theta \frac{dP_{\alpha}^{m_Y}}{d\theta} \sin \theta d\theta = (n_Y-1) \epsilon_{n_Y}^{m_Y} \chi_{Y-1} - (n_Y+2) \epsilon_{n_Y+1}^{m_Y} \chi_{Y+1}$$

$$\text{where } \epsilon_{n_Y}^{m_Y^2} = \frac{n_Y^2 - m_Y^2}{4n_Y^2 - 1} = B_{n_Y}^{m_Y^2} = A_{n_Y+1}^{m_Y^2} \quad \text{B.2}$$

Similarly, using A. 6 it can be shown that

$$\sum_{\alpha} c_{\alpha} \chi_{\alpha} \int_0^\pi P_{n_Y}^{m_Y} P_{n_d}^{m_Y} \cos \theta \sin \theta d\theta = n_Y (n_Y-1) \epsilon_{n_Y}^{m_Y} \chi_{Y-1} + (n_Y+1)(n_Y+2) \epsilon_{n_Y+1}^{m_Y} \chi_{Y+1} \quad \text{B.3}$$

The following integrals of triple products of Legendre function arise naturally from the spectral transformation of the

vorticity and divergence equations

$$H_{\alpha\gamma\beta} = \frac{C_\alpha - C_\beta}{2} L_{\alpha\gamma\beta} \quad \text{B.4}$$

where 
$$L_{\alpha\gamma\beta} = \int_0^\pi P_\gamma \left( m_\alpha P_\alpha \frac{dP_\beta}{d\theta} - m_\beta P_\beta \frac{dP_\alpha}{d\theta} \right) d\theta$$

$$I_{\alpha\gamma\beta} = C_\beta K_{\alpha\gamma\beta} \quad \text{B.5}$$

where 
$$K_{\alpha\gamma\beta} = \int_0^\pi P_\gamma \left( \frac{m_\alpha m_\beta P_\alpha P_\beta}{\sin^2 \theta} - \frac{dP_\alpha}{d\theta} \frac{dP_\beta}{d\theta} \right) \sin \theta d\theta$$

$$J_{\alpha\gamma\beta} = C_\alpha C_\beta \int_0^\pi P_\alpha P_\gamma P_\beta \sin \theta d\theta \quad \text{B.6}$$

Here  $\alpha, \beta, \gamma$  are wave vectors defined as  $\alpha = \kappa_\alpha + i m_\alpha$  etc., and the  $P_\alpha$  are the normalized associated Legendre functions of the first kind.

The symmetry properties of the interaction matrices may be obtained from the above equations.

$$L_{\alpha\gamma\beta} = -L_{\beta\gamma\alpha}$$

B.7

$$L_{\alpha^* \gamma^* \beta^*} = -L_{\alpha\gamma\beta}$$

Further by integration by parts gives (Silberman, 1954)

$$L_{\alpha\gamma\beta} = (-1)^{m_\alpha} L_{\alpha^*\beta\gamma} = (-1)^{m_\beta} L_{\gamma\alpha\beta^*} \quad \text{B.8}$$

so that in consideration of the evaluation of  $L_{\alpha\gamma\beta}$  one need only consider positive values of  $m_\alpha, m_\beta, m_\gamma$ .

Following essentially the development of Silberman (loc. cit.) the following expression of  $L_{\alpha\gamma\beta}$  in terms of integrals of the type B.6 may be obtained.

$$L_{\alpha\gamma\beta} = E_{\alpha\gamma\beta} - E_{\beta\gamma\alpha} \quad \text{B.9}$$

$$\text{where } E_{\alpha\gamma\beta} = m_\beta \left[ \frac{(2n_\alpha+1)(n_\alpha-m_\alpha)!}{(n_\alpha+m_\alpha)!} \right]^{\frac{1}{2}} \sum_q \left[ \frac{(2n_q+1)(n_q+m_\alpha)}{n_q-m_\alpha} \right]^{\frac{1}{2}} \int_0^\pi P_q P_\gamma P_\beta \sin\theta d\theta$$

and  $q \equiv n_q + i m_\alpha$   $n_q = n_\alpha - 1, n_\alpha - 3, \dots, m_\alpha + 1$  or  $m_\alpha$ .

Consider now  $K_{\alpha\gamma\beta}$ .

$$K_{\alpha\gamma\beta} = \int_0^\pi P_\gamma \left( \frac{m_\alpha m_\beta P_\alpha P_\beta}{\sin^2\theta} - \frac{dP_\alpha}{d\theta} \frac{dP_\beta}{d\theta} \right) \sin\theta d\theta \quad \text{B.10}$$

The  $P_\alpha$  satisfy the following differential equation

$$\frac{d}{d\theta} \left( \sin\theta \frac{dP_\alpha}{d\theta} \right) + \left( n_\alpha(n_\alpha+1) - \frac{m_\alpha^2}{\sin^2\theta} \right) \sin\theta P_\alpha = 0 \quad \text{B.11}$$

Integrating the following expression by parts gives

$$\int_0^{\pi} P_Y \frac{dP_{\beta}}{d\theta} \frac{dP_{\alpha}}{d\theta} \sin\theta d\theta = P_Y \frac{dP_{\beta}}{d\theta} P_{\alpha} \sin\theta \Big|_0^{\pi} - \int_0^{\pi} P_{\alpha} \frac{d}{d\theta} (P_Y \frac{dP_{\beta}}{d\theta} \sin\theta) d\theta$$

Since  $\frac{dP_{\beta}}{d\theta}$  can be expressed as a linear combination of  $P_Y$ 's and no  $P_Y$  has singularities at the poles, the first term on the right hand side is equal to zero;

$$\int_0^{\pi} P_Y \frac{dP_{\beta}}{d\theta} \frac{dP_{\alpha}}{d\theta} \sin\theta d\theta = - \int_0^{\pi} P_{\alpha} \frac{d}{d\theta} (P_Y \frac{dP_{\beta}}{d\theta} \sin\theta) d\theta \quad \text{B.12}$$

Differentiating through the right hand side of B.12 gives

$$\int_0^{\pi} P_Y \frac{dP_{\beta}}{d\theta} \frac{dP_{\alpha}}{d\theta} \sin\theta d\theta = - \int_0^{\pi} P_{\alpha} P_Y \frac{d}{d\theta} (\sin\theta \frac{dP_{\beta}}{d\theta}) d\theta - \int_0^{\pi} P_{\alpha} \frac{dP_Y}{d\theta} \frac{dP_{\beta}}{d\theta} \sin\theta d\theta$$

Using B.11 results in the following expression

$$\begin{aligned} \int_0^{\pi} P_Y \frac{dP_{\beta}}{d\theta} \frac{dP_{\alpha}}{d\theta} \sin\theta d\theta &= \int_0^{\pi} P_{\alpha} P_Y \left( n_{\beta}(n_{\beta}+1) - \frac{m_{\beta}^2}{\sin^2\theta} \right) \sin\theta P_{\beta} d\theta \\ &- \int_0^{\pi} \frac{dP_Y}{d\theta} P_{\alpha} \frac{dP_{\beta}}{d\theta} \sin\theta d\theta \end{aligned} \quad \text{B.13}$$

Similarly, expansion about the other term gives

$$\begin{aligned} \int_0^{\pi} P_Y \frac{dP_{\beta}}{d\theta} \frac{dP_{\alpha}}{d\theta} \sin\theta d\theta &= \int_0^{\pi} P_{\beta} P_Y \left( n_{\alpha}(n_{\alpha}+1) - \frac{m_{\alpha}^2}{\sin\theta} \right) \sin\theta P_{\alpha} d\theta \\ &- \int_0^{\pi} \frac{dP_Y}{d\theta} P_{\beta} \frac{dP_{\alpha}}{d\theta} \sin\theta d\theta \end{aligned} \quad \text{B.14}$$

Addition of B.13 and B.14 gives

$$\begin{aligned}
 2 \int_0^{\pi} P_{\gamma} \frac{dP_{\beta}}{d\theta} \frac{dP_{\alpha}}{d\theta} \sin \theta d\theta &= \left[ n_{\alpha}(n_{\alpha}+1) + n_{\beta}(n_{\beta}+1) \right] \int_0^{\pi} P_{\alpha} P_{\gamma} P_{\beta} \sin \theta d\theta \\
 &\quad - (m_{\alpha}^2 + m_{\beta}^2) \int_0^{\pi} \frac{P_{\alpha} P_{\beta} P_{\gamma}}{\sin^2 \theta} \sin \theta d\theta \\
 &\quad - \int_0^{\pi} P_{\gamma} \frac{d(P_{\alpha} P_{\beta})}{d\theta} \sin \theta d\theta
 \end{aligned}$$

B.15

Thus  $2 K_{\alpha \gamma \beta}$  is given by

$$\begin{aligned}
 2 K_{\alpha \gamma \beta} &= - \left[ n_{\alpha}(n_{\alpha}+1) + n_{\beta}(n_{\beta}+1) \right] \int_0^{\pi} P_{\alpha} P_{\gamma} P_{\beta} \sin \theta d\theta \\
 &\quad + (m_{\alpha} + m_{\beta})^2 \int_0^{\pi} \frac{P_{\alpha} P_{\beta} P_{\gamma}}{\sin^2 \theta} \sin \theta d\theta + \int_0^{\pi} \frac{dP_{\gamma}}{d\theta} \sin \theta \frac{d(P_{\alpha} P_{\beta})}{d\theta} d\theta
 \end{aligned}$$

Integrating the last term on the right hand side by parts and using equation B.11 one obtains

$$\int_0^{\pi} \frac{dP_{\gamma}}{d\theta} \sin \theta \frac{d(P_{\alpha} P_{\beta})}{d\theta} d\theta = \int_0^{\pi} P_{\alpha} P_{\beta} \left( n_{\gamma}(n_{\gamma}+1) - \frac{m_{\gamma}^2}{\sin^2 \theta} \right) P_{\gamma} \sin \theta d\theta$$

Since  $m_\alpha + m_\beta = m_\gamma$  for non vanishing of the interactions,

$K_{\alpha\gamma\beta}$  can be expressed as

$$K_{\alpha\gamma\beta} = \frac{n_\gamma(n_\gamma+1) - n_\alpha(n_\alpha+1) - n_\beta(n_\beta+1)}{2} \int_0^\pi P_\alpha P_\gamma P_\beta \sin\theta d\theta$$

or more simply

$$K_{\alpha\gamma\beta} = \frac{c_\gamma - c_\alpha - c_\beta}{2} \int_0^\pi P_\alpha P_\gamma P_\beta \sin\theta d\theta$$

B.16

Thus all of the interaction matrices are expressible in terms of integrals of the product of three Legendre polynomials. An expression for integrals of the type  $\int_0^\pi P_\alpha P_\gamma P_\beta \sin\theta d\theta$  has also been presented by Silberman (loc. cit.)

$$\int_0^\pi P_\alpha P_\gamma P_\beta \sin\theta d\theta = \frac{(n_\beta + n_\alpha - n_\gamma - 1)!! \left[ (2n_\gamma + 1)(2n_\alpha + 1)(2n_\beta + 1) \right]^{\frac{1}{2}}}{(n_\beta + n_\gamma - n_\alpha)!! (n_\alpha + n_\beta + n_\gamma + 1)!! (n_\alpha + n_\gamma - n_\beta)!!} \\ \times \left[ \frac{(n_\gamma + m_\gamma)! (n_\gamma - m_\gamma)! (n_\beta - m_\beta)! (n_\alpha - m_\alpha)!}{2 (n_\alpha + m_\alpha)! (n_\beta + m_\beta)!} \right]^{\frac{1}{2}} \\ \times \sum_{h=0}^{n_\gamma - m_\gamma} \frac{(-1)^{\frac{1}{2}(n_\beta - n_\alpha + n_\gamma) + m_\beta + h} (n_\beta + m_\beta + h)! (n_\alpha + n_\gamma - m_\beta - h)!}{(n_\gamma - m_\gamma - h)! h! (n_\beta - m_\beta - h)! (n_\alpha - n_\gamma + m_\beta + h)!}$$

where  $k!! = k(k-2)(k-4)\dots 2$  or  $1$ , and  $0!! = (-1)!! = 1$

as well, any terms with the single factorial of a negative number are considered equal to zero. It is also implicitly assumed that

$m_\alpha + m_\beta = m_\gamma$ . The above integral vanishes unless the following

conditions are fulfilled

$$\pi_\alpha + \pi_\beta + \pi_\gamma = \text{even}$$

$$|\pi_\beta - \pi_\alpha| \leq \pi_\gamma \leq \pi_\alpha + \pi_\beta$$

These selection rules result in similar selection rules for the interaction matrices which are summarized in the following table.

#### SELECTIONS RULES

Interaction Matrix	$H_{\alpha\gamma\beta}$	$L_{\alpha\gamma\beta}$	$I_{\alpha\gamma\beta}$	$K_{\alpha\gamma\beta}$	$J_{\alpha\gamma\beta}$
Wave Rule	$m_\alpha + m_\beta = m_\gamma$	$m_\alpha + m_\beta = m_\gamma$	$m_\alpha + m_\beta = m_\gamma$	$m_\alpha + m_\beta = m_\gamma$	$m_\alpha + m_\beta = m_\gamma$
Triangle Rule	$ \pi_\alpha - \pi_\beta  < \pi_\gamma$ $< \pi_\alpha + \pi_\beta$	$ \pi_\alpha - \pi_\beta  \leq \pi_\gamma$ $\leq \pi_\alpha + \pi_\beta$	$ \pi_\alpha - \pi_\beta  \leq \pi_\gamma$ $\leq \pi_\alpha + \pi_\beta$	$ \pi_\alpha - \pi_\beta  \leq \pi_\gamma$ $\leq \pi_\alpha + \pi_\beta$	$ \pi_\alpha - \pi_\beta  \leq \pi_\gamma$ $\leq \pi_\alpha + \pi_\beta$
Parity Rule	$\pi_\alpha + \pi_\beta + \pi_\gamma = \text{odd}$	$\pi_\alpha + \pi_\beta + \pi_\gamma = \text{odd}$	$\pi_\alpha + \pi_\beta + \pi_\gamma = \text{even}$	$\pi_\alpha + \pi_\beta + \pi_\gamma = \text{even}$	$\pi_\alpha + \pi_\beta + \pi_\gamma = \text{even}$
Additional Rules	$\pi_\alpha \neq \pi_\beta$	$m_\alpha^2 + m_\beta^2 \neq 0$	$\pi_\alpha \neq 0; \pi_\beta \neq 0$	$\pi_\alpha \neq 0; \pi_\beta \neq 0$	$\pi_\alpha \neq 0; \pi_\beta \neq 0$
The quantity vanishes unless the specified condition is fulfilled					

The symmetry and redundancy relations for the interaction matrices are as follows

$$L_{\alpha\gamma\beta} = -L_{\beta\gamma\alpha} = -L_{\alpha^*\gamma^*\beta^*}$$

$$L_{\alpha\gamma\beta} = (-1)^{m_\alpha} L_{\alpha^*\beta\gamma} = (-1)^{m_\beta} L_{\gamma\alpha\beta^*}$$

where  $\alpha^* = \pi_\alpha - i m_\alpha$  etc.,

$$H_{\alpha\gamma\beta} = H_{\beta\gamma\alpha} = -H_{\alpha^*\gamma^*\beta^*}$$

$$K_{\alpha\gamma\beta} = K_{\beta\gamma\alpha} = K_{\alpha^*\gamma^*\beta^*}$$

$$J_{\alpha\gamma\beta} = J_{\beta\gamma\alpha} = J_{\alpha^*\gamma^*\beta^*}$$

B.17

Since all of the interaction matrices can be expressed in terms of integrals of the type  $M_{\alpha\gamma\beta} = \int_0^\pi P_\alpha P_\gamma P_\beta \sin\theta d\theta$ , they can be evaluated by taking advantage of not only their own symmetry and redundancy relations, but also those of  $M_{\alpha\gamma\beta}$

$$M_{\alpha\gamma\beta} = M_{\beta\gamma\alpha}$$

$$M_{\alpha^*\gamma\beta} = (-1)^{m_\alpha} M_{\alpha\beta\gamma}$$

$$M_{\alpha\gamma\beta^*} = (-1)^{m_\beta} M_{\gamma\alpha\beta}$$

B.18

Thus in computing the interaction matrices only positive wave vectors need be considered.